The molecular dysregulation of Excitation contraction coupling in patients with congenital muscle disorders

Inauguraldissertation

zur

Erlangung der Würde eines Doktors der Philosophie

vorgelegt der

Philosophisch-Naturwissenschaftlichen Fakultät

der Universität Basel

Von

Ori   Rokach

Von Israel

Basel, 2015

Genehmigt von der Philosophisch-Naturwissenschaftlichen Fakultät

auf Antrag von

Prof Jean Pieters

Prof Susan Treves

Prof Christoph Handschin

Basel, 08 Dezember 2015

Prof. Dr. Jörg Schibler

Dekan

Acknowledgments:

I wish to express my appreciation to Prof Susan Treves and Prof Francesco Zorzato for supervising this work and assisting when needed.

In addition I would like to thank all the lab members that were supporting me along the journey while preparing and writing this work.

I would like to express my gratitude to my family and friends for their support.

I cordially thank Prof Jean Pieters, Prof Christoph Handschin and Prof Markus Ruegg, who accepted to be members of my PhD committee.

Table of Contents

Abstract:

Excitation contraction coupling (ECC) is the process whereby an action potential spreading throughout the muscle membrane activates muscle contraction, by releasing Ca^{2+} from the Sarcoplasmic Reticulum (SR). Ca^{2+} release from the SR is mediated by the Ryanodine Receptor located on the SR membrane. Any alterations in the architecture of the intercellular muscle membrane compartments or mutations in the RYR1 gene are associated with neuromuscular disorders such as Central core disease, Multi minicore disease, Central nuclear myopathy or congenital fiber type disproportion.

In the last few decades, ECC characteristics were extensively investigated in our lab, on myotubes originating from patient's muscle satellite cells. In the 1st paper entitled "Establishment of human skeletal muscle- derived cell line: biochemical, cellular and electrophysiological characterization", we studied the ECC in an immortalized human muscle cell line (HMCL-7304), which helps to overcome many of the technical limitations of working with primary muscle cells from human patients. ECC in HMCL-7304 was characterized with qPCR and western blotting as well as super resolution microscopy (SIM), Ca^{2+} imaging and electrophysiological measurements. We discovered that HMCL-7304 have a phenotype closer to slow twitch muscles than fast twitch muscles. HMCL-7304 can be used as a platform to investigate genetic mechanisms of muscle disorders, as shown in our 2nd publication; "RyR1 deficiency in congenital myopathies disrupts excitation contraction coupling", where we simulated the downregulation of RyR1 expression as seen in patients with recessive RYR1 mutations, by silencing RyR1 expression in the HMCL-7304.

Patients with recessive RYR1 mutations have been shown to downregulate RyR1 expression in skeletal muscles. This is in contrast to what is observed in patients with dominant RYR1 mutations, in whom we could not find reduction in the RyR1 expression. In patient's muscle biopsies where RyR1 expression is reduced, all isoforms of InsP3R Receptors (ITPR1-

ITPR3) were found to be up-regulated. Ca^{2+} release was not altered by the reduction of RyR1 expression using siRNA in HMCL or by blocking of IP3Rs using Xestospongin, rejecting the possibility for InsP3R functional compensation for the downregulation of RyR1.

The potential mechanisms causing downregulation of RyR1 in patients with recessive RYR1 mutations is addressed in our 3rd publication; "Epigenetic changes as a common trigger of muscle weakness in congenital myopathies". Patients with downregulation of RyR1, exhibit decreased expression of muscle specific microRNAs and increased expression of HDAC4 and HDAC5. Additionally hyper-methylation of CpG Island in the RYR1 gene was observed. Down regulation of RyR1, downregulation microRNAs and upregulation of HDAC4 and HDAC5 was also observed in patients with Nemaline myopathy, reflecting common epigenetic changes activated in congenital myopathies. Using HDAC or DNMT inhibitors can target common downstream pathways activated in muscles of patients with congenital myopathies offers an interesting new approach for the amelioration of muscle function

List of Abbreviations:

ACTA- α actin

AD- Autosomal dominant

ADP/ATP- Adenine di/tri phosphate

AGO- Argonate

ALS- Amyotrophic lateral sclerosis

AMPK- AMP activated protein kinase

Ang II- Angiotensin II

AP- Action potential

ApoCaM- Ca^{2+} free calmodulin

AR- Autosomal recessive

BIN1- Amphiphysin 2

BMD- Backer muscular distrophy

C/EBP-α - CCAAT/enhancer binding protein

CAF1- Chromatin assembly factor 1

CaM- Calmodulin

CaMKII – Ca^{2+}/Calmoduln dependent protein kinase

CBP- CREB binding protein

CCD- Central core disease

CDK4- Cyclin dependent kinase 4

CFL- Cofilin

CFTD- Congenital fiber type disproportion

cHC- constitutive heterochromatin

CICR- Ca^{2+} induced Ca^{2+} release

4 cmc- 4 chloro-m-cresol

CNM- Central nuclear myopathy

COX- Cytochrome oxidase

CPI- CpG islands

CRU- Ca^{2+} release unit

CSQ- Calsequestrin

DACH2- Dachshund Family Transcription Factor 2

DGCR8- DiGeorge Syndrome Critical Region Gene 8

DHPR- Dihydropyridine receptor

DMD- Duchenne muscular dystrophy

DNM2- Dynamin 2

DNMT- DNA methyltransfrase

DOT1- Disruptor of telomeric silencing 1

EC- Euchromatin

ECC- Excitation contraction coupling

ECCE- Excitation coupled calcium entry

ECM- Extra cellular matrix

EDL- Extensor digitorum longus

FGF- Fibroblast growth factor

fHC- facultative heterochromatin

FKBP- FK506 binding protein

FSHD- Facioscapulohumoral muscular dystrophy

GIT1- GPCR kinase 2 binding protein 1

GLUT- Glucose transporter

HAT- Histone acetyl transferase

HC- Heterochromatin

HDAC- Histone de acetylase

HEK- Human embryonic kidney

hmC- Hydroxymethyl- cytosine

HMCL- Human muscle cell line

HNF1-α - Hepatocyte nuclear factor 1 homeobox A

HNF4 - Hepatocyte nuclear factor 4

HP1- Heterochromatin protein 1

hTERT- telomerase reverse transcriptase

HVA- High voltage activated

IL10- Interleukin 10

ITPR- IP3 receptor gene

IVCT- In vitro contracture test

JP- Janctophilin

JP45- Junctional SR protein 45

KBTBD13- Klech repeat and BTB containing 13

KLHL- Klech like family member

KO- Knock out

lncRNA – Long non coding RNA

LSR- Longitudinal SR

LVA- Low voltage activated

MBD- Methyl binding domain

MCAD- Medium chain acetyl CoA dehydrogenase

Me1/Me2/Me3- mono/di/tri methylated

MECP- Methyl CpG binding protein

MEF2- Myocyte enhancer factor 2

MG- Mitsugumin

MH- Malignant hyperthermia

miRs- microRNAs

MITR- MEF interacting transcription factor

MmD- Multi minicore disease

MTM1- Myotubularin 1

MuRF1- Muscle RING-finger protein-1

MYOD- Myogenic differentiation

NADH- Nicotinamide adenine dinucleotide

NCX- Na^+/Ca^{2+} exchanger

NEB- Nebulin

NEM- Nemaline myopathy

NES- Nuclear export signal

NF-E2 - Nuclear Factor, Erythroid-Derived 2

NLS- Nuclear localization sequence

NMDA- N- methyl-D-aspartate

PAX- Pair box

PCAF- P300/CBP associated factor

PcG- Poly comb group

PCM1- Pericentriolar material protein 1

PCNA- Proliferating cell nuclear antigen

PGC- 1α - Peroxisome proliferator-activated receptor gamma coactivator 1-alpha

PKA- Protein kinase A

PKD- Protein kinase D

PLCγ- Phospholipase C

pRB- Phospho retinoblastoma

PRC2- Polycomb repressive complex 2

PRE- PcG response element

PRMT- Protein arginine N- methyltransferase

PTEN- Phosphatase and tensin homolog

RISC- RNA induced silencing complex

ROS- Reactive oxygen species

Rtt106- Histone chaperone Rtt106

RYR- Ryanodine receptor

SAM- S Adenosylmethionine

SAR- Sarcoluminin

SEPN1- Selenoprotein 1

SERCA- Sarcoplasmic/ Endoplasmic Ca^{2+} ATPase

SMYD1- SET and MYND domain 1

SOCE- Store operated Ca^{2+} entry

SOL- Soleus

SP1- Specificity protein 1

SR- Sarcoplasmic reticulum

SRP- Sarcoplasmic reticulum protein

STIM1- Stromal interaction molecule 1

SUMO- Small Ubiquitin like modifier

SWI/SNF- SWItch/Sucrose Non-Fermentable

TNNT- Troponin T

TPM- Tropomyosin

TRDMT1- TRNA Aspartic Acid Methyltransferase 1

TRE- TrxG response element

TRIC-A- Trimeric intercellular cation selective channel A

TRPC- Transient receptor potential protein Ca^{2+} entry channel

Trx1- Thioredoxin 1

TrxG- Thrithorax Group

TSA- Trichostatin A

TSS- Transcription start site

UHRF1- Ubiquitin like containing PHD and RING finger domain 1

UTR- Untranslated Region

VGCC- Voltage gated Ca^{2+} channel

ZEB- Zinc finger E-box-binding homeobox

List of Figures:

Chapter 1- Introduction:

1. Excitation Contraction Coupling and Ca^{2+} Homeostasis:

1.1 Excitation Contraction Coupling and Ca^{2+} Homeostasis:

Excitation **C**ontraction **C**oupling- The physiological mechanism that leads to an increase of Ca^{2+} in the vicinity of the skeletal muscle contractile proteins, Myosin and Actin. This physiological mechanism consist of two steps: Depolarization of the T tubular membrane that activates the dihydropyridine receptor an L-type voltage gated Ca^{2+} channels (VGCC) and release of Ca^{2+} from the sarcoplasmic reticulum (SR) to the cytoplasm trough the Ryanodine receptor Ca^{2+} channel 1 (RyR1).
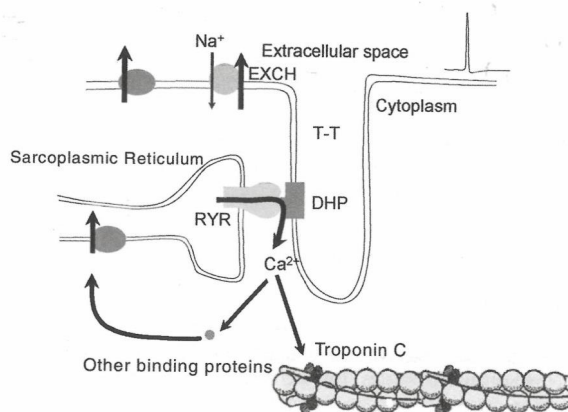
Figure 1.11: **Excitation contraction coupling**: Action potential propagates along the plasma membrane and into the T-tubules and activates the dihydropyridine receptor, a voltage dependent Ca^{2+} channel that activates the RyR1 located on the terminal cisternae. RyR1 releases Ca^{2+} from the SR that leading to muscle contraction. Ca^{2+} uptake back into the SR is performed mainly by the SERCA pumps [1].

RyR1s are located on the terminal cisternae of the sarcoplasmic reticulum membrane and are directly activated by the DHPR a Voltage Gated Ca^{2+} Channel, through inward current of Ca^{2+}. In skeletal muscle, 50% of RyR1 activation is through a direct interaction of the DHPR on the plasma membrane or on the transverse tubules, an invagination of the plasma membrane into the muscle fiber [2]. The DHPR is a hetero-pentamer formed by the subunits; α1, α2, β, γ

and δ. The transmembrane domain S4 of α1 subunit is a voltage sensor that upon charge movement creates a conformational change that enables the physical interaction with the RyR1, located on the terminal cisternae [3, 4]. The allosteric interaction of the RyR1 with the DHPR, activates RyR1 and allows Ca^{2+} to flow from the SR to the myoplasm through RyR1. In Skeletal muscle, RyR1 and DHPR face one another, creating the "Ca^{2+} release unit" (CRU) that responds to the action potential (AP) reaching the T tubules membrane [5, 6]. However, RyRs that do not face DHPRs are activated by a positive feedback mechanism termed Ca^{2+} induced Ca^{2+} release (CICR). CICR was first discovered in frog muscles and is believed to be more significant in amphibian muscles than in mature mammalian muscle fibers, although CICR is believed to have an important role in the synchronization of rapid Ca^{2+} release from the SR [7, 8]. After its release from the SR and following muscle contraction, Ca^{2+} is pumped back to the SR leading to muscle relaxation, by Sarcoplamic/Endoplasmic Reticulum Calcium ATPase (SERCA) and Na^+/Ca^{2+} exchanger (NCX) [9, 10]. The SERCA consists approximately 80% of the total protein present on the longitudinal SR (LSR) and thus plays a fundamental role in regulating Ca^{2+} homeostasis in muscle. The LSR links between two terminal cisternae, and its location relative to the SR is shown in Figure 1.12.
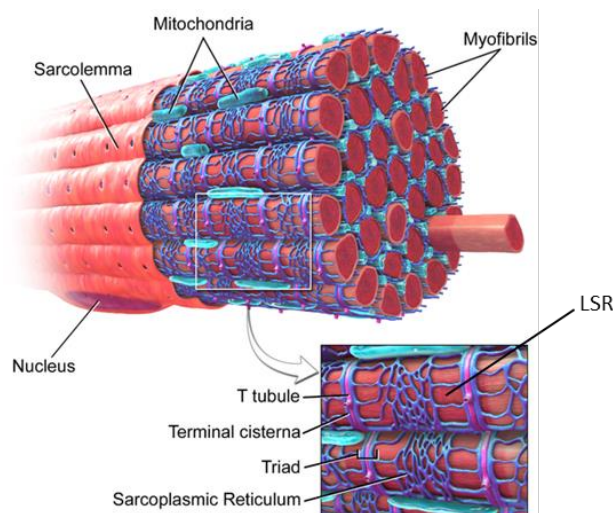
Figure 1.12: Schematic representation of the Sarcoplasmic Reticulum compartments [11].

Fractionation of the SR compartments enables to investigate many proteins that are important for the ECC. In the next figure and in the text bellow, some of these proteins will be discussed (Figure 1.13).

1 RyR	4 SERCA	7 JP-45	10 SRP-27/TRIC
2 DHPR	5 TRISC	8 Junctate	11 Junctophilin
3 CSQ	6 Junctin	9 MG-29	
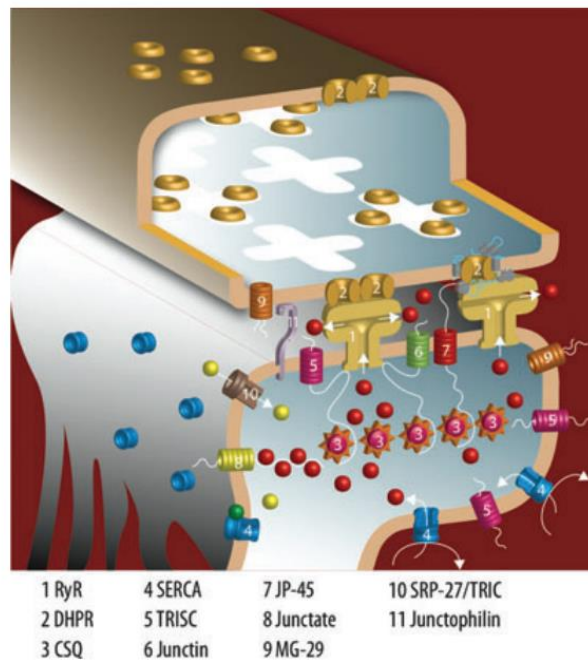
Figure 1.13: **Schematic representation of the protein components of skeletal muscle sarcoplasmic reticulum [12].**

Beside the RyR1, many proteins are contained within the SR, including Calsequestrin (CSQ) a Ca^2 buffering protein of the SR, which binds about 80 mole of Ca^2 per one mole of protein with low affinity. Upon Ca^{2+} binding, CSQ changes its conformation and its affinity to the RyR. Reports suggest that RyR activity can be modulated by CSQ and other proteins such as Junctin and Triadin that responsible for anchoring CSQ (figure 1.13). There are two variants of CSQ; CSQ1 is more abundant in fast type II fibers and CSQ2 is more abundant in slow type I fibers [13].

After Ca^{2+} is released into the myoplasm, it binds to troponin thereby eliminating the inhibition caused by troponin and tropomyosin on the interaction between actin and myosin;

removal of the inhibition allows actin and myosin to interact and slide, an event that leads to muscle contraction [14].

Apart from CSQ, there are other proteins involved in the binding and buffering of Ca^{2+} in the SR, including calreticulin, parvalbumin and sarcalumenin (SAR) [15]. Parvalbumin has been shown to be more expressed in rodent fast fibers and is less abundant in higher mammals such as humans [16]. SAR is located in the longitudinal tubuli and terminal cisternae and has been shown to have multiple roles including; stimulating Ca^{2+} uptake by interacting with SERCA1, Ca^{2+} release by modulating the activity of RyR1 and Ca^{2+} storage by serving as Ca^{2+} buffer [17-20].

Janctophilin (JP) are a family of proteins that help stabilize the junction between the plasma membrane and the SR. In skeletal muscle, both JP1 and JP2 are highly expressed and facilitate the physical interaction between the RyR1 and DHPR, by linking the transverse tubules and the SR membrane. As mentioned previously this interaction plays a major role in Ca^{2+} release that permits muscle contraction (number 11, figure 1.13) [21]. JP1 homozygous KO is lethal, 20 hours after birth. Interestingly, JP KO leads to swollen terminals, lower number of triads and incomplete formation of the junctional complexes. Consequently, there is a reduction in the contractility of the muscle and abnormal sensitivity to extracellular Ca^{2+} [12].

JP45 is a 45KD polypeptide containing a single transmembrane segment that interacts with CSQ via its luminal carboxyl terminus. In addition it has been shown to interact with the DHPR via its cytoplasmic amino terminus. KO or over expression of JP45 result in the decrease of voltage dependent Ca^{2+} release [22-24].

Mitsugumin-29 (MG29) is a membrane protein containing 4 transmembrane domains, belonging to the synaptophysin family. It has been shown that MG29 interacts with the RyR1 and increases the probability for RyR1 to open without affecting the channel current amplitude. KO of MG29 leads to vacuolated SR, swollen transverse tubules and misaligned triads. Indeed MG29 favors the formation of triadic structures. Interestingly, MG29 KO mice experience fatigue more rapidly comparing to W.T mice [25, 26].

Junctate is a 33KD ER/SR membrane spanning domain expressed in a variety of excitable and non- excitable tissues. AβH-J-J is the gene that encodes Junctate, together with Junctin and

beta hydroxylase (figure 1.14). Junctate and Junctin play an important role in the regulation of intercellular Ca^{2+}. Junctate forms a multimolecular complex with inositol 1,4,5-trisphosphate receptor (InsP3R) and canonical transient receptor potential protein Ca^{2+} entry channel (TRPC), mediating Ca^{2+} release from the ER and Ca^{2+} entry, respectively.
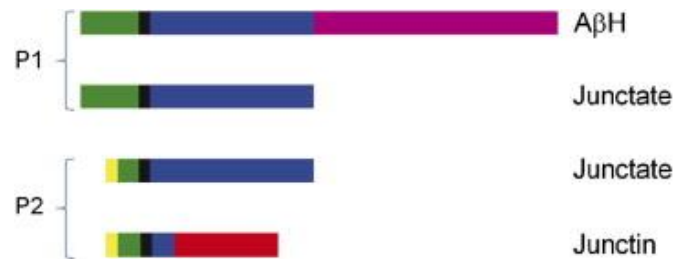
Figure 1.14: Schematic representation of the alternatively spliced AβH-J-J locus. The N terminal domain of AβH and Junctin are encoded by two different promoters (P1 and P2 respectively). Each region is presented in different color: green, AβH-type N-terminal cytoplasmic regions; black, transmembrane region; blue, highly charged acidic luminal regions; purple, AβH catalytic domain; yellow, junctin type N-terminal region; red, junctin-specific basic luminal region [27].

The regulation of transcripts expression arising from the AβH-J-J locus is very complex, as there are two promoters. Promoter 1 is similar to other housekeeping genes, though P2 is regulated in a tissue specific fashion, for instance by the muscle specific transcription factor MEF2 (myocyte enhancer factor 2). Interestingly, P2 is activated only in excitable tissues like striated muscle [27, 28].

SRP27/TRIC – known as Mitsugumin-33, TRIC-A (Trimeric intercellular cation selective channel) or SR protein 27 (SRP27) is expressed in excitable tissue and especially in fast fiber type. SRP27 amino terminus is exposed to the ER/SR and its carboxyl terminus is exposed to the cytosol. Reconstitution in lipid bilayers and Ca^{2+} imaging experiments suggests the SRP27 is a monovalent cation channel. This channel is believed to counter-balance the charge movement due to influx of Ca^{2+} conducted by RyR1 [29, 30].

Store Operated Calcium Entry (SOCE) is a mechanism responsible for maintaining the Ca^{2+} levels in the SR. When Ca^{2+} levels in the intracellular stores are low, Ca^{2+} is transported from the extra cellular milieu into the myoplasm in order to replenish the stores.
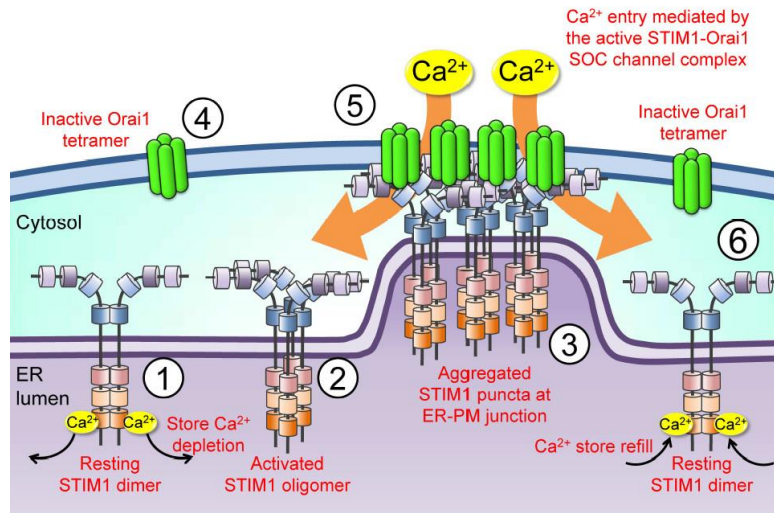
Figure 1.15: STIM1 dependent SOCE activation [31].

The molecular mechanism of SOCE involves two proteins; stromal interactions molecule (STIM1) and Calcium permeable Orai Channel (Orai1). STIM1 is a single-pass transmembrane protein that has a Ca^{2+} binding domain located in the SR luman, termed EF-hand domain (Helix-loop–helix structural domain). The EF hand domain binds Ca^{2+} within the loop, allowing it to sense Ca^{2+} levels in the SR lumen. When Ca^{2+} levels are low and Ca^{2+} is not bound to STIM1, STIM1 oligomerizes through its intra-luminal EF domains and interacts with Orai1, located on the plasma membrane. Orai1 is a tetrameric ion channel that interacts with the cytosolic, coil coiled domain of STIM1 and mediates entry of Ca^{2+} ions from the extracellular environment. Upon oligomerization, STIM1 forms multiple punctuated structures that are directed to regions with close proximity to the plasma membrane, named plasma membrane junctions (Figure 1.15). This mechanism of Ca^{2+} influx however, is very slow, occurring in seconds, while skeletal muscle ECC occurs in msec, leading many investigators to suggest that other mechanisms are activated in SR store refilling. Interestingly, it was recently shown that STIM1 interacts with RyR1 as well as with canonical transient receptor potential channels (TRPC), significantly contributing to SOCE [32-34].

21

Apart from SOCE, excitation coupled calcium entry (ECCE) allows entry of Ca^{2+} into the SR by prolong activation of muscle depolarization (that is independent of the Ca^{2+} stores). ECCE require functional L type Ca^{2+} channels, functional RyR1 and involves Ca^{2+} influx through the L type Ca^{2+} channels. The exact mechanism of ECCE is still elusive, though it was shown that ECCE occurs rapidly and on the triadic region [35, 36].

The regulation of Ca^{2+} reuptake to the SR is well maintained especially during exercise, when Ca^{2+} ions have to be efficiently removed from the myoplasm and pumped back into the SR in order to allow the relaxation of the sarcomeres. As mentioned previously in skeletal muscle the removal of Ca^{2+} is mainly performed by the activity of the ATP dependent SERCA and to a lesser extent by the activity of the Na^+/ Ca^{2+} Exchanger (NCX).

1.2 Ca^{2+} Homeostasis in different muscle fiber types:

Muscle fiber types in mammals can be divided into 4 major groups: type 1 - slow twitch and three fast twitch fiber types- type 2A, 2B (not expressed in human but in other mammals) and 2X. These fiber types were classified according to the myosin heavy chain isoforms that they express. The distribution and the quantity of fast and slow fibers may vary between different muscles depending on their function.

Continuous low intensity activity for example, posture and long lasting repetitive activities, requires more slow twitch fibers, however jumping, kicking and strong maximal contraction, requires fast twitch fibers. Extensor digitorum longus (EDL) has a much higher frequency in firing pattern (70-90Hz) compared with slow soleus (SOL) that has low frequency of firing (approx. 20Hz) but long resistance to fatigue. Interestingly, in normal female inbred Lewis rats 75.7%±2.2 of the fibers composing EDL are type 2B, 18.8%±1.7 type 2A and only 5.5%±1 are type 1 slow fibers. However SOL contains 96%±2.9 of type 1 muscle fibers [37].

Tension and force development of SOL is significantly slower than in EDL muscles, where the response to an action potential is faster. Apart from force development, the decay in muscle tension of EDL occurs earlier, compared to SOL muscle.

Ca^{2+} transients have a direct impact on the dynamic properties of the muscle fibers. Interestingly, the kinetic parameters of Ca^{2+} transients show two clusters of values; corresponding to type 1 slow fibers or fast 2A fibers with low decay rate and fast 2X or fast 2B fibers with high decay rate (figure 1.2).
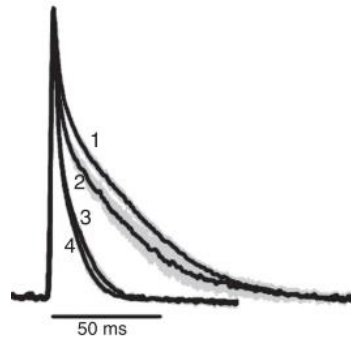
Figure 1.2: Ca^{2+} transient in mouse single muscle fiber identified according to their myosin composition using mag-fluo 4 AM (1- slow, 2- 2A, 3- 2X and 4- 2B fibers) [38].

As mentioned previously, SERCA pumps Ca^{2+} ions back to the SR using the energy produced from ATP hydrolysis, allowing the relaxation of the muscle. There are 10 isoforms of SERCA that exists in vertebrates, though in human skeletal muscle there are 2 main isoforms, SERCA1a and SERCA2a [39]. SERCA1 is expressed in fast twitch type II fibers and SERCA2 in slow twitch type I fibers. SERCA density in the SR is 5-7 times larger in fast type II fibers compared to type I fibers, allowing the fast uptake of Ca^{2+} ions. Interestingly, ADP has a higher inhibitory effect on SERCA in fast fibers, in comparison with SERCA in slow fibers. Thus that lower responsiveness to ADP of slow fibers may contribute to the prevention of muscle fatigue and enabling continuous activity. NCX isoforms (NCX 1-3) contributes to the removal of Ca^{2+} from the cytoplasm in both fiber types but slightly more in type 1 slow fibers [38, 40].

Calcium homeostasis in the different compartments of the muscle fibers is crucial for normal physiological activity of skeletal muscle. The contractility of the muscle fiber depends on an adequate concentration of Ca^{2+}; the cytosolic free Ca^{2+} levels is higher in type I fibers compared to type II fibers. The difference of free cytosolic Ca^{2} between fast and slow fibers, dictates Ca^{2+} secondary messengers and neuromuscular activity.

1.3 The Ryanodine Receptor (RYR):

1.3.1 Structure and function:

The Ryanodine receptor (RyR) is a high molecular weight protein (565 KD for each monomer) that assembles as a homo-tetramer (2.3MDa) in order to function as a calcium release channel. There are 3 isoforms of the RYR gene; RYR1, which is highly expressed in skeletal muscle and to a lesser extent in cerebellum, smooth muscles, testis, adrenal gland, B-lymphocytes and dendritic cells. RYR2 is highly expressed in the heart, brain and smooth muscle cells and RYR3 is expressed in a variety of tissues and in developing skeletal muscle [41].

Cryo-EM studies have revealed that the RyR receptor has a mushroom- like shape with a bulky N terminal cytoplasmic domain, comprising its regulatory domains. While the last 1000 amino acids encode for the trans-membrane domain including the Ca^{2+} pore [42, 43]. A number of small proteins including FKBP12 interact with the cytoplasmic domain stabilizing the channel and giving rise to a large macromolecular signaling complex. The last year several publications have described the fine structure of the RyR, one of them describing the crystal structure using single particle electron microscopy (Cryo- EM, Figure 1.31).
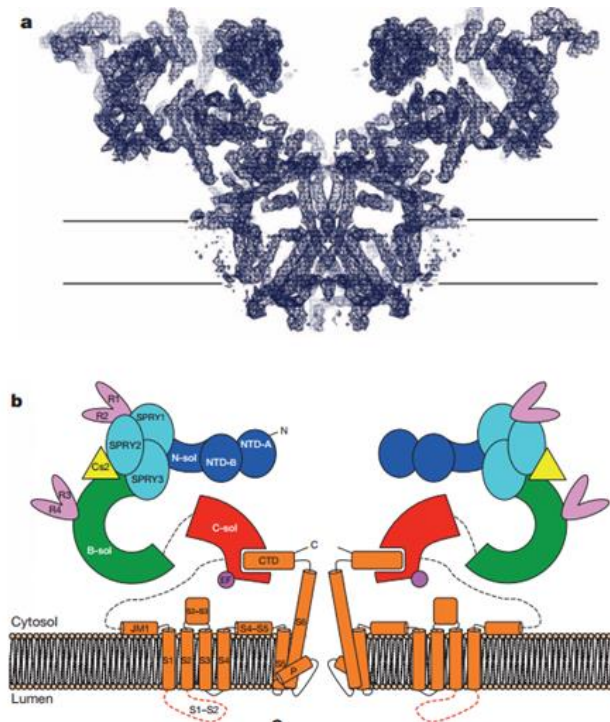
Figure 1.31: **The architecture of the RyR in 4.8 Å resolution**. A. Slab of density on blue mesh, B. Schematic representation of RyR1, B-sol, bridge solenoid; C-sol, core solenoid; N-sol, N-terminus solenoid [2].

Studies on the structure have shown that the RyR1 has a 4 fold symmetry, being made up by 4 protomers surrounding the central ion-conducting pore. 80% of the RyR1 mass is in the cytosol and this is thought to be involved in the regulation of the channel. There are 6 transmembrane domains plus the pore domain, sharing a strong homology with voltage gated sodium and potassium channels [44]. The α-solenoid scaffold incorporates 5 domains: RY12, RY34, SPRY1, SPRY2 and SPRY3, Interestingly, RY34 contains a known phosphorylation site for PKA (Ser-2843). As presented in figure 1.31b, S5 and S6 are make up the pore of the channel. S1-S4 are similar to voltage sensor transmembrane domains that can interface with the pore transmembrane domains. Remarkably, the brevity of the construction suggests hosting only one Ca^{2+} ion at the time [2]. The selectivity filter of the RyR is highly conserved and contains the following amino acid sequence: Gly-X-Arg-X-Gly_3-X-Gly-Asp, which was found in other channels

as well, including the IP3 receptor and potassium channels [45]. Furthermore it has been shown that Asp and Gly are crucial for the selectivity of the channel [44].

1.3.2 Regulation:

The RyR1 is highly regulated by proteins and enzymes, as well as other modulators, such as Ca^{2+} and Mg^{2+}. Ca^{2+} modulates the activity and the conductance of the channel. When Ca^{2+} binds to the A sites, it increases the activity of the RyR1. However, when Ca^{2+} binds to the I site the conductance of the channel decreases; both I and A sites are located in the cytosolic domain of the Ryanodine Receptor 1 [46]. Ca^{2+} does not only bind directly to the RyR1 but to the small ubiquitously expressed proteins, calmodulin (CaM) and S100A. CaM can exist in two forms; Ca^{2+}-CaM or Ca^{2+} free CaM (ApoCaM). Several reports have indicated that RyR have 4-6 binding sites to ApoCaM and 1 binding site for Ca^{2+}- CaM. However, in other reports it was found that for skeletal muscle and cardiac RyR isoforms, each RyR subunit can bind to a single Ca^{2+}-CaM or single ApoCaM molecule. In addition it was shown that the binding site for CaM on the RyR is located in the same region (Amino acid residues; 3630-3637). ApoCaM concentration is high at nM concentration of Ca^{2+}, known to activates the RyR1 by increasing it's sensitivity to CICR [47-50]. Skeletal muscle and heart also express a member of the S100A family, S100A1 binds to the RyR1 and promotes Ca^{2+} release. Ca^{2+}-CaM and Ca^{2+}- S100A1 compete for the same binding site termed RyRP12 on the cytosolic domain of every RyR protomer. The binding of S100A increases the probability for RyR1's open state, indeed KO of S100A1 attenuates the rise of Ca^{2+} evoked by an action potential [51, 52].

FK506 binding protein 12 (FKBP12) interacts with each protomer of RyR1 and stabilizes the "closed channel conformation". FK506 has shown to promote the dissociation of FKBP12 from RyR1 (The EC50 of the dissociation from the RyR1 is 0.12-0.5µM). SR vesicles stripped of FKBP12 have a higher probability of being in the open conformation compared to FKBP12-containing vesicles. According to some studies FKBP12 disassociates from RyR1 upon phosphorylation by Protein Kinase A (PKA); similar results were observed for the cardiac isoform (RyR2) [53, 54].

Interestingly, the cardiac RyR2 interacts with 4 molecules of FKBP12.6, (each interacting with 1 protomer of RyR2). However, unlike the mechanism observed in RyR1, upon disassociation of FKBP12.6 from RyR2, the channel is not activated, though this issue is controversial [55-58]. Nevertheless, RyR2 can be phosphorylated by CaMKII on Serine 2815, and in some studies this phosphorylation has been shown to activate RyR2 without the disassociation of FKBP12.6 [59].

1.4 The dihydropyridne receptor: an L-type Voltage Gated Ca^{2+} Channel of skeletal muscle:

Voltage Gated Ca^{2+} Channels mediate Ca^{2+} entry into cells in response to membrane depolarization (Figure 1.41A). Different VGCCs have different thresholds of activation in a variety of cell types and they are characterized as High Voltage Activated (HVA) or Low Voltage Activated (LVA). The pore unit α1, named CAV is encoded by 10 genes CACNA1A-CACNA1S that have different chromosomal locations and contains positively charged, voltage sensor subunit-S4 (Figure 1.41B, C) .Based on the pharmacological and biophysical characteristics of the channel, VGCC were characterized as N, L, T, P/Q and R types. L type VGCCs are expressed in specialized tissues, for instance Cav1.1 is mainly expressed in skeletal muscle, whereas Cav1.2 is expressed in the heart and smooth muscle (Figure 1.41B) [60]. The S4 subunit (Figure 1.31c) undergoes a conformational change allowing it to interact with the RyR1, upon action potential [61].
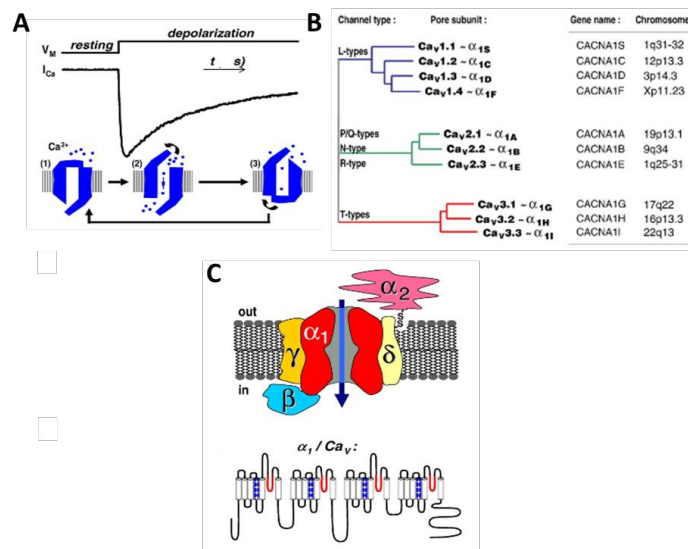
Figure 1.41: VGCC Structure and Function (A) schematic presentation of VGCC activation and inactivation upon membrane depolarization. **(B)** Channel types and their chromosomal location **(C)** The oligomeric structure of the VGCC; the pore forming unit – α1 and the regulatory forming units β, γ,δ and α2. The pore forming unit of the channel α1 is composed of voltage sensor in blue (S4) and the pore region in red [62].

α1S (DHPR) interacts with the RyR1, located on the SR membrane leading to Ca^{2+} release from the SR. Loops II and III of the α1 subunit interact with the RyR1 channel, while the β subunit of the DHPR may act as an "anchor" that docks the DHPR to the RyR1 (Figure 1.42). Additionally, the β subunit affects the channel gating properties and the trafficking of α1 subunit. α2/δ subunits are encoded by the same gene and linked by disulfide bounds. Interestingly, they enhance membrane trafficking and increase current amplitude [63].
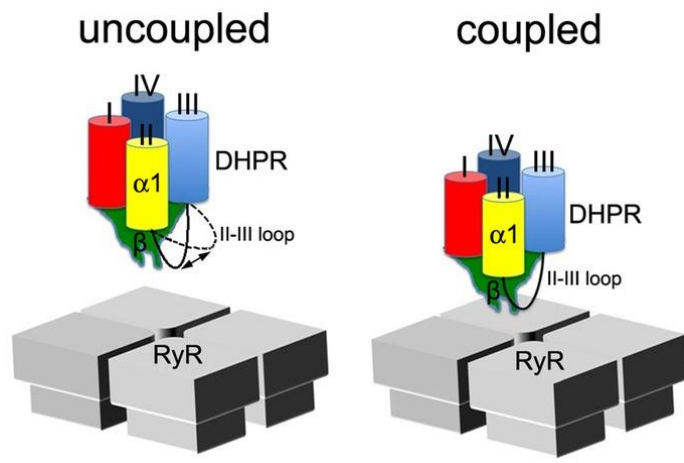
Figure 1.42: Model of physical coupling between DHPR and RyR1 [63].

2. Disorders of ECC and Congenital Neuromuscular Disorders:

Congenital myopathies are clinical conditions that are diagnosed on the basis of the patient's clinical manifestations and histopathological features of the muscle biopsy in combination with proper genetic testing. The three main congenital myopathies are Nemaline myopathy, Core myopathies and Centronuclear myopathy. A major portion of patients shows involvement of extraocular muscle, facial musculature and normal or elevated levels of creatine kinase.

2.1 Malignant Hyperthermia (MH):

Malignant hyperthermia is a pharmaco-genetic disorder triggered by volatile anesthetics in genetically predisposed individuals. Examples of trigger agents include halothane, sevoflurane, deslurane and the depolarizing muscle relaxant succinylcholine. MH is defined as hyper-metabolic reaction of the skeletal muscle that involves:

- Tachycardia
- Acidosis of the blood
- Increased oxygen consumption
- CO_2 over production
- Muscle rigidity
- High body temperature

The incidence of an MH reaction is approximately every 1:10000- 1:25000 anesthetics. A genetically susceptible patient may not develop an MH reaction at every contact with a triggering agent. Though mutations in the RYR1 gene are linked to predisposition to develop an MH reaction, at present it is not known why some patients trigger but not others. The frequency of developing MH is twice higher in male patients compared to female patients. It

has been shown that all ethnic groups are equally affected and can develop MH with a similar probability. Interestingly, 52% of the patients that develop MH are 15 years old or younger but this may relate more to the anesthetic agent used rather than to the effect of age per se.

An MH reaction is thought to be caused by the uncontrolled release of calcium from the SR leading to muscle rigidity, over- activation of the SERCA and Ca^{2+} extrusion systems. Depletion of ATP (during MH reaction) leads to loss of membrane integrity leading to Hyperkalemia and Rhabdomyolysis. Untreated patients die from high core body temperature (exceeding $41C^o$ and up to $44\ C^o$), Kidney failure, Heart failure or Bowel Ischemia. In order to counteract an MH episode, the trigger agent (anesthetic) must be interrupted, the patient is placed in a cooling ice bath and dantrolene, the only approved drug, must be immediately administered.

In most cases the genetic cause of Malignant Hyperthermia is linked to dominant mutations in the Ryanodine Receptor 1 (RYR1) and to date more than 100 mutations have been casually linked to the MH susceptibility trait. Till approximately 10 years ago, MHS was diagnosed using the in vitro contracture test (IVCT) an invasive procedure by which contracture of isolated muscle biopsies in vitro (obtain from the patients under regional anesthesia) are assessed after administration of either the trigger agent halothane or the RyR1 activator Caffeine. For many individuals where the family mutation in the RYR1 has been identified, the IVCT is no longer performed, and the genomic DNA of the patient is examined for the presence of the familial causative mutation. If no mutation is found then the IVCT is performed in order to exclude a risk of an MH reaction during surgery [64, 65]. Interestingly, SR Ca^{2+} release channels isolated from MH pigs exhibit higher CICR and increased sensitivity to Caffeine, Halothane, 4 chloro-m cresol (4cmc) and t-tubules depolarization. In addition MH pigs had reduced inhibition of Ca^{2+} and Mg^{2+} [66]. The porcine model of MH (R615C) exhibited a lower threshold of contraction that arises from earlier depolarization, activating voltage dependent Ca^{2+} release [67, 68].

2.2 Central Core Disease (CCD):

Central Core Disease is the most common congenital myopathy occurring with a frequency of 3-5/100,000 and is characterized histologically by the appearance of central cores along the muscle fibers.
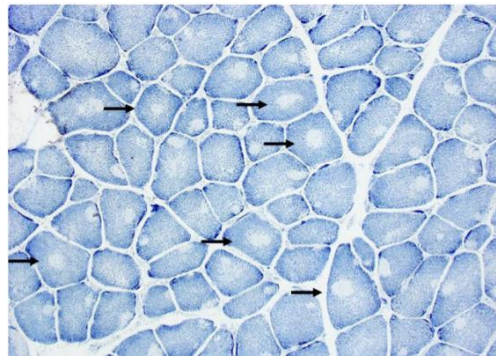
Figure 2.21: Histopathological appearance of a biopsy from a patient with Central Core Disease. NADH staining of Rectus Femoris transverse section [69].

The cores are defined as areas lacking oxidative staining and are typically found in type 1 fibers. Electron microscopy shows absence/reduction of mitochondria, myofibrillar disorganization and accumulation of abnormal Z band material within the core area. Some of the cores have normal "structured" myofibrilar organization that preserves the ATPas activity. The diagnosis of the disease in patients entering a neuromuscular diagnostic center are based on the presence of weak muscles and the concomitant presence of histopathological hallmarks in the muscle biopsy; muscle MRI and mutations analysis may help confirm the diagnosis. Patients with CCD may present with one or several clinical features including:

- Hypotonia.
- Motor development delay, which can be variable among patients.
- Muscle stiffness and weakness, there is no proved association between the amounts of cores and the degree of weakness.
- Proximal muscle weakness in the hip girdle and axial muscles.

- Orthopedic complications (contractures, club foot)
- Malignant hyperthermia susceptibility (MHS) – condition activated by volatile anesthetics in medical procedures (discussed in the previous section 2.1).

Respiratory involvement in patients with CCD is not frequent but some patients especially during childhood, required regular respiratory assessment or even invasive respiratory assistance limiting their daily activities. CCD is predominantly caused by dominant mutations in the RYR1 mainly located on the C terminus of the protein, (Figure 2.22) [69].
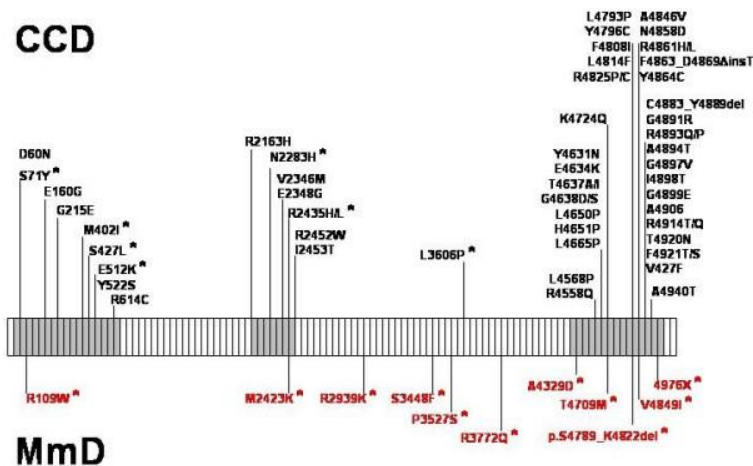
Figure 2.22: Schematic representation of the RYR1 with the distribution of recessive (Associated with MmD, in red) and dominant mutations (Associated with CCD, in black) [70].

Transient expression of Rabbit RYR1 cDNA in HEK293 cells (either W.T RYR1, mutated with CCD mutation and mutated RYR1 linked to MH) provided interesting insight. Cells transfected with CCD- RYR1 mutant showed higher resting Ca^{2+} compared to cells expressing the W.T or the MH- RYR1 mutant. Cells expressing MH and CCD-RYR1 mutants released less Ca^{2+} after pharmacological activation compared to the W.T expressing cells. Taken together these results suggest that CCD mutations lead to "leaky" channel [71]. Immortalized B

lymphocyte isolated from CCD patients were also used to investigate Ca^{2+} homeostasis. Ca^{2+} release from the intracellular stores occurred in the absence of any RyR activating pharmacological agents in CCD patients, though a similar phenomena was not seen in cells obtained from healthy individuals. Significantly reduced intercellular stores were measured by assessing the peak of Ca^{2+} elicited by Thapsigargin. Lastly, normal sensitivity to the RyR inhibitor Dantrolene was observed [72]. Other experiments on the function of mutations linked to CCD, showed that they did not affect the sensitivity of RyR1 to pharmacological activators nor the resting Ca^{2+} concentration, however significant decrease of Ca^{2+} release was observed upon RyR1 activation [73].

2.3 Multi Mini-core Disease (MMD):

MmD is histologically characterized by the presence of multiple cores appearing in the muscle biopsy as well as clinical features characteristic of congenital myopathies. The immediate phenotype of the disease appears at a very early age with spinal rigidity, scoliosis and respiratory impairments. MmD is a genetic heterogeneous disease caused most frequently by recessive mutations in Selenoprotein 1 (SEPN1) or recessive mutations in RYR1; in the latter case the mutations are either homozygous or compound heterozygous . As opposed to patients with CCD, patients with MmD with recessive RYR1 mutations, often present with Opthalmoplegia (weakness or paralysis of the extraocular muscle) along with other clinical features as described in figure 2.31. MmD usually appears in infancy or childhood with hypotonia or muscle weakness and reduced fetal movements. There are some cases appearing in adults that involve progressive respiratory and heart failures.

Feature	*SEPN1*-related MmD	*RYR1*-related MmD
Clinical		
Extraocular involvement	-	++
Bulbar involvement	+	+
Respiratory involvement	+++	+
Scoliosis	+++	++
Malignant hyperthermia susceptibility	-	+
Histopathology		
Type 1 predominance/uniformity	+	+++
Increase internal nuclei	+	+++
Multiple large cores ("multicores")	+	+++
Numerous small cores ("minicores")	+++	+

(-) = feature not reported, (+) = feature reported, (++) = common feature, (+++) = very common feature

Figure 2.31: clinical and pathological features that can help distinguish between SEPN1 related or RYR1 related forms of MmD [70].

Figure 2.31 outlines the differences in the clinical and histopathological features of MmD caused by recessive mutations in the RYR1 and SEPN1. Few patients diagnosed with MmD, especially patients with proved RYR1 recessive mutations have clinical Malignant Hyperthermia (MH) episodes triggered by volatile anesthetic. Some of the patients with MmD caused by SEPN1 and RYR1 mutations have bulbar muscle involvement that influences their ability to swallow or speak.
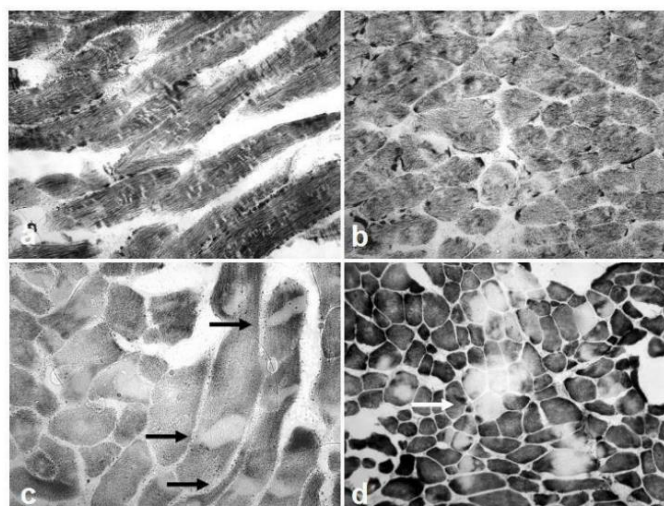
Figure 3.22: Histopathological features of Multi Minicore Disease. A. NADH staining for transverse segments of 3 years old patient B. NADH staining for horizontal segments of 3 years old patient C. NADH staining for transverse segments of 9 years old patient D. Cytochrome oxidase (COX) staining for horizontal segments of 9 years old patient **[70].**

Although not always true and of limited diagnostic values it seems that biopsies from MmD patients harboring recessive RYR1 mutations exhibit multiple cores distributed along the fibers (multicores), while MmD associated with recessive SEPN1 mutations show multiple small lesions scattered along the fibers. In other words, core morphology can vary in size and shape depending on the genetic mutation underlying the disease. Like the cores observed in patients with CCD, observation of muscle samples from patients with MmD by EM shows that the cores disrupt the muscle structure, cause myofibrillar disorganization and alter the structure of the SR, T – tubules and cause loss of the otherwise highly ordered sarcomeric architecture.

2.4 Central Nuclear Myopathy (CNM):

Central Nuclear Myopathy is a genetically heterogeneous congenital myopathy characterized histologically by the presence of centralized nuclei within the muscle fiber (figure 2.41) as well as the appearance of small fibers (figure 2.42 A), hypotrophy of type 1 fibers, a mild increase in connective and fat tissue and Z line streaming in areas adjacent to the nuclei (figure 2.42 C, D).

The clinical features vary between patients, depending on the genetic cause for the disease. The most sever phenotype is X linked and caused by mutations in the MTM1 gene; it mainly affects males though rare cases of affected females due to skewed X inactivation have been reported [74].The clinical features of patients born with X linked MTM1 (XMTM) manifest at birth or soon after and include severe muscle weakness, hypotonia, external ophtalmoplegia and respiratory failure. In the majority of cases, the disease leads to early death within the first few months of age, although some patients survive until adolescence and beyond [74]. The product of the MTM1 gene is myotubularin 1, a phosphoinositide phosphatase whose activity plays an important role in phospholipid metabolism by specifically removing phosphate from phosphatidylinositol 3-phosphate and phosphatidylinositol 3,5-biphosphate [75]. MTM1 contains a tyrosine phosphatase domain that is thought to play a role in signal transduction, cell growth and differentiation [76]. MTM1 is ubiquitously expressed and studies are under way in

order to understand why patients with MTM1 mutations have such a severe skeletal muscle phenotype, with sparing of the heart and other tissues. Of importance, most if not all of the mutations identified to date in patients result in the absence of the MTM1 protein product.
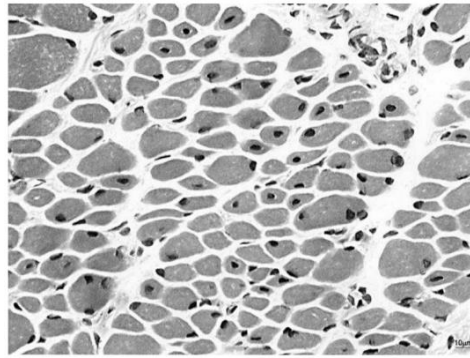
Figure 2.41: **H&E stained muscle biopsy taken from 3 months old female infant with X linked CNM, due to a mutation in MTM1.** This patient has skewed X inactivation that leads to severe phenotype [74].

Apart from the X linked form of CNM, there are Autosomal Recessive (AR) and Autosomal Dominant (AD) forms of the disease that are caused by mutations in Dynamin2 (DNM2) and amphiphysin 2 (BIN1) genes, respectively. DNM2 is a large GTPase known to be involved in many cellular process, through association with the microtubular network (endocytosis, membrane trafficking, actin assembly and centrosome function). BIN1 is responsible for membrane remodeling, curvature and has a role in the organization of the T tubules. The interaction between BIN1 and DNM2 is necessary for normal muscle function and for the positioning of the nuclei [69, 77]. The clinical features of patients with BIN1 and DNM2 mutations are milder than the features characterizing X linked CNM.

In the past decade however, a number of patients diagnosed with CNM were shown to harbor recessive mutations in the RYR1 gene [78].
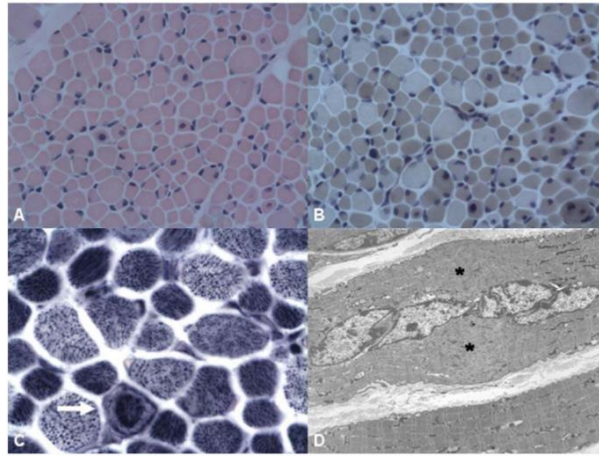
Figure 2.42: **Histopathological features of RYR1 related CNM in patients. A.** H&E staining in transverse section presents variability in fiber size, mild increase in endomysial connective tissue and little adipose tissue. Central nuclei appear mainly in small fibers. **B.** ATPase staining of transverse section shows predominance darker staining on Hypotrophic type 1 fibers with some dark staining on type 2 fibers as well. **C.** Transverse section stained against NADH shows that there is a darker predominance of type 1 hyotrophic fibers. **D.** longitudinal section of Electron Microscopy show central nuclei aligned in chain. In addition, minicores formation and Z line streaming formation appears in proximity with the nuclei [78].

The histopathological data of many patients shows central nuclei mainly appearing in small fibers (figure 2.42 A), Hypotrophy of fiber type 1 compared to fiber type 2 (figure 2.42 B), mild increase of connective tissue and fat tissue in the muscle and Z line streaming next to the nuclei (figure 2.42 D). The clinical features of CNM due to RYR1 mutations are neonatal hypotonia, reduced fetal movement feeding difficulties and extraocular involvement. No Malignant Hyperthermia (MH) reactions have been reported in these patients to date.

2.5 Nemaline Myopathy (NEM):

Nemaline Myopathy is defined histopathologically by the presence of inclusion bodies, (nemaline bodies; Greek *Nema* is thread) within the muscle fibers. Muscle weakness and hypotonia are apparent from the neonatal period but some patients are also diagnosed during childhood or adulthood. These patients characteristically exhibit depressed or the absent of

deep tendon reflexes. Muscle weakness of the face, neck flexors and proximal limb muscles is severe. Nemaline myopathy is clinically classified into 6 groups, depending on the severity and if there is respiratory involvement: severe neonatal congenital myopathy (16% of NEM patients), Amish NEM, Intermediate congenital (20%), Typical congenital (46%), childhood onset (13%) and adult onset (4%). The survival rate of these patients is very much dependent on the severity of the disease. Most surviving patients are able to walk [79].

Mutations in at least 10 genes have been associated with Nemaline Myopathy including α Tropomyosin – slow (TPM3), Nebulin (NEB), α ACTIN (ACTA1), β Tropomyosin (TPM2) and Troponin T1 (TNNT1), Cofilin 2 (CFL2), Kelch repeat and BTB (POZ) domain-containing 13 (KBTBD13) and Kelch-like family members 40 and 41 (KLHL40 and KLHL41). The majority of Nemaline patients have mutations in α actin (ACTA) and Nebulin (NEB) [79, 80].
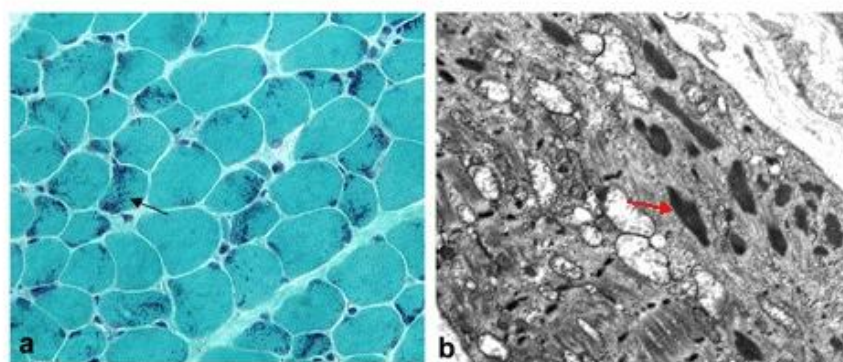
Figure 2.5: Pathology of Nemaline myopathy. A. Gomori Trichome staining in frozen sections showing Nemaline bodies (rods). Dark blue structures scattered throughout the muscle fibers**. B**. Rods structures in transmission electron microscopy (15K magnification) [79].

The diagnosis of the disease is performed by Gomori Trichome staining and shows the presence of rod shaped structures. By electron microscopy, the rods seem to be due to disruption in the myofibrillar pattern and accumulation of thin filaments in areas devoid of sarcomeric structures [79].

3. MicroRNAs Structure and Function:

3.1 Structure and Function:

MicroRNAs (*miRs*) are non-coding small RNAs regulating the expression of many genes. MicroRNAs play an important role in embryogenesis and development, as well as in human diseases. From a physiological point of view, their presence leads to transcriptional silencing by a mechanism involving their specific binding to the 3' un-translated region (3' UTR) of a messenger RNA and the subsequent recruiting of Argonaute family proteins (AGO). AGO interacts with factors that inhibit translations, mediating mRNA deadenylation and mRNA decay. The nucleotides located in positions 2nd-7th from the 5' end are crucial for the recognition of the mRNA target (seed sequence), however the nucleotides in position 8th and 13th-16th contribute significantly less to the specificity of the binding. The biosynthesis of miRNA is tightly controlled and its dysregulation can lead to cancer or neuro-developmental disorders.

In mammalian cells microRNAs are transcribed by RNA polymerase II (RNA pol ll) creating long primary transcripts, termed pri- miRNA. The secondary structure of the pri-miRNA is a loop that embeds the mature microRNA sequence (figure 3.11).
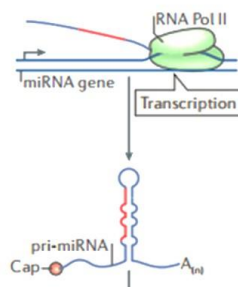
Figure 3.11: pri- miRNA illustration, Modified from [81].

Most of the genes encoding human microRNAs are located within introns of non-coding or coding gene sequences, even though few microRNAs have been identified located within the coding sequence of a gene (Figure 3.12C). MicroRNAs that are located within an intron can be

co-transcribed with the proximal gene, since they share the same promoter; nevertheless in some cases the microRNA promoter is distinct from that of its adjacent gene, as is its transcription. MicroRNAs that are located in close proximity to other microRNAs can create a cluster, termed polycistronic transcription unit.
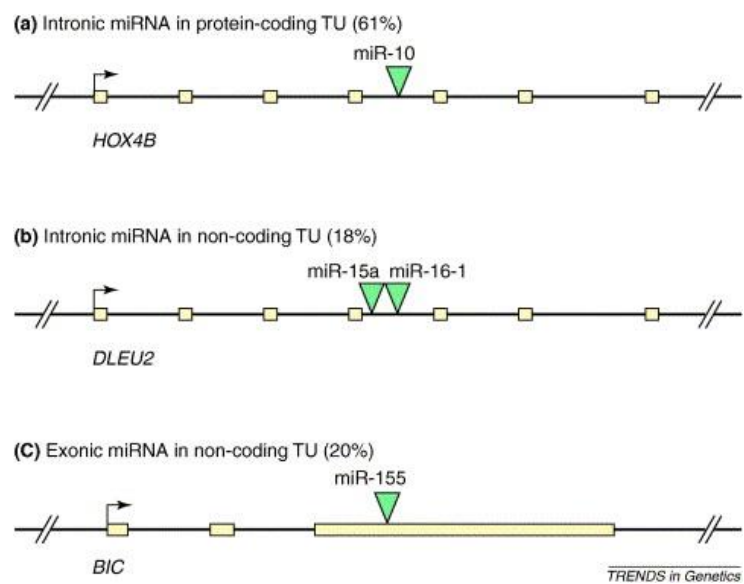
Figure 3.12: Genomic organization and structure of miRNA gene. A. Intronic miRNA (miR10) in a protein coding transcriptional unit (HOX4B gene). Green triangle- the binding location of the microRNA, the exon is marked in yellow.   B. Intronic miRNA cluster (miR15a; miR16-1) in a non-coding transcript (DLEU2) C. The location of exonic miR155 in a non-coding transcript (BIC) [82].

MicroRNA expression is regulated by transcription factors, including P53, MYOD, ZEB1 and ZEB2. For instance MYOD regulates the cluster of miR1/206. [83].

The pri- microRNA that is shown in figure 3.13 consists of a stem of 33-35 bp in length, a terminal loop and single stranded RNA in both 3' end and 5' end. The subsequent steps involved in the microRNA maturation entail Dorsha activity that releases a small hairpin pre-microRNA of 65bp. The complex that Dorsha creates with DGCR8 and with the pri-miRNA is called Microprocessor (figure 3.14).
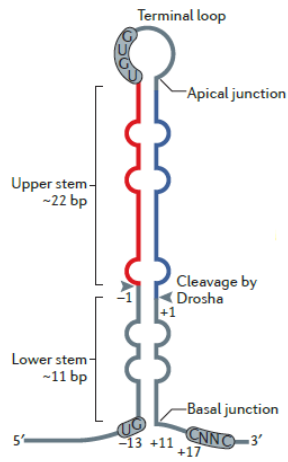
Figure 3.13 : Pri- microRNA structure, taken from [81]

Dorsha is an RNase III type endonuclease that interacts with double stranded RNA, through DGCR8's double stranded binding domain (dsRBD). At its carboxyl terminus, there are tandem RNase III domains (RIIIDa and RIIIDb); RIIIDb cuts the 5' strand and RIIIDa cuts the 3' strand leading to two 3' nucleotide overhangs. Cutting is carried out 11bp away from the basal junction and 22bp away from the apical junction (figure 3.13).
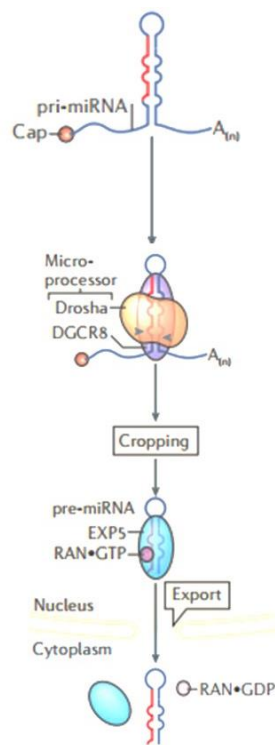
Figure 3.14 : **microRNA biosynthesis,** taken from [81]

The regulation on pri- miRNA processing is very tight. The activity of microprocessor can be regulated by post translational modifications, nuclear localization and protein stability. For instance, Histone deacetylase 1 (HDAC1) can deacetylates DGCR8 and increase DGCR8's affinity for the pri-miRNA. Additionally, phosphorylated MECP2 (methyl-CpG-binding protein 2) can sequester DGCR8 and when MECP2 is dephosphorylated, DGCR8 is released and microRNAs are produced. Dorsha and DGCR8 Knock out are embryonically lethal in mice at E 7.5. DGCR8 KO in stem cells leads to the inability of the cells to proliferate and differentiate explaining the termination of embryogenesis.

The next step in the maturation of the pre-miRNA is its transport to the cytosol through a complex termed Exportin 5 (encoded by XPO5) and RAN-GTP (GTP binding protein). When GTP is hydrolysed to GDP+Pi, pre-miRNA is released into the cytosol. Exportin5 recognizes the dsRNA that is bigger than 14 nucleotides and single stranded molecules of 1-8

nucleotides (3' overhang). KO of *XPO5* leads to a decrease in matured microRNAs but not to increase in pre-miRNA accumulation in the nucleus. The fact that the mature microRNAs are not completely depleted, suggests that there is another system that exports pre-microRNAs out of the nucleus and that protects the nucleus from nucleolytic attack. Exportin 5 is well regulated and responds to internal stress such as DNA damage through activation of AKT.

Once it reaches the cytoplasm the pre-miRNA is further processed and cleaved by Dicer. Dicer cleaves the terminal loop of the pre-miRNA, creating double stranded RNA. *Dicer-1* KO mice are embryonically lethal (7.5 E) and its silencing in stem cells affects proliferation and differentiation, similar to the phenotype of *DCGR8* KO stem cells. Tandem RNase domains are located in the C-terminus of the Dicer similarly to the Dorsha and in the N-terminus, there is a helicase domain that recognizes the terminal loop of the pre-miRNA. The 3' two nucleotide overhang, created by Dorsha are favorable to be bound by the Dicer, as a result Dicer cleaves 21-25 nucleotide away from the 3' end of the double stranded RNA.
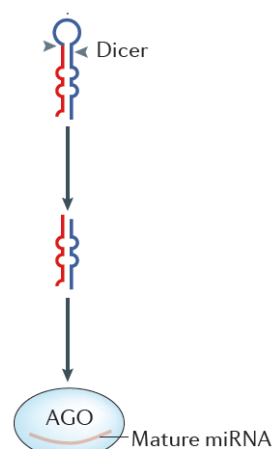
Figure 3.15 : **Pre- microRNA structure,** taken from [81]

The double stranded RNA, generated by Dicer is loaded onto the AGO2 protein that is responsible for miRNA mediated silencing. Double stranded RNA binds to AGO, forming an effector complex called RNA Induced silencing complex (RISC). The RISC complex is responsible for the loading of the double stranded RNA and unwinding it so it can specifically

44

interact with the target RNA. In Drosophila, the mechanisms of miRNA mediated transcription inhibition has been investigated in detail and it seems that its mechanism of action depends on of the *AGO* isoforms that are expressed for instance [81, 84]:

1. AGO2 prevents protein-protein interaction, which inhibits the interaction between initiation factor 4E and initiation factor 4F. This interaction is required for the assembly of the preinitiation complex on the mRNA [84, 85].
2. AGO1 prevents translation by promoting deadenylation and enhancing mRNA degradation [86].

3.2 Muscle Specific MicroRNAs:

Muscle specific microRNAs (MyomiRs) have a major impact on muscle development and muscle physiology. These microRNAs include miR1, miR133 and miR206, they are abundant in skeletal muscle and appear to be essential for proper skeletal muscle or cardiac muscle development and function. For instance, miR1 inhibits cardiac development by repressing myoblast differentiation through the repression of Histone deacetylase 4 (HDAC4, transcription repressor of myogenesis) [87]. miR133 enhances myoblasts proliferation by repressing serum response factor (SRF) that are responsible for myogenesis [88]. The genes that encode miR133 (miR133a-1, miR133a-2 and miR133b), miR1 (miR1-1 and miR1-2) and miR206 are expressed in a bicistronic fashion. There are 3 loci expressing these microRNAs: miR1-1/miR133a-2 are clustered on chromosome 10 in humans and on chromosome 2 in mouse, miR1-2/miR133a-1 are clustered on chromosome 18 in human or mouse and miR206/miR133b are clustered on chromosome 6 in human and chromosome 1 in mouse. The mature sequence of miR1-1 and miR1-2 is identical, as well as the mature sequences of miR133a-1 and miR133a-2. However, MiR133b is different from miR133a by 1 nucleotide located in the 3' end of miR133b [89] [90]. During the development of human fetus, the expression of miR1, miR133 and miR206 are significantly increased. Moreover, the expression of these microRNAs is proportional to the ability of myoblasts to become myotubes.

MyoD (myogenic differentiation factor D) is known to play a significant role in muscle development and particularly with the expression of miR133, miR1 and miR206 [91]. MyoD and MEF2 regulate the intragenic enhancer activity of miR1-2/miR133a-1 in the somite myotomes and in skeletal muscle fibers during embryogenesis. Similar mechanisms were shown to repeat in the miR1-1/miR133a-2 locus, further confirming the major role of MEF2 in skeletal muscle and heart development [92].

As described in a previous section, microRNAs play an important role in cell proliferation and differentiation through the regulation of muscle specific transcription factors; Paired BOX 3 (PAX3) and Paired BOX 7 (PAX7). For instance, miR27b inhibits cell proliferation and promotes differentiation by targeting PAX3 [93]. In addition, miR486 plays an important role in myoblast proliferation [94], while some findings report that miR486 together with miR206 induce myoblasts differentiation by targeting PAX7 [95]. In muscle satellite cells there are two subpopulations of stem cells; PAX7^{low} and PAX7^{high}, how the distribution occurs is not known yet. MiR431 targets the 3' UTR of PAX7, and enriches the subpopulation of low expressed PAX7 in satellite cells. Enrichment of PAX7^{low} subpopulation contributes to muscle regeneration and differentiation. Interestingly, when transgenic mice over-expressing miR431 were bred with mdx mice there was a significant reduction of the dystrophic phenotype of the mdx mice [96].

3.3 MicroRNA and Skeletal Muscle Disorders:

During the past decades and mainly thanks to the human genome sequencing project, the genetic mutations underlying a large number of neuromuscular disorders have been identified. Recently however, it has become apparent that some muscle disorders are associated with misregulation of microRNA expression. In a model of skeletal muscle hypertrophy, miR1 and miR133 were significantly decreased, while Pri-miRNA 206 levels were increased, though the mature form of miR206 was found to be constant [87]. Furthermore injection of double stranded miR1, miR133 and miR206 into rat skeletal muscle accelerates

regeneration opening novel perspectives to improve the muscle phenotype of patients with muscle dystrophies due to lack of regeneration [97].

In a mouse model for Amyotrophic lateral sclerosis (ALS), which exhibits paralysis, muscle atrophy and denervation, miR206 was found to be significantly elevated, probably as a protective response since deficiency of miR206 enhance disease progression. The protective effect of miR206 seems to involve targeting of HDAC4; in fact miR206 Inhibits HDAC4 expression and leads to an increase in the expression levels of fibroblast growth factor binding protein 1 (FGFBP1) that potentiates the bioactivity of FGF. FGF promotes re-innervation of the neuromuscular junction, which contributes to the regeneration of the neuromuscular synapse (figure 3.3) [98].
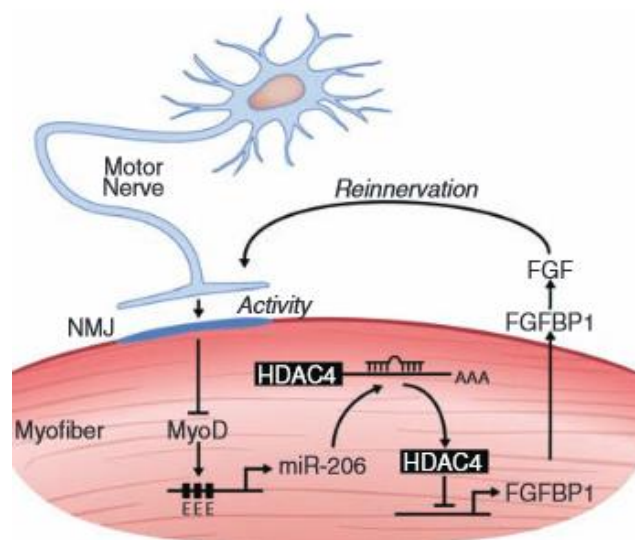
Figure 3.3: miR206 dependent re-innervation [98].

MiR486 is also enriched in skeletal muscle and plays an important role in cell proliferation, migration and wound healing. MiR486 over- expression in myoblasts leads to cell proliferation, whereas silencing of miR486 inhibits cell migration and wound repair. MiR486 targets PTEN, a phosphatase that induces cell cycle arrest followed by cell death [94]. In Duchenne muscular dystrophy (DMD) miR486 decreases significantly however this is not the

case in Backer muscular dystrophy (BMD) in which there is a production of an incomplete but partially functional dystrophin. [99, 100].

Alterations in the expression levels of myomiRs has also been observed in patients with Facioscapulohumeral muscular dystrophy (FSHD) where increased levels of miR133, miR1 and miR206 were found. In FSHD, alterations in the expression level of more than 29 different microRNAs was found, indicating that in the future following the levels of myomiRs may have a diagnostic value and may be useful to monitor drug response or disease progression [101, 102]. FSHD is a very common muscular dystrophy caused by a deletion in the 3300 bp macrosatellite D4Z4 repeat, located in the long arm of chromosome 4. Deletion of this area causes chromatin relaxation and transcriptional de-repression of this region (through hypo-methylation of the region). De-repression of this region leads to the detection of sense and antisense double stranded transcripts. Interestingly, the double stranded transcripts can serve as targets for the Dicer that cleaves them and creates miRNAs/siRNAs. Currently, it is not known if these microRNAs are functional or if they can cause local chromosomal silencing or specific loci silencing [103].

Finally the importance of proper myomiR expression was recently illustrated by the creation of a mouse model lacking miR133a-1 and miR133a-2; these mice exhibited a late onset of centronuclear myopathy type II (fast twitch) phenotype, impaired mitochondrial function, disarray of muscle triads and fast to slow myofibril conversion. The mechanism whereby these changes occur is not known even though an increase of Dyanmin 2 has been postulated to play a role [92].

4. Chromatin Organization and Transcription Regulation:

4.1 Chromatin Organization:

The chromatin is organized in a condensed state (Heterochromatin) or in a de-condensed state (Euchromatin). Heterochromatin can be further separated into facultative Heterochromatin (fHC) or Constitutive Heterochromatin (cHC), the latter being transcriptionally silent during differentiation. cHC areas are usually important for chromosomal integrity and stability, such as centrosomes and telomeres. Facultative Heterochromatin (fHC) is also transcriptionally silent but has the potential to interconvert to Euchromatin (EC), which is transcriptionally active. Intriguingly, fHC can have several states of condensation range for instance in promoter compaction of inactive genes [104].

Chromatin is packaged into structural units, termed nucleosomes. Each nucleosome packages 147 base pairs of DNA and has DNA extension to 170-240 bp (linker DNA, figure 4.1). The histone octamer contains 2 copies of the 4 core histones H2A, H2B, H3 and H4 and H1 histone, the latter regulates the expression of nearby genes by modulating the packaging state of the DNA. H2A and H2B or H3 and H4 form heterodimers that can each organize 30 bp of DNA, through the DNA loops (binding sites) L1L2 and α helixes, α1α1 (figure 4.11).
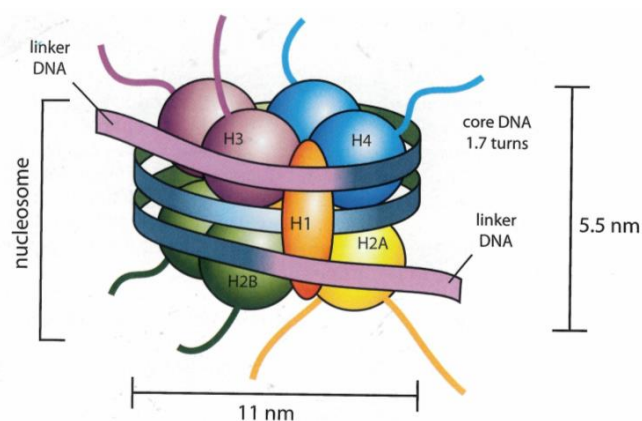
Figure 4.11: **The nucleosome core particle and the histone octamer. N terminus tails stretched out of the histone octamer [105].**

Under physiological conditions the octameric structure is not stable in the absence of DNA. Binding of DNA is not sequence specific and octamers can interact with any area within the genome, creating interfaces between the hydrogen atoms of the amide chains and the phosphate-oxygen atoms of the DNA backbone. However, it has been shown that appropriate spacing of AA and TT facilitates the interaction with the octamer.

The $(H3-H4)_2$ tetramer is created first and binds to the DNA with higher ionic force than the dimer (H3-H4). Binding of the dimers H2A-H2B to the DNA follows immediately after the binding of the $(H3-H4)_2$ tetramer. Initially, H3-H4 is synthetized and histone chaperone ASF1 transfers H3-H4 to other histone chaperons CAF1 and Rtt106 in order to form the $(H3-H4)_2$ tetramer, depositing it on newly synthetized DNA fork through association with PCNA. Apart from replication dependent nucleosome assembly, transcription dependent nuclear assembly has been associated with the activity of histone chaperone HIRA that interact with RNA pol II and recruit newly synthetized H3-H4. A similar mechanism was shown to occur in telomere regions, through the association with the histone chaperone DAXX [106].
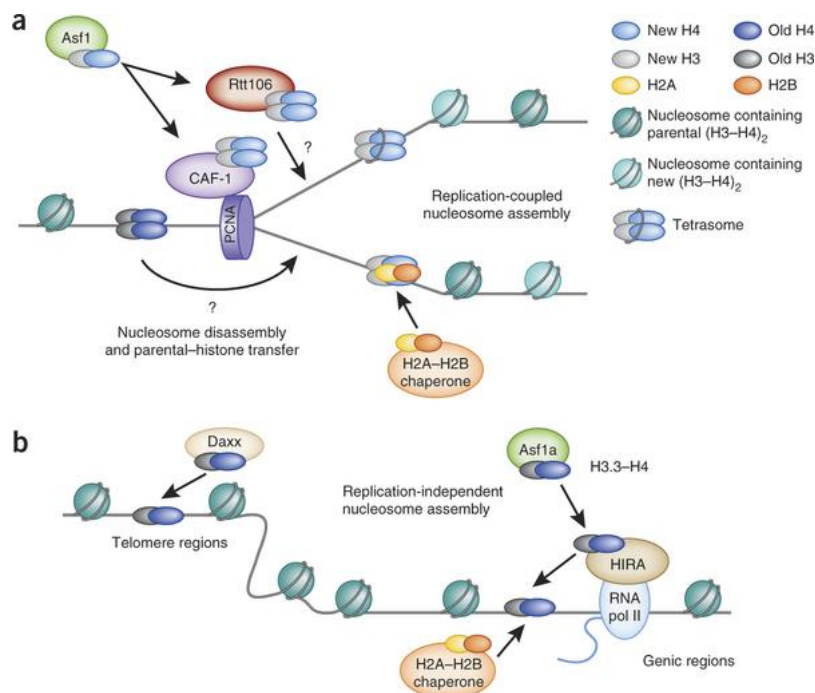
Figure 4.12: Histone chaperones coordinate to regulate DNA replication–coupled nucleosome assembly (a) and replication-independent nucleosome assembly (b) [106].

The nucleosome is a highly dynamic structure and is rarely fixed in a given position; ATP-dependent chromatin remodeling factors can enhance its mobility. The histone H1 functions as a linker to stabilize the nucleosome by reducing sliding of the octamer. In addition H1 controls the nucleosome's mobility and controls gene expression in a positive or negative manner [105, 107, 108].

4.2 Chromatin Remodeling Post-Translational Modifications of Histone:

4.2.1 Preface:

Nucleosomal DNA has to be unwrapped in order to allow transcription factors and transcription regulators to have access to the DNA. Exposing the DNA to the transcriptional machinery requires two main mechanisms: chromatin remodeling and chromatin modifications. One of the structurally and functionally conserved complexes for chromatin remodeling is the complex SWI/SNF. This is an ATP dependent chromatin remodeling complex that contains subunits such as SNF5 that are responsible for interacting with the nucleosome and modulate DNA-histone interactions. SWI/SNF is a relatively large complex that has 12 subunits and is conserved in many species: in Drosophila it is called BAP and in Humans, BAF. This complex interacts with transcription factors, leading the complex to a specific region on the chromatin. SWI/SNF complex anchors to the DNA 20bp upstream from the intended location and pulls the DNA, creating a loop. This process is energetically unfavorable and requires hydrolysis of ATP. There is a positive correlation between the loop sizes to the amount of hydrolyzed ATP required. The loop continues to spread until it reaches the site where the DNA separates from the nucleosome. Even though this process is very accurate, it can cause "nucleosomal sliding" to nearby nucleosomes.

Chromatin modifications contribute to the exposure of DNA in order to allow the transcriptional machinery to interact with the DNA; DNA exposure occurs by spontaneous

conformational changes leading to the unwrapping of the DNA and nonspontaneous covalent bond modification of the linker histone 1 (H1). H1 is responsible for the stem structure formation, approximately 30bp in length that binds to the nucleosome and serves as a "gate" for remodeling factors to unwrap the DNA (Figure 4.21).
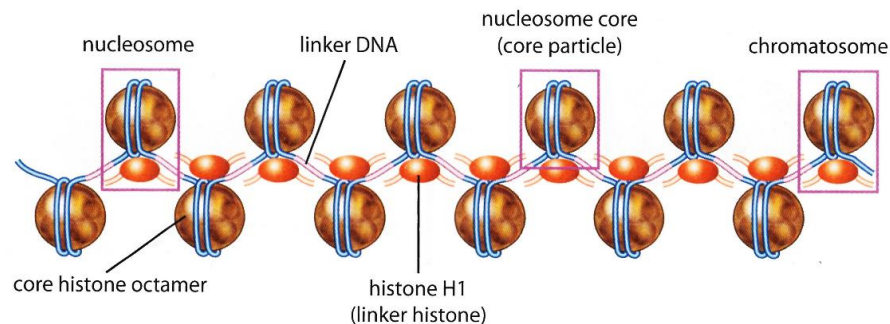
Figure 4.21: **The contribution of Histone H1 to the stem structure of the chromatin [105].**

Covalent post translational modifications of histones such as histone acetylation and methylation of certain amino acids located on the N- teminal tails of histones, determines the regulation of transcription in different loci [105]. There are several post translational modifications that can influence chromatin remodeling and transcriptional regulation, including phosphorylation of serine and threonine residues, methylation of lysine and arginine, acetylation and de-acetylation of lysine and ubiquitilation or sumoylation of lysine residues. In the next chapters, histone acetylation and methylation will be extensively discussed.

4.2.2 Histone Acetylation:

Histone Acetylation on lysine residues is almost always associated with active gene transcription. The acetylation occurs on lysine residues located on the NH2 terminal tail of histones. Acetylation of lysine by acetyltransferases decreases the positive charge of the basic histone tails and modulates the electrostatic histone tail interactions. Acetylation causes un-packaging of chromatin fibers by disrupting tail interaction within the nucleosome and with neighboring nucleosomes, resulting in opening of the chromatin (Figure 4.22).
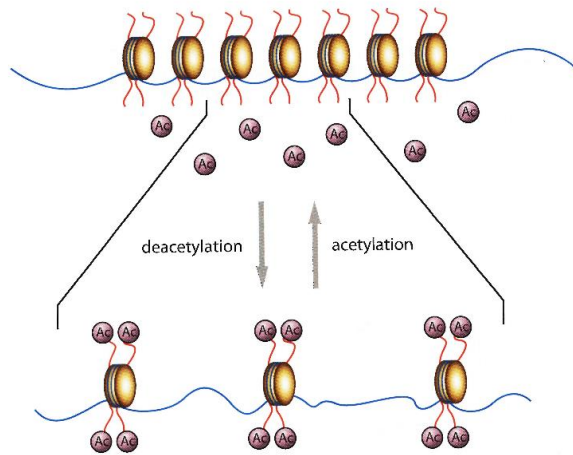
Figure 4.22: Acetylation forces the N terminal tails apart and enables open chromatin conformation [105].

Lysine acetylation can occur in several positions along the histone tails, for instance, on the H3- lysine residues 4, 9, 14, 18, 23, 36, 45 and 79. Acetylated nucleosomes can create open conformations to a particular area and create steric disturbances on adjacent regions, which can reinforce the open chromatin conformation in neighboring regions. In order to prevent transcriptional activity in adjacent regions, there is another "layer" of regulation driven by Bromodomain containing proteins [105].

Bromodomains are hydrophobic pockets highly conserved among transcription factors that bind acetylated lysine. Indeed Bromodomains interact with the open conformation of chromatin and allow the binding of other sequence specific transcription factors.

Bomodomains are highly conserved and the human proteome produces 61 different bromodomains distributed in 46 different nuclear and cytoplasmic factors. For instance, the Histone acetyl-transferases (HAT) P300/CBP, the histone methyl-transferases MLL, other transcription factors and chromatin remodeling complexes [105, 109].

4.2.2.1 Histone acetyl – transferases (HATs):

Histone acetyl-transferases (HATs) transfer the acetyl group from Acetyl-coA to the receiving lysine located on the histone tails. A-type HATs are located in the nucleus and are responsible for transcription related acetylation events, however B-type HATs are responsible for the acetylation of newly synthetized histones in the cytoplasm, transported to the forming nucleus upon DNA replication [110]. It has been shown that the activation of HATs is partially mediated by the activity of kinases, such as Cyclin E/ Cyclin 2 dependent kinase 2 during cell cycle progression. HATs are mostly active when they are part of protein complexes and their activity is subjected to other regularity partners such as transcription factors and other nuclear proteins. For instance, CBP or the closely related P300 are HATs whose enzymatic activity depends on the following sequence specific transcription factor : HNF1-α, HNF4, Sp1, Zta, NF-E2, C/EBP-α [111].

4.2.2.2 Histone De- Acetylases (HDACs):

Histone deacetylases (HDACs) antagonize the function of HATs and are responsible for the de-acetylation of histones, leading to a closed conformation of the chromatin. HDACs lack DNA binding domains and the interactions with DNA occurs through transcription factors, an interaction that allows the transcriptional regulation of specific subsets of genes. Indeed HDACs are very specific with respect to gene inhibition. There are 11 mammalian HDAC proteins with highly conserved deacetylase domains. HDACs are classified into 4 groups; Class I, Class IIa, Class IIb and Class IV. Additionally another group of deacetylases, termed Sirtuins was identified and this is commonly referred to as class III (Figure 4.222) [112-114].
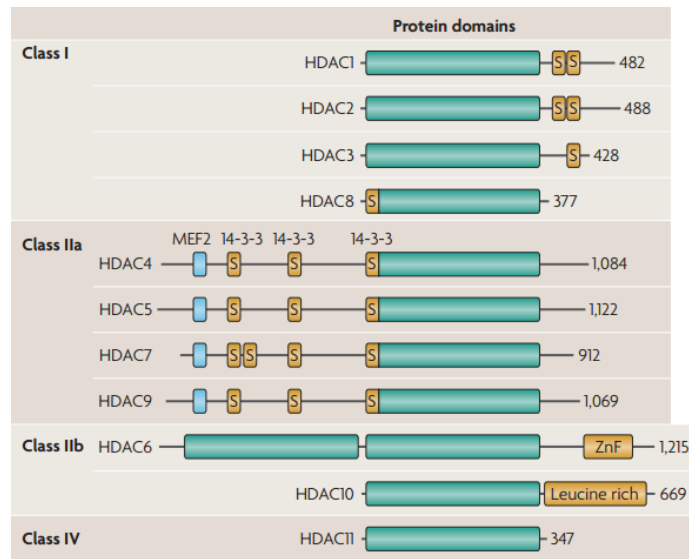
 Figure 4.222: HDACs super family distribution: Green rectangles – conserved HDAC domains, Blue squares- MEF2 binding sites, Yellow squares marked with S – binding sites of 14-3-3 protein and ZnF- Zinc Finger [113].

Class I HDACs consists of HDAC1, HDAC2, HDAC3 and HDAC8, they are ubiquitously expressed and localize in the nucleus. Class I HDACs contain a highly conserved deacetylase domain with short amino and carboxyl tails.

Class IIa HDACs consists of HDAC4, HDAC5, HDAC7 and HDAC9 with long N terminal extensions. These extensions have conserved binding sites for MEF2 and binding sites for the adaptor protein 14-3-3 (figure 4.222). 14-3-3 sequesters Class IIa HDAC from the nucleus to the cytoplasm upon phosphorylation by Calcium/Calmodulin- dependent protein kinase (CaMK) and Protein kinase D (PKD). The removal of class IIa HDACs from the nucleus allows P300 (HAT) to associate with MEF2 and activate transcription. HDAC4, HDAC5 and HDAC9 are enriched in skeletal muscle, brain and heart. HDAC7 is enriched in endothelial cells and in T cell precursors derived from the thymus. MEF2 interacting transcription factor (MITR), a splice variant of HDAC9 that lacks the catalytic domain of HDAC9, can bind to MEF2 and repress its activity. These results indicate that the catalytic domain of HDAC9 is not necessary for the repression of MEF2 activity. The catalytic domain of Class IIa HDACs is highly conserved and a tyrosine residue, located within the catalytic domain, is changed in vertebrates to histidine, which leads to a 1000 fold reduction of its enzymatic activity. Taken together Class IIa HDACs are considered

to be very potent transcriptional repressors even in the absence of their catalytic domain. The repressional efficiency of Class IIa HDACs can be further increased by recruiting class I HDACs through their C terminal domain or by interacting with Heterochromatin protein 1 (HP1), which binds to methylated Cytosine within DNA sequences [112-114].

Class IIb HDACs; are made up of HDAC6 and HDAC10. HDAC6 is a cytoplasmic enzyme and its substrates are cytoskeletal proteins, such as α tubulin and cortactin as well as other cytoplasmic proteins such as chaperons and IFNαR (Interferon receptor). HDAC6 is the only HDAC that has two catalytic domains and a Zinc finger domain. Not much is known on HDAC10, although recently it was shown to be involved in autophagy mediated cell survival and sensitivity of tumor cells to cytotoxic drug treatment. HDAC11 is a class IV HDAC and it is enriched in muscle, kidney, brain and testis. Little is known about it's function, though it was recently shown that HDAC11 represses the expression of interleukin 10 (IL10), which influences immune cells tolerance versus immune cells reactivity, a critical "decision" that has a major effect on autoimmune responses and transplantations [112-116].

4.2.2.2 A Histone Deacetylase 4 (HDAC4):

HDAC4 is a class IIa HDAC that interacts with tissue specific transcription factors, via it's N- terminal domain. HDAC4 has been identified as a regulator of PAX7 (Pair Box 7), as loss of HDAC4 reduces PAX7 expression and that of its target genes. Down-regulated PAX7 expression leads to loss of satellite cell proliferation, an event that is normally induced upon muscle damage [117].

HDAC4 shuttles from the cytoplasm to the nucleus through its nuclear localization sequence (NLS). The de-phosphorylation of serine 298 by Protein Phosphatase 2 (PP2A) creates a conformation change that exposes the NLS and allows entry of HDAC4 into the nucleus. On the other hand, phosphorylation of HDAC4 on Ser246, Ser467 and Ser632 enables its binding to

the Phosphoserine domain of 14-3-3, which sequesters HDAC4 from the nucleus and inhibits its transcriptional repressive functions [118].
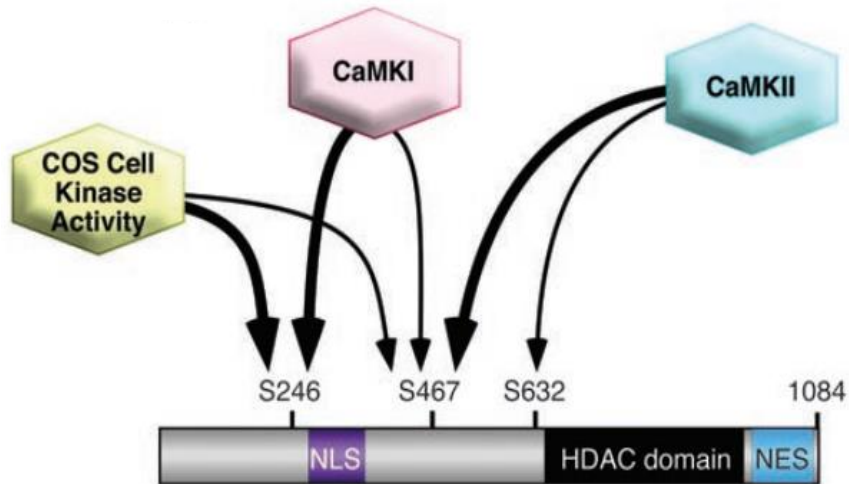
Figure 4.222A: CaMKI and CaMKII Phosphorylation sites [119].

HDAC4 phosphorylation by CaMKII is specific and does not occur in other class IIa HDACs, though CaMKI and PKD can phosphorylate both HDAC4 and HDAC5. The reason why CaMKII phosphorylates only HDAC4 is due to the unique docking site for CaMKII located on HDAC4 that is not present in other class IIa HDACs. CamKII induces cytosolic accumulation of HDAC4 and shuttles together with HDAC4 to the cytoplasm [119].
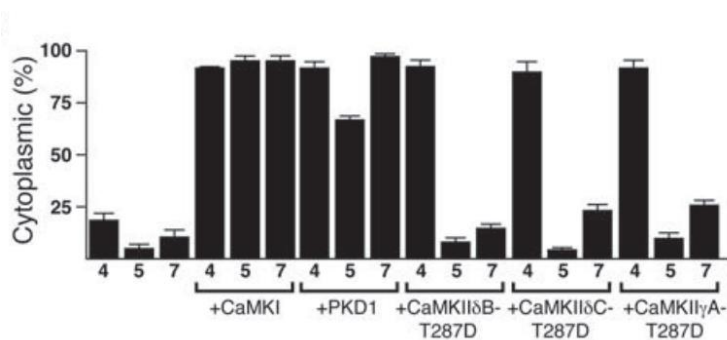
Figure 4.222A.2: Quantitative analysis of HDAC4, HDAC5 and HDAC7 cytoplasmic localization. T287D mutation in CaMKII (auto-activated CaMKII) leads to HDAC4 predominant localization to the cytoplasm [119].

Figure 4.222A2 shows the definite localization of HDAC4 in the cytoplasm of COS cells, after constitutive expression of CaMKII. All active forms of CaMKII with the point mutation T287D lead to its auto-activation, and to the cytoplasmic localization of HDAC4. Such results are not observed for other class IIa HDACs, supporting the concept that CaMKII influences the subcellular localization of HDAC4 alone while PKD/CaMKI influence the localization of all class IIa HDAC members [119].

As mentioned previously HDAC4 interacts with MEF2C and exploits its NLS in order to enter the nucleus. The shuttling of HDAC4 from the cytoplasm to the nucleus is also regulated by factors such as Thioredoxin 1 (Trx1). Over expression of Trx1 suppress the nuclear export of HDAC4 in response to reactive oxygen species (ROS) induced by Phenylephrine. Oxidation of Dnajb5 (heat shock protein 40) on Cys274/Cys276 and Oxidation of HDAC4 on CYS667/Cys669, enhances its interaction with Trx1 creating a complex that inhibits the nuclear export of HDAC4, independently from the phosphorylation status of HDAC4.

The half-life of HDAC4 is 8 hours and the half-life of its mRNA is 4 hours, indicating that HDAC4 is unstable in comparison to other enzymes. HDAC4 proteolysis is likely to be executed by caspase 3, which is also known to be involved in the degradation of MEF2 family members. The cleavage PEST sequence site of HDAC4 is at Asp 289, which is not conserved in other class IIa HDACs. Cleavage of HDAC4 by Caspase 3 does not allow HDAC4 to shuttle into the nucleus and inhibit MEF2, moreover the involvement of Caspase 3 proves an important link between HDAC4 and caspase- mediated apoptosis [120-122].

HDAC4 can be sumoylated at lysine 559 and its substitution with arginine causes HDAC4 to lose its repressional activity [123]. Apart from it's de-acetylase activity, HDAC4 is also SUMO (Small Ubiquitin like Modifier) E3 ligase that sumoylates Lys424 and Lys439 on MEF2. Sumoylated Lys424 prevents the acetylation of MEF2 by CBP (CREB- Binding protein) on lys424, which potentiates HDAC4 repression. Intriguingly, the transcription activity of MEF2 can also be regulated by sumoylation and acetylation on Lys 424 [124].

In addition to the nuclear substrates of HDAC4 such as histones, there are other nuclear and cytoplasmic substrates, for instance P53 and Z disc associated protein (MLP) respectively. The de-acetylation of P53 by HDAC4 increases the transcriptional repression following DNA damage. MLP is a sensor for cardiac mechanical stretch, which plays a major role in muscle contraction regulation. Interestingly, MLP is de-acetylated by HDAC4 and acetylated by PCAF, which is the first evidence for the involvement of HDAC4 and PCAF in muscle contraction regulation [125, 126].

4.2.2.2 B Histone Deacetylase 5 (HDAC5):

HDAC5 is a class IIa HDAC that shuttles between the cytoplasm and nucleus under the control of CaMKs. Upon phosphorylation of HDAC5 by CaMKI, HDAC5 is exported to the cytoplasm thereby repressing its transcriptional activity. In a recent experiment it was shown that the addition of 50µM NMDA (N-methyl-D-aspartate) to cultured cortical neurons induces neuronal cell apoptosis by exporting HDAC5 to the cytoplasm. Indeed, ectopic expression of nuclear HDAC5 leads to inhibition of NMDA induced apoptosis. The Class IIa HDAC inhibitor, Trichostatin A (TSA) promotes NMDA induced apoptosis by suppressing the activity of HDAC5 [127].

HDAC5 regulates the transcriptional activity of genes involved in metabolism in C2C12 cells. Knockdown of HDAC5 caused an increase in glucose uptake, overexpression of GLUT4 and insulin stimulated glycogen synthesis. [128] Moreover, overexpression of HDAC5 in the heart leads to a decrease of gene expression involved in substrate handling and energy production, such as *Hexokinase II*, *PGC 1α* and medium chain acetyl CoA dehydrogenase (*MCAD*) [129].

4.2.3 Histone Methylation:

Histone methylation occurs on all basic residues that is Lysine, Arginine and Histidine. Lysine residues can be mono-methylated (me1), di-methylated (me2) and Tri- methylated (me3) (Figure 4.23). Arginine residues can be mono-methylated and di-methylated symmetrically (me2s) and asymmetrically di-methylated (me2a). Histidine residues have been reported to be mono-methylated only [105].
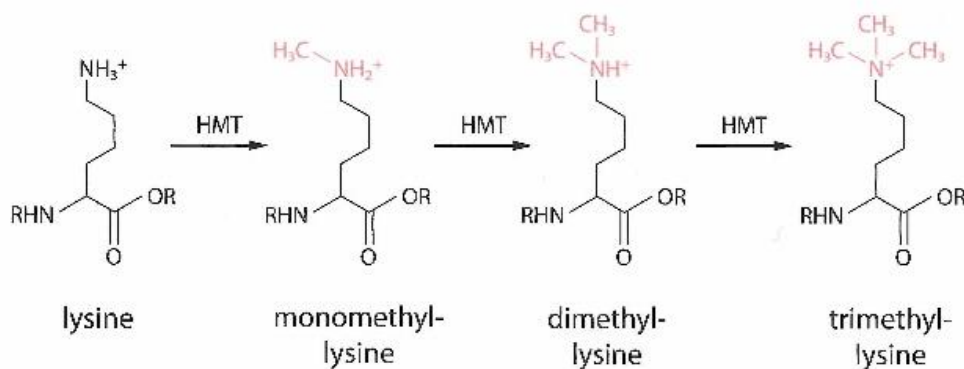
Figure 4.23: **Lysine residues methylation scheme by Histone methyl- transferases (HMT) [105].**

The mostly discussed methylations on lysine residues of histone 3 are H3K4, H3K9, H3K27, H3K36 H3K79 and on lysine residues of histone 4, H4K20. Arginine residues that are methylated on histone 3 and studied heavily are H3R2, H3R8, H3R17, H3R26 and H4R3 (the latter is on histone 4). Indeed, many basic residues are discovered to be methylated on H2A, H2B, H3 and H4. These methylations were believed to be irreversible, although lately there are many reports proving the opposite.

There are three families of enzymes that methylate histones using S- Adenosylmethionine as a substrate. The first two, methylate lysine residues such as SET domain containing proteins and DOT1 like proteins. The third family methylates arginine residues and is termed Arginine N- methyltransferase (PRMT). Methyltransferases are recruited to the region of interest by specific DNA sequences such as Poly comb group (PcG) response elements (PREs)

and Thrithorax group (TrxG) response elements (TREs). In addition, there are other factors that are responsible for the recruitment of Histone methyltransferases, such as long non coding RNAs (lncRNAs) that specifically bind to DNA sequences and to protein complexes mediating histone methylation.

The recognition process of methylated histones is executed by proteins with methyl binding domains, such as PHD fingers, WD40 repeats, CW domains and PWWP domains. The consequence of histone methylation is context dependent, for instance H3K4me3 is mostly a transcriptional activator, whereas H3K27me3 is mostly a transcriptional repressor. In addition, the level of methylation determines function, for instance H3K4me1 is associated with enhancer activity, although H3K4me3 is linked to promoter activity. Histone methylation is a very important epigenetic marker that is maintained throughout evolution being present in C. elegans and D. melanogaster, and unlike DNA methylation that is more prominent in higher eukaryotes [130].

4.2.4 Histone Post translational modification in skeletal muscle:

The influence of post translational modification on histones in skeletal muscle during the proliferation and differentiation is not yet fully understood. The myogenic program of muscle specific gene expression starts after the expression of muscle specific transcription factors, such as MyoD. MyoD is inhibited by HDAC1 (Class I HDAC) and HDAC1 expression levels decrease significantly during skeletal muscle differentiation. Furthermore during differentiation pRb (phospho-retinoblastoma) binds to HDAC1 and prevents its inhibitory interaction with MyoD. P300 and PCAF (P300/CBP associated factor) acetylate MyoD and help to recruit other HATs to muscle specific genes. Accumulation of HATs leads to the increase of MyoD-dependent gene expression. As mentioned previously, similar mechanism exists with Class II HDACs and MEF2.
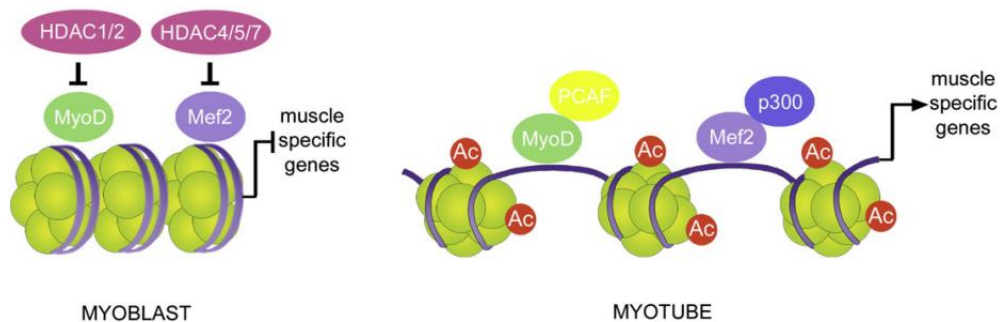
Figure 4.241: Histone acetylation and de- acetylation regulate myogenesis [131].

In order to keep muscle stem cells in a primed state, there is a loss of inhibitory H3K27 Tri-methylation along the genome and high abundance of H3K4me3 at transcriptional start sites (TSS). The Polycomb repressive complex 2 (PRC2) establishes gene silencing by Tri-methylation of H3K27. The lack of the enzymatic subunit of PRC2 leads to impaired stem cells proliferation and alterations in muscle specific gene expression.

Ubiquitinylation of histones has a major influence on transcription initiation and elongation, which can be enhanced by other modifications such as histone methylation. For instance, H3K4me3 mediates histone Ubiquitinylation, however H3K36me3 mediates histone de-ubiquitilation. Additionally, H2B Ubiquitinylation levels decrease significantly during muscle cell differentiation, and interestingly a patient with "early onset inclusion body myopathy" exhibited impaired decrease in H2B Ubiquitinylation [132]. These results suggest that histone ubiquitnylation may play a role in muscle disease.

Global deletion of single HDACs in mice is often lethal in the prenatal phase owing to severe developmental defects. In mice with HDAC1 and HDAC2 full knockout in skeletal muscle, there is 40% of lethality due to respiratory complications. Approximately 60% of the mice survive the first day of life, but subsequently develop a progressive myopathy, skeletal muscle degradation and centrally nucleated myofibrils. However when only 3 alleles are missing (out of 4 alleles encoding HDAC1 and HDAC2), the mice are viable and display normal muscle architecture [131].

Upon innervation, muscle mass is preserved and muscle proteolysis is prevented. On the other hand, when innervation is prevented muscle proteolysis and atrophy take place. Myogenin is known to regulate the expression levels of E3 ligase; MuRF1 and atrogin1, which are responsible for the increase of muscle proteolysis and atrophy with the absence of innervation. HDAC 4 and 5 inhibit the expression of the repressor DACH2 that are Myogenin repressors (Figure 4.242) [133]. In double HDAC4 and HDAC5 knock-out mice , Myogenin was not up-regulated and the mice did not respond to the lack of innervation by undergoing proteolysis and atrophy [134].
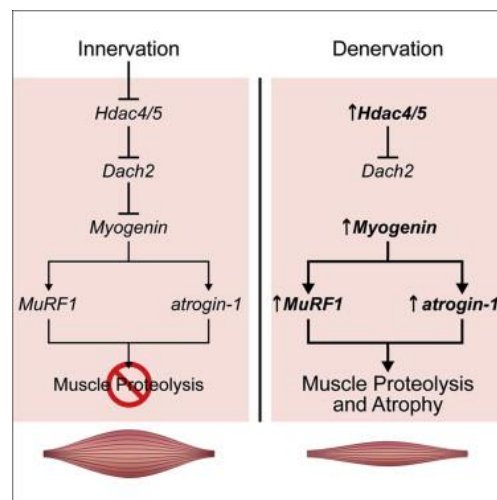
Figure 4.242: Innervation and denervation influence on muscle proteolysis and atrophy. Upon denervation HDAC4 and HDAC5 are highly expressed and as consequence muscle proteolysis and atrophy are taking place [134].

HDAC4 and HDAC5 are highly expressed in skeletal muscle tissue, any alterations in their expression can lead to diseases such as ALS. ALS patients have high expression levels of HDAC4 and the severity of the disease correlates with HDAC4 upregulation [135]. HDAC inhibitors are already confirmed to improve patient's conditions with immunological disorders, cancer or neuromuscular diseases. For instance, in Duchenne muscular dystrophy there is a major amelioration of the symptoms when HDAC inhibitors are used in mice. In mdx mice HDAC

inhibitors increase myofibrilar size, decrease inflammatory infiltration to the muscle tissue and prevent the formation of fibrotic scars [136].

4.3 DNA Methylation:

4.3.1 Preface:

DNA methylation is a common modification that is associated with the control of gene expression. Methylation patterns are not uniform throughout the genome and are mainly concentrated within the coding sequence. 80% of DNA methylations are discovered within CpG dinucleotides, which are concentrated in regions termed CpG Islands (CGIs). There are promoters that contain few CpG dinucleotides (CpG dinucleotide every 100 bp) and promoters that contain 10 fold more CpG dinucleotide. Tissue specific housekeeping genes belong to the group of promoters with low CpG dinucleotide concentration.
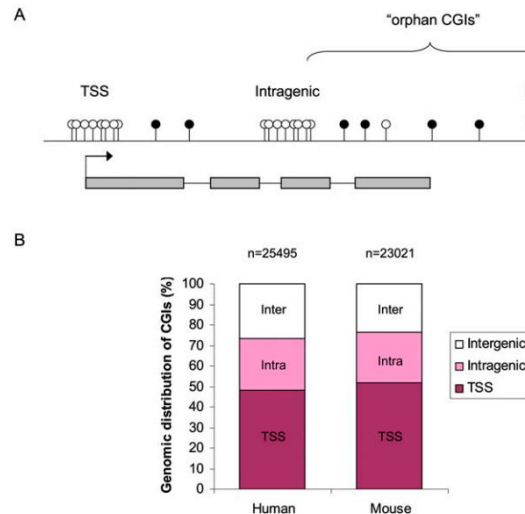
Figure 4.31: **The genomic distribution of CpG Islands**. TSS; Transcription start site, Intragenic; within the gene body, Intergenic; between annotated genes and Orphan CpG Islands; with unknown function. **Filled circles**- methylated CpG residues, **Empty circles**- unmethylated CpG residues [137].

During evolution, areas with a high abundance of CpG Islands have become less methylated, while areas containing few CpG Islands are more methylated. High-throughput experiments show that the amount of CpG Islands in humans is higher than that present in the mouse genome (25495 and 23021 respectively per haploid genome) [137]. 50% of the CpG Islands in mouse and human are annotated with TSS-Transcription Start Site (Figure 4.31b). The other half is distributed between intergenic and intragenic CpG Islands and these are termed "orphan" to express the uncertainty over their significance and function.

CpG Islands are often un-methylated even within genes that are not active, since methylation does not initiate gene silencing but rather locks genes in a silent mode. During X chromosome inactivation, DNA methylation takes place after the appearance of other silencing modifications, such as H3K27 tri-methylation, in other words, DNA methylation is essential for the maintenance of "leak-proof" X chromosome.

The presence of transposable elements (repetitive sequences constituting about 45% of the human genome) is postulated to pose a threat to the integrity of the genome. Thus, silencing transposons by DNA methylation is crucial for the survival of the host and serves as the main mechanism for the inhibition of transposomal activity. DNA Methyltransferase 1 (DNMT1) is the only gene known to be vital for repression of transposons in mammalian somatic cells [138].

During mammalian development, CpG poor promoters appear to be highly methylated especially after the epiblast phase. Highly methylated chromatin recruits methylcytosine binding proteins 1 and 2 (MECP1, MECP2, etc…) that contain MBDs (Methyl Binding Domains). MBDs are motifs of 75 amino acids that are highly conserved. In Humans there are 4 MBDs (MBD1-MBD4). The interaction of MBD and DNA takes place in the major groove, where two methyl groups are pointed out from the helix structure. Recognition regions that transcription factors bind to may be masked by methylation of CpG islands, leading to transcription repression. Moreover highly methylated regions are known to create chromatin condensation and cause inaccessibility of transcription factors [105, 137].

4.3.2 DNA Methyl-Transferases:

Cytosine methylation is catalyzed by DNA Methyltransferases (DNMTs), in fact these enzymes are the only enzymes able to transfer methyl group from S- adenosylmethionine (SAM) to cytosine.
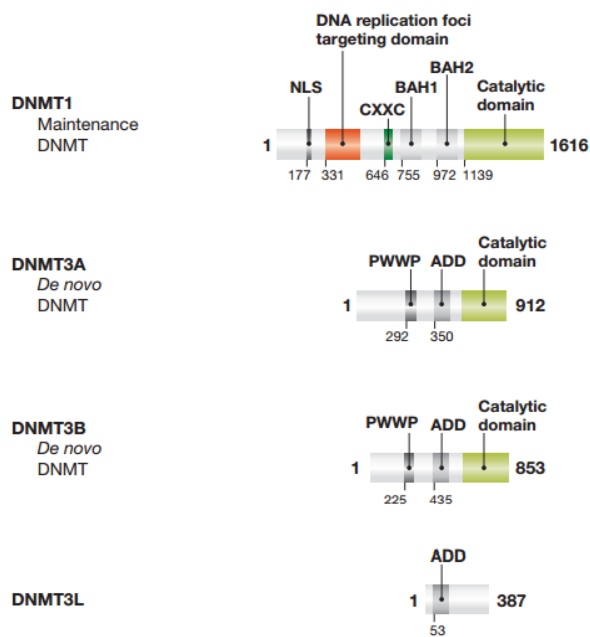
Figure 4.32: **DNMTs structure and function:** Schematic presentation of DNMTs with their different domain displayed [139].

There are several DNMTs that are enzymatically active in mammals; DNMT1, DNMT3A, DNMT3B and DNMT3L, the latter is a regulatory DNMT lacking catalytic acivity.

DNMT1 is a maintenance DNA Methyltransferase, which is responsible for methylating cytosine in the newly synthesized strand when 5 methycytosine is present in the template strand, creating an exact parallel pattern in the newly synthesized DNA strand. Because of its function, *DNMT1* is localized to the replication foci during the S phase through its interaction with the SRA domain of UHRF1 (Ubiquitin-like, containing PHD and RING finger domains 1). In

other words, UHRF1 is a E3 ubiquitin ligase that interacts with DNA and recruits DNMT1 [139, 140]. DNMT1 maintains the same pattern of methylation in the daughter strand and in fact KO mice for *DNMT1* lose 90% of their methylations and die in early stage of embryogenesis. In cancer cells, DNMT1 was shown to have *de novo* activity, which is unusual under physiological condition since the CXXC domain binds to the un-methylated dinucleotide and together with the BAH1 domain, create a linker between the catalytic site and the unmethylated CG. Binding of the DNMT1 to the parallel strand 5 methylcytosine, increases the enzymatic efficiency by 10 fold through allosteric activation and increase in specificity, which allows accurate and effective methylation of the unmethylated cytosine partner in the daughter strand. Figure 4.32 also shows that DNMT1 has a nuclear localization signal (NLS) that enables the entry of DNMT1 into the nucleus.

DNMT2 in human is encoded by the gene *TRDMT1*. DNMT2 does not fulfill similar activity that of other DNMTs since DNMT2 methylates certain tRNAs and prevents their cleavage by ribonucleases (eg. tRNA$^{asp\,(GTC)}$, tRNA$^{val\,(AAC)}$ and tRNA$^{gly\,(GCC)}$) [141].

DNMT3A, DNMT3B and DNMT3L are *de novo* DNA methyltransferases. DNMT3A and DNMT3B are closely related and both contain PWWP, PHD like ADD domain and catalytic domain. ADD domain is known to interact with non-modified lysine 4 in H3, H3K4. PWWP domain interacts with trimethylated lysine 36 in H3, H3K36me3, which helps to increase the activity of DNMT3A. DNMT3L has no catalytic domain and binds to DNMT3A, increasing its enzymatic activity [141].

Chapter 2 - Results:

1. Establishment of a human skeletal muscle-derived cell line: biochemical, cellular and electrophysiological characterization

In the last few decades scientists have isolated single muscle fibers originating mainly from small rodents, in order to closely investigate the cellular properties involved in ECC. Obtaining such highly differentiated cells (muscle fibers) in tissue culture for a long period of time is almost impossible. However, differentiating satellite cells to myotubes in vitro starting from patient's biopsies is performed almost routinely in our laboratory in order to investigate if alterations in ECC occur in patients with specific neuromuscular disorders [142, 143]. However, the use of myotubes holds many limitations, for instance non-homogenous culture such as fibroblasts "contamination", slow growth/differentiation and limited amount of cell divisions as well as the fact that myotubes cannot differentiate further into fibers. Nevertheless, considering these drawbacks, there is a need for an immortalized human muscle cell line. In this publication we characterized the ECC of an immortalized human muscle skeletal cell line (HMCL- 7304), which originated from satellite cells obtained from a healthy 19 year old female with no overt neuromuscular disorders. In order to create the immortalized cell line, telomerase reverse transcriptase (*hTERT*) and cyclin dependent kinase 4 (*CDK4*) vectors were overexpressed [144, 145]. Our first step was to determine the expression levels of several genes involved in ECC. The transcripts levels were compared with those expressed in muscle biopsies from healthy individuals. Our results show that SERCA1 levels were very low in the HMCL-7304 leading to the slow Ca^{2+} uptake in the cells compared to mature muscle. Immunofluorescence images showed that myotubes have a low level of organization of RYR1 and DHPR, though their Ca^{2+} release in respond to KCl and 4-cmc that was normal.

Here we characterized the immortalized human muscle cell line that can, in the future, be genetically manipulated and used as a platform for the investigation of neuromuscular disorders.

Author contribution: In the 1st publication entitled "Establishment of a human skeletal muscle-derived cell line: biochemical, cellular and electrophysiological characterization" Ori Rokach prepared cultures, performed experiments and analyzed the data shown in figures 1 and 3, Martin Rausch and Francesco Zorzato performed SIM microscopy experiments and Nina D Ullrich performed the electrophysiological experiments, Haiyan Zhou performed the western blot on figure 1_b and Vincent Mouly established the immortalized cell line. Susan Treves wrote the manuscript and oversaw the experiments.

Establishment of a human skeletal muscle-derived cell line: biochemical, cellular and electrophysiological characterization

Ori ROKACH*†, Nina D. ULLRICH‡, Martin RAUSCH§, Vincent MOULY‖, Haiyan ZHOU¶, Francesco MUNTONI¶, Francesco ZORZATO*,**1 and Susan TREVES*,**1

*Department of Anaesthesia, University Hospital Basel, Hebelstrasse 20, 4031 Basel, Switzerland, †Department of Biomedicine, University Hospital Basel, Hebelstrasse 20, 4031 Basel, Switzerland, ‡Department of Physiology, University of Bern, Bern, Switzerland, §Novartis Biomedical Institute, Postfach 4002 Basel, Switzerland, ‖Thérapie des maladies du muscle strié, Institut de Myologie, UM76, UPMC, Université Paris 6, Paris, France, ¶Dubowitz Neuromuscular Centre, Institute of Child Health, University College London, 30 Guilford Street, London WC1N 1EH, U.K., and **Department of Life Sciences and Biotechnology, University of Ferrara, Ferrara, Italy

Excitation–contraction coupling is the physiological mechanism occurring in muscle cells whereby an electrical signal sensed by the dihydropyridine receptor located on the transverse tubules is transformed into a chemical gradient (Ca^{2+} increase) by activation of the ryanodine receptor located on the sarcoplasmic reticulum membrane. In the present study, we characterized for the first time the excitation–contraction coupling machinery of an immortalized human skeletal muscle cell line. Intracellular Ca^{2+} measurements showed a normal response to pharmacological activation of the ryanodine receptor, whereas 3D-SIM (super-resolution structured illumination microscopy) revealed a low level of structural organization of ryanodine receptors and dihydropyridine receptors. Interestingly, the expression levels of several transcripts of proteins involved in Ca^{2+} homoeostasis and differentiation indicate that the cell line has a phenotype closer to that of slow-twitch than fast-twitch muscles. These results point to the potential application of such human muscle-derived cell lines to the study of neuromuscular disorders; in addition, they may serve as a platform for the development of therapeutic strategies aimed at correcting defects in Ca^{2+} homoeostasis due to mutations in genes involved in Ca^{2+} regulation.

Key words: excitation–contraction coupling, gene expression, immortalized muscle cell, ryanodine receptor, skeletal muscle, super-resolution microscopy.

INTRODUCTION

Skeletal muscle is a highly differentiated tissue made up of myofibres, a syncytium of cells filled with myofibrils and containing sarcomeres that generate the force necessary for muscle contraction. In the last few years, a number of techniques have been developed to isolate single muscle fibres from small rodents allowing detailed investigations of the functional properties of the EC (excitation–contraction) coupling mechanism at the ultrastructural, biochemical and cellular levels in normal and pathological conditions [1–4]. Because of their high degree of differentiation and specialization, it is difficult to maintain differentiated muscle fibres in culture for more than a few days [5] and it is nearly impossible to obtain mature fibres starting from precursor satellite cells. Nevertheless, starting from newborn mice, one can obtain cultures of contracting and striated myotubes that can be used for a number of manipulations. As to human muscle cells, primary cultures can be obtained *in vitro* by culturing satellite cells from biopsies and differentiating them into myotubes [6–9], but there is a clear necessity to develop cell lines from control and diseased individuals which will develop into myotubes and which can be exploited as a platform for drug screening, and for biochemical, cellular and physiological characterization [10–13].

For the last two decades, our laboratories, as well as others, have established primary cultures from human biopsies and characterized their intracellular Ca^{2+} homoeostasis, with particular emphasis on EC coupling, how endogenous mutations in the RyR (ryanodine receptor) Ca^{2+} channel (RyR1) affect its functional properties and some downstream effects of Ca^{2+} dysregulation such as subcellular localization of the transcription factor NFAT (nuclear factor of activated T-cells), pro-inflammatory cytokine release and production of reactive nitrogen species [9,14,15]. However, the use of primary cultures has some inherent drawbacks mainly relating to the fact that they are generally slow-growing and will undergo a limited number of divisions. To overcome this problem, immortalization of human myogenic cells has been established both from a normal individual [16,17] and from patients with different neuromuscular diseases [17–20]. In the present study, we characterized a new cell line derived from a normal individual with no overt neuromuscular disorder. We show that the myotubes derived upon differentiation by serum withdrawal express the transcripts and protein components of the skeletal muscle EC coupling machinery. In addition, we established by 3D-SIM (super-resolution structured illumination microscopy) the subcellular distribution of RyR1 and of the DHPR (dihydropyridine receptor) and assessed Ca^{2+} release via RyR by using optical and

electrophysiological techniques. This human skeletal muscle cell line HMCL-7304 is a tool of paramount importance to study on a larger scale the changes occurring in human muscles under a variety of pathological conditions.

EXPERIMENTAL

Cell culture

The immortalized myoblast cell line was established from the intercostal skeletal muscle of a 19-year-old female donor with no neuromuscular disorder, by double transfection with recombinant retroviruses containing h*TERT* (human telomerase reverse transcriptase) cDNA and *CDK4* (cyclin-dependent kinase 4) cDNA, as described previously [16,17]. The experiments were approved by the Author's Institutional Ethical Committee and were in accordance with the Declaration of Helsinki (2008) of the World Medical Association. The donor gave written informed consent to the work. Immortalized myoblasts were maintained in skeletal muscle cell growth medium (PromoCell) in a low-oxygen atmosphere (5 % O_2 and 5 % CO_2) at 37 °C. In order to induce differentiation, once the density had reached approximately 80 %, cells were rinsed once with PBS (pH 7.2) (Life Technologies) and incubated with skeletal muscle differentiation medium (PromoCell). The process of differentiation took 5 days on average, after which multinucleated myotubes were clearly visible under low magnification. Hereinafter, the human muscle derived-cell line will be referred to as HMCL-7304.

Ca^{2+} concentration measurements

HMCL-7304 cells were grown and differentiated on glass coverslips coated with 10 μg/ml laminin (Life Technologies). Once myotubes had formed, cells were loaded with the fluorescent Ca^{2+} indicator Fluo-4/AM (Fluo-4 acetoxymethyl ester) (Life Technologies) for 40 min at 37 °C as described previously [15]. Cells were rinsed once with Krebs–Ringer medium (pH 7.4) containing 2 mM $CaCl_2$ and then coverslips were mounted on to a 37 °C thermostatically controlled chamber which was continuously perfused with Krebs–Ringer medium (pH 7.4); individual cells were stimulated with the indicated agonists (KCl, 4-chloro-*m*-cresol, caffeine) made up in Krebs–Ringer medium (pH 7.4) containing no added Ca^{2+} plus 100 μM La^{3+} in order to monitor changes in the free cytosolic Ca^{2+} concentration ($[Ca^{2+}]_i$) due to release from intracellular stores. Individual cells were stimulated by means of an eight-way 100-mm-diameter quartz micromanifold computer-controlled microperfuser (ALA Scientific Instruments), as described previously [14]. Online fluorescence images were acquired using an inverted Nikon TE2000 TIRF (total internal reflection fluorescence) microscope equipped with a dry Plan Apochromat ×20 objective [0.17 NA (numerical aperture)] and an electron multiplier Hamamatsu CCD (charge-coupled device) camera C9100-13. Changes in $[Ca^{2+}]_i$ were analysed using the MetaMorph imaging system (Molecular Devices) and the average pixel value for each cell was measured as described previously [14,15].

Electrophysiological measurements and confocal Ca^{2+} imaging

Myoblasts were grown on laminin-coated glass-bottomed 35-mm-diameter dishes (MatTek). After differentiation into myotubes, cells were patch-clamped in the whole-cell configuration with low-resistance borosilicate glass micropipettes (1–3 MΩ) using an Axopatch 200B amplifier (Axon Instruments) controlled by

Table 1   Sequences of primers used in the present study

Primer	Forward primer sequence	Reverse primer sequence
RYR1	5′-ATCTCCCGCCTTAGCCATACTTCT-3′	5′-GGACCTCTACGCCCTGTATC-3′
RYR3	5′-CAGTCCCTATCTGTCAGAGCC-3′	5′-CATGGCCGTATAACAGGGTCC-3′
CAV1.1	5′-ACGAACATGCACCTAGCCAC-3′	5′-ACGAACATGCACCTAGCCAC-3′
CASQ1	5′-CACCCAAGTCAGGGGTACAG-3′	5′-GTGCCAGCACCTCATACTTCT-3′
CASQ2	5′-CATTGCCCATCCCCAACAAACC-3′	5′-AGAGTGGGTCTTTGGTGTTCC-3′
DES1	5′-AACCAGGAGTTTCTGACCACG-3′	5′-TTGAGCCGGTTCACTTCGG-3′
MYH1	5′-GGGAGACCTAAAATTGGCTCAA-3′	5′-TTGCAGACCGCTCATTTCAAA-3′
MYH2	5′-AGAAACTTCGCATGGACCTAG-3′	5′-CCAAGTGCCTGTTCATCTTCA-3′
SERCA1	5′-GGTGCTGGCTGACGACAACT-3′	5′-AAGAGCCAGCCACTGATGAG-3′
SERCA2	5′-CTCCATCTGCCTGTCCAT-3′	5′-GGCTGACGGCTTCCAAGT-3′

a custom-written data-acquisition software developed by LantibodiesView (National Instruments). The external solution contained 150 mM triethylammonium methylsulfonate, 2 mM $CaCl_2$, 1 mM $MgCl_2$, 10 mM Hepes, 0.001 mM TTX (tetrodotoxin) and 1 mM 4-aminopyridine; the pH was adjusted to 7.4 with CsOH. The pipette solution contained 140 mM $CsCH_3SO_3$, 10 mM Hepes, 6 mM $MgCl_2$, 11.5 mM $CaCl_2$, 4 mM Na_2ATP, 20 mM EGTA, 14 mM $CrPO_4$, 0.1 mM leupeptin and 0.1 mM Fluo-3 potassium salt; the pH was adjusted to 7.2 with CsOH [21]. The reference electrode was connected to the bath solution with an agar bridge (4 % agar in 3 M KCl). All measurements were carried out at room temperature (25 °C). Holding potential was kept at -80 mV. Stepwise depolarizations were applied to activate the voltage-dependent DHPR and to trigger Ca^{2+} release mediated by RyR1, the intracellular Ca^{2+}-release channel located in the SR (sarcoplasmic reticulum) membrane. Detailed voltage-clamp protocols are indicated. In order to determine the current–voltage relationship, long depolarizations of 800 ms were applied. Currents were analysed in IgorPro (Wavemetrics). Peak current amplitude was calculated from the difference between membrane currents before and during application of 500 mM $CdCl_2$ (ΔI_{CaL}). For the investigations of electromechanical coupling between the DHPR and RyR1, short depolarizations (50 ms) were applied. Changes in the $[Ca^{2+}]_i$ were monitored using the fluorescent Ca^{2+} indicator Fluo-3 (Biotium), which was loaded into the cell via the patch pipette. Using a MicroRadiance laser-scanning confocal microscope (Bio-Rad Laboratories), Fluo-3 was excited at 488 nm with an argon ion laser, and emission light was collected above 500 nm. Linescan images were recorded at a rate of 50 lines/s, analysed in ImageSXM (free software based on NIH Image) [22] and processed further using IgorPro. Changes in $[Ca^{2+}]_i$ are shown as relative changes in fluorescence ($\Delta F/F_0$).

qPCR (quantitative real-time PCR) experiments

Total RNA was extracted from differentiated HMCL-7304 myotubes and biopsies from healthy individuals, using TRIzol® (Life Technologies) as described previously [23]. cDNA was synthesized with the High Capacity cDNA synthesis kit (Applied Biosystems) and the primers listed in Table 1. Transcript levels were quantified using SYBR® Green reagent on an Applied Biosystems platform (7500 fast real-time PCR system) and levels were normalized to desmin expression.

Mouse muscle fibre isolation

Mouse FDB (flexor digitorum brevis) fibres were enzymatically dissociated at 37 °C for 60 min in a cell culture incubator in

Tyrode's solution containing 0.20% collagenase I (Sigma Fine Chemicals) and placed on glass coverslips coated previously with 1.5 μl of laminin (1 mg/ml) (Life Technologies) as described previously [23].

Immunofluorescence

For immunofluorescence, myotubes cultured on glass coverslips were fixed with 4% (w/v) paraformaldehyde at room temperature for 15 min, washed and permeabilized with 0.1% Triton X-100 in PBS for 1 h before blocking with 3% (v/v) goat serum for 30 min, followed by 1 h of incubation in mouse anti-(fast myosin) monoclonal antibody (1:100 dilution; Sigma Fine Chemicals, catalogue number M4276) and mouse anti-(slow myosin) monoclonal antibody (1:50 dilution; Novo NCL, Leica Biosystems, catalogue number NCL-MHC) at room temperature. Coverslips were washed in 0.1% Triton X-100 in PBS and incubated with goat anti-(mouse IgG) secondary antibody conjugated to Alexa Fluor® 594 (Life Technologies, catalogue number A-11005) for 1 h at room temperature, followed by thorough washing in PBS. Nuclei were stained with Hoechst 33258 (Invitrogen) for 10 min. Slides were mounted in aqueous mounting medium and viewed with a Leica DMR fluorescent microscope equipped with a ×20 HC-PL Fluotar objective (0.50 NA). The percentage of fast and slow myosin-positive HMCL-7304-derived myotubes was calculated by counting the number of myosin-positive cells divided by the total number of cells as visualized by brightfield microscopy in the same area. For super-resolution microscopy, mouse FDB fibres or human skeletal muscle myotubes were fixed with 3.7% (w/v) paraformaldehyde (in PBS) for 30 min at room temperature, rinsed twice with PBS and permeabilized with 1% Triton X-100 in PBS for 30 min. After rinsing and blocking non-specific sites with 1:100 blocking solution (Roche), cells and fibres were incubated with anti-RyR1 monoclonal antibody (Thermo Scientific, catalogue number MA3-925) or goat anti-Ca$_v$1.1 (Santa Cruz Biotechnology, catalogue number sc-8160) antibody for 3 h at room temperature (10 μg/ml final concentration diluted in PBS with 0.01% Tween 20). Slides were rinsed with PBS containing Tween 20 five times for 5 min each and incubated with the appropriate secondary conjugate (Alexa Fluor® 555 or Alexa Fluor® 647, diluted 1:500 in PBS containing Tween 20) overnight at 4°C. Slides were rinsed with PBS containing Tween 20 and mounted with 10% (v/v) glycerol in PBS. Staining was visualized with a Zeiss Elyra microscope equipped with ×63 oil Plan-Apochromat (1.4 NA) objective. Raw datasets consisted of images acquired with three different grid angles and five different grid phases. Super-resolution images were calculated from the raw data using the built-in algorithm. The baseline was just shifted (not truncated) to allow inspection for potential ghosts arising from sample imperfections.

Electrophoresis and immunoblotting

Microsomes were prepared from differentiated HMCL-7304-derived myotubes as described previously [24]. Protein concentration was determined using Protein Assay Kit II (Bio-Rad Laboratories) using BSA as a standard. SDS/PAGE, protein transfer on to nitrocellulose membranes and immunostaining were performed as described previously [24]. The following primary antibodies were used: mouse anti-RyR1 (Thermo Scientific, catalogue number MA3-925), rabbit anti-RyR1 (a gift from Professor Vincenzo Sorrentino, University of Siena, Siena, Italy), goat anti-Ca$_v$1.1 (Santa Cruz Biotechnology,

catalogue number sc-8160), rabbit anti-CSQ1 (calsequestrin 1) (Sigma, catalogue number C0743), rabbit anti-CSQ2 (Epitomics, catalogue number 2962-1), goat anti-SERCA1 (sarcoplasmic/endoplasmic reticulum Ca^{2+}-ATPase 1) (Santa Cruz Biotechnology, catalogue number sc-8093), goat anti-SERCA2 (Santa Cruz Biotechnology, catalogue number sc-8095) and mouse anti-MYH1 (myosin heavy chain 1) (Millipore, catalogue number 05-716). Secondary peroxidase conjugates were Protein G–peroxidase (Sigma, catalogue number P8170) and peroxidase-conjugated goat anti-(mouse IgG) (Sigma, catalogue number A2304). The immunopositive bands were visualized by chemiluminescence using the Super Signal West Dura kit (Thermo Scientific).

Statistical analysis and graphical software

Statistical analysis was performed using Student's t test; means were considered statistically significant when the P value was <0.05. When more than two groups were compared, analysis was performed by the ANOVA test followed by the Bonferroni post-hoc test using GraphPad Prism 4.0 software. Origin software was used to generate dose–response curves and obtain EC$_{50}$ values; images were assembled using Adobe Photoshop CS (version 8.0).

RESULTS

Expression levels of transcripts and proteins involved in EC coupling in cell line-derived myotubes

In order to functionally characterize the HMCL-7304-derived myotubes, we chose several genes that are well known to play a crucial role in skeletal muscle EC coupling. Transcript levels were quantified and compared with those present in muscle biopsies obtained from five healthy individuals. Figure 1(A) shows the relative expression levels on a logarithmic scale of different transcripts. Interestingly, we found that the *RYR1* transcript was significantly lower (approximately 300-fold) than in differentiated muscle ($P < 0.0001$), and there was no up-regulation of *RYR3* mRNA, which was also significantly reduced in HMCL-7304 myotubes. *SERCA1* and *CSQ1* transcript levels were significantly lower (~1000-fold) in the cell line ($P < 0.003$), whereas there was a 10-fold increase in the expression of the *CSQ2* transcript. *SERCA2* showed similar mRNA levels in the biopsies and the cell line as did *CAV1.1*, suggesting that expression of the L-type Ca^{2+} channel may appear at an early stage of development. The transcript levels of *MYH1* and *MYH2*, that are characteristically expressed in slow-twitch and fast-twitch muscles respectively were lower in HMCL-7304 compared with biopsies; however, immunofluorescence shows that the slow myosin isoform is present in a larger percentage of HMCL-7304 cells, compared with fast myosin, with approximately 51% slow to 13% fast (36% negative for both fast and slow isoforms) (Figure 1B). Taken together, these results suggest that the differentiated myotubes express proteins that are more abundant in slow-twitch muscles.

We are aware that the presence of a transcript does not necessarily reflect protein expression, thus we tested microsomes prepared from HMCL-7304-derived myotubes by immunoblotting. Figure 1(C) confirms that MYH1, SERCA1, SERCA2, Ca$_v$1.1 and RyR1 were all expressed. The double-immunopositive band seen in the RyR1 Western blot does not represent RyR3, since both bands were present when a RyR1-specific polyclonal antibody was used, thus the lower band is probably a degradation product. No bands were visualized when blots were probed with anti-CSQ1 antibodies (not shown), but a
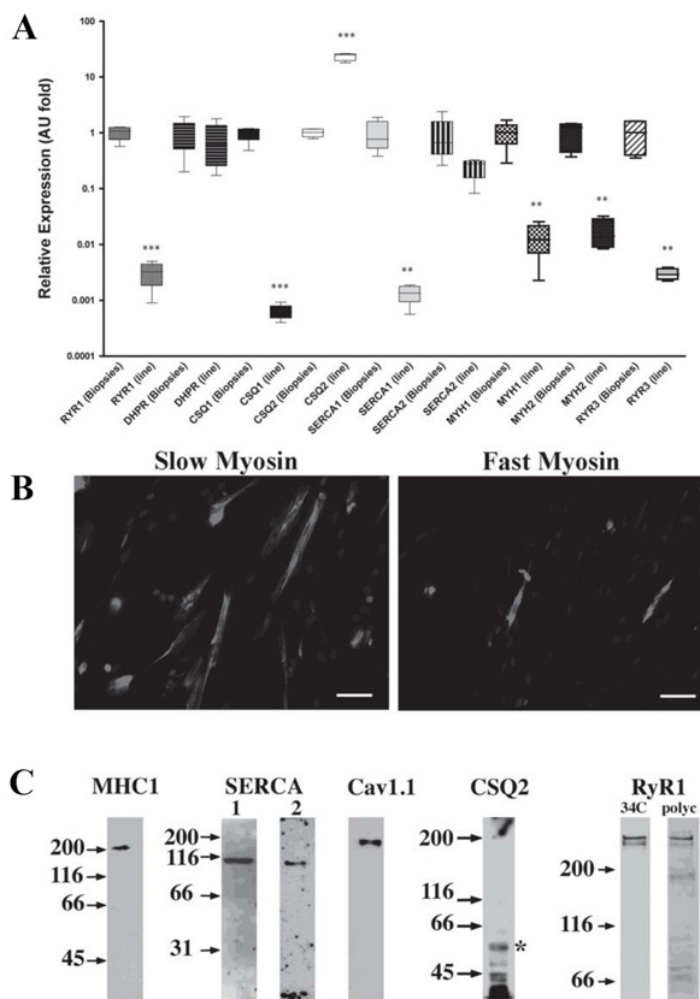
Figure 1   Expression of EC coupling-associated proteins in HMCL-7304-derived myotubes

(**A**) qPCR results of the relative expression levels of the indicated transcripts in HMCL-7304-derived myotubes compared with those in mature muscle biopsies. Expression levels were normalized for desmin content and are expressed as relative transcript content in biopsy/HMCL-7304-derived myotubes. The results are represented as box-and-whisker plots performed on four or five controls and on the mytoube cell line. ***$P < 0.0001$; **$P < 0.07$ (Student's t test). (**B**) Immunofluorescence of HMCL-7304-derived myotubes stained with anti-(fast myosin) and -(slow myosin) and DAPI and observed with a Leica DMR fluorescence microscope with a ×20 objective. Scale bar, 50 μm. (**C**) Western blot analysis of RyR1 and CASQ2 (70 μg/lane), Ca$_v$1.1, SERCA1, SERCA2 and MYH1 (MHC1) (50 μg/lane). Blots were prepared and developed as detailed in the Experimental section; for RyR1 the commercial monoclonal antibody 34C as well as the RyR1-specific polyclonal antibodies recognize the same high-molecular-mass band corresponding to the RyR. Thus the lower, less intense, immunopositive band probably represents a proteolytic product. The asterisk (*) indicates CSQ2.

band migrating with an approximate molecular mass of 55 kDa (asterisk) was present when myotube microsomes were probed with anti-CSQ2 antibodies.

Cellular localization of EC coupling proteins

In mature skeletal muscle, EC coupling occurs and is fully dependent on the architecture of highly structured intracellular Ca^{2+} release units, whereby the voltage-sensing L-type Ca^{2+} channel is present in the transverse tubules and faces the terminal cisternae of the SR containing the RyR1 Ca^{2+} release channels. The SR contains the Ca^{2+}-binding protein CSQ, whereas the SERCAs are located on the longitudinal SR. In order to define the cellular localization of these proteins in mature myotubes, we used a 3D-SIM microscope, because, compared

with conventional confocal fluorescence microscopy and STED (stimulated emission depletion) microscopy, it offers improved axial resolution (approximately 300 nm) [25]. Figure 2 shows the immunostaining of Ca$_v$1.1 and RyR1 both in myotubes (panels A–F) and in enzymatically dissociated mouse FDB fibres (panels G–I). As expected in FDB fibres, the staining with anti-Ca$_v$1.1 shows a double row of fluorescent particles (Figure 2G) that mostly overlap with particles which are stained with anti-RyR1 antibodies (Figure 2H). Human myotubes also show fluorescent particles whose distribution does not follow the highly regular pattern observed in mature FDB fibres. However, when observed at high magnification, it becomes apparent that human myotubes display areas containing multiple parallel longitudinal rows of fluorescence particles which are stained with anti-Ca$_v$1.1 antibodies (Figure 2D, double arrows). A large fraction of particles stained with anti-Ca$_v$1.1 antibodies
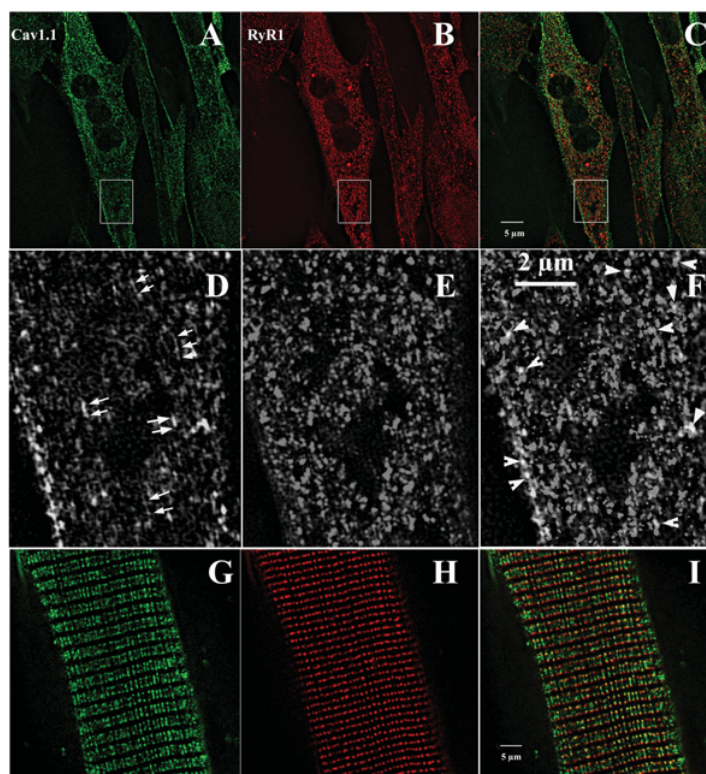
Figure 2   Cellular localization of RyR1 and Ca$_v$1.1 in differentiated myotubes compared with mouse FDB fibres by 3D-SIM microscopy

Human myotubes (**A–F**) and mouse FDB fibres (**G–I**) were stained with anti-Ca$_v$1.1 (**A**, **D** and **G**) and anti-RyR1 (**B**, **E** and **H**) antibodies and examined using a Zeiss Elyra/ZEN 2010 microscope with a ×63 oil Plan-Apochromat (1.4 NA) with three rotations. (**D**), (**E**) and (**F**) are higher magnifications of the boxed areas shown in (**A**), (**B**) and (**C**) respectively. Double arrows in (**D**) represent nascent T-tubules; arrowheads in (**F**) show co-localization of RyR1 and C$_v$a1.1.

co-localize with particles stained with anti-RyR1 antibodies (Figure 2F, arrowheads) and may represent Ca^{2+}-release units involved in EC coupling. In the next set of experiments, we assessed the EC coupling characteristics of HMCL-7304-derived myotubes, by studying RyR-mediated Ca^{2+} release and Ca$_v$1.1-mediated Ca^{2+} currents either by optical methods or by using the patch-clamp technique in the whole-cell configuration.

Functional properties and pharmacological activation of Ca^{2+} release

Figure 3 shows the results obtained in cells loaded with the fluorescent Ca^{2+} indicator Fluo-4; stimulation of cells with 60 mM KCl caused an immediate increase in the resting [Ca^{2+}]$_i$ which decayed back to resting values within approximately 5 s (Figure 3B); the peak increase in [Ca^{2+}]$_i$ was similar irrespective of whether cells were stimulated via activation of the DHPR L-type Ca^{2+} channel by KCl-induced depolarization, or by direct activation of the RyR1 with 4-chloro-m-cresol and caffeine (Figure 3C). Figures 3(D), 3(E) and 3(F) show concentration-dependent peak Ca^{2+}-release curves elicited by caffeine, 4-chloro-m-cresol and KCl respectively, as well as the calculated EC$_{50}$ values. These results are similar to those obtained in primary human muscle myotubes explanted from biopsies from control individuals [14,15].

We then investigated the voltage-dependence of membrane currents (I_{CaL}) from the DHPR in voltage-clamped HMCL-7304 myotubes. Starting from a holding potential of -80 mV and an initial pre-step to -40 mV, cells were stimulated by repetitive depolarizing steps of 800 ms in 10 mV increments to increasing membrane potentials. Figure 4(A) shows five steps of the stimulation protocol (upper trace) and the corresponding membrane currents (below) during control conditions (trace a, continuous line) and during inhibition of I_{CaL} with Cd^{2+} (trace b, dotted line). The calculated difference current (ΔI_{CaL}, trace c) is indicated by the dashed line and peak current amplitudes at the end of the depolarizing steps are used for further analysis. Figure 4(B) summarizes the voltage-dependence of current activation and reveals a half-maximal activation ($V_{1/2}$) at -9 mV.

A parallel investigation of electromechanical coupling was achieved using a combination of voltage-clamp and confocal Ca^{2+} imaging. Cells were imaged in the linescan mode at close proximity to the position of the patch pipette. Membrane depolarization triggered significant Ca^{2+} release, indicating functional coupling between the DHPR and RyR1. Depolarization-induced Ca^{2+} release was monitored and recorded in linescan images. Figure 5(A) shows a voltage-clamped HMCL-7304 myotube loaded with Fluo-3; the position of the linescan is indicated in the illustrated myotube. Short depolarization (50 ms) starting from the holding potential of -80 mV to $+10$ mV activated the DHPR and triggered Ca^{2+} release from the SR. The resulting Ca^{2+} transient is displayed in the linescan image and in the corresponding line profile. Of note is the slow return
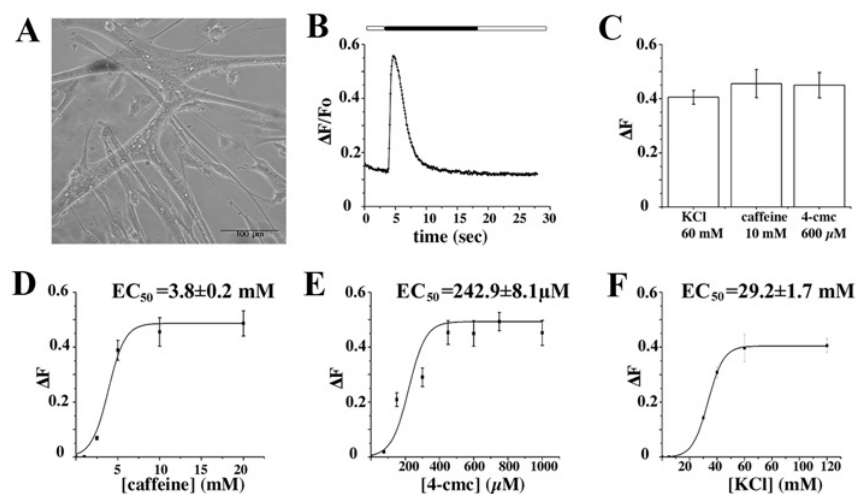
Figure 3 Characterization of RyR1-mediated Ca^{2+} release in HMCL-7304-derived myotubes

Myotubes were loaded with 5 μM Fluo-4 and Ca^{2+} release from intercellular stores was measured in Krebs–Ringer medium containing no added Ca^{2+} plus 100 μM La^{3+} as described in the Experimental section. (**A**) Photomicrograph of a fully differentiated myotube 5 days after differentiation. (**B**) Representative Ca^{2+} transient elicited by the addition of KCl; the unfilled bar above the trace indicates Krebs–Ringer medium containing 100 μM La^{3+}; the filled bar indicates stimulation with 60 mM KCl in 100 μM La^{3+}. Images were acquired every 100 ms with an electron multiplier Hamamatsu CCD C9100-13 camera and data were analysed using Metamorph imaging software. (**C**) Peak Ca^{2+} transients induced by 60 mM KCl, 10 mM caffeine or 600 μM 4-chloro-m-cresol (4-cmc); results are means$\pm$S.E.M. ΔF (peak fluorescence − resting fluorescence) of 15 measurements. (**D–F**) Dose–response curves to caffeine, 4-chloro-m-cresol (4-cmc) and KCl. Each point represents the mean$\pm$S.E.M. ΔF of at least ten different myotubes. The data were fitted using a Boltzmann equation using Origin 6.0 software.
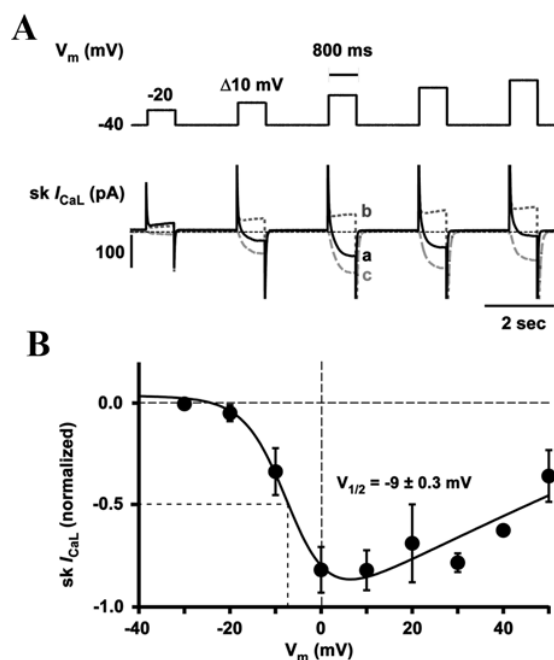
Figure 4 Skeletal L-type Ca^{2+} currents in HMCL-7304

(**A**) Whole-cell patch-clamp recordings of single HMCL-7304 myotubes: cells were stimulated from a holding potential of −80 mV and a pre-step to −40 mV to increasing depolarizing potentials (see stimulation protocol). Membrane currents (sk I_{CaL}) were recorded in control solution (trace a, continuous line) and during inhibition of I_{CaL} with CdCl$_2$ (500 μM, trace b, dotted line). Original current traces and calculated difference current (ΔI_{CaL}, trace c, dashed line) are shown. (**B**) Current–voltage relationship of sk I_{CaL} reveals a half-maximal current activation at −9$\pm$0.3 mV.

of the [Ca^{2+}]$_i$ to resting levels, which might be consistent with a low level of SERCA1 expression in immature myotubes (see Figure 1A). As expected, increasing membrane depolarization results in greater Ca^{2+} release, which saturates at a membrane potential of approximately 0 mV. Figure 5(B) shows the Ca^{2+} transient amplitude in response to increasing depolarization in a single protocol, and Figure 5(C) summarizes the voltage-dependence of Ca^{2+} release. In order to minimize side effects from long periods of scanning and accumulation of cytosolic Ca^{2+} due to slow Ca^{2+} extrusion processes, data points for peak Ca^{2+} transients in Figure 5(C) have been collected from repeated short linescan recordings (6 s). Ca^{2+} transients elicited under voltage clamp revealed a half-maximal release activation ($V_{1/2}$) at −32 mV.

DISCUSSION

In the present paper, we describe the biochemical, cellular and physiological characteristics of a novel cell line generated from human skeletal muscle. The necessity to establish cell lines of human origin from 'normal' individuals or patients affected by a number of neuromuscular conditions has been apparent for the last few decades, but early attempts to immortalize human myoblasts capable of differentiating into mature myotubes were unsuccessful (for example, see [26,27]). In the present paper, we report the successful myotube differentiation from myoblasts of the newly generated immortal human muscle cell line HMCL-7304 derived from a healthy individual and characterize its features at the biochemical, structural and functional levels, showing that its phenotype is similar to myotubes from primary cultures.

In the last few years, a number of groups have exploited vectors expressing hTERT and CDK4 and have reported successful immortalization of myoblasts from 'normal' individuals and individuals affected by various forms of muscular dystrophies
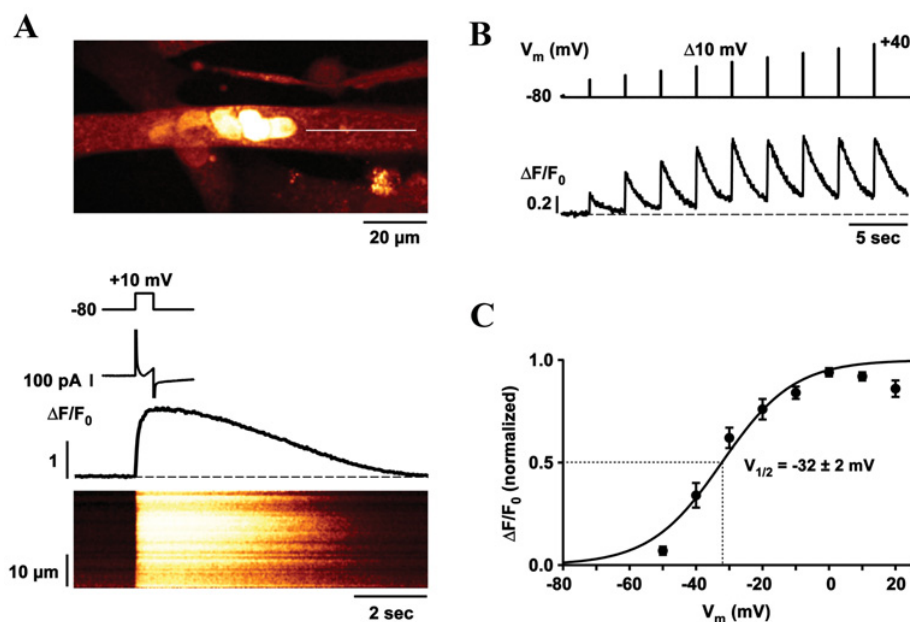
Figure 5   Depolarization-induced Ca^{2+} release in HMCL-7304 myotubes

(**A**) Patch-clamped HMCL-7304 myotube loaded with Fluo-3. The area of the linescan recording is indicated. Stimulation protocol, current response, line profile and linescan image of the Ca^{2+} transient are displayed in their respective temporal relation. (**B**) Stimulation protocol and line profile of the resulting Ca^{2+} transients in a single protocol reveals the increase in Ca^{2+} release upon increasing membrane depolarization. (**C**) Voltage-dependence of Ca^{2+} release. Peak Ca^{2+} transient amplitudes have been extracted and plotted as a function of the stimulation potential. Half-maximal Ca^{2+} release amplitude is achieved at -32 ± 2 mV.

and dysferlinopathies [16–20,28]. The possibility of generating such immortalized cell lines able to differentiate into myotubes constitutes an important tool to investigate human neuromuscular diseases much as the murine skeletal muscle C2C12 cell line has been exploited in the last few decades by laboratories worldwide to investigate key aspects of skeletal muscle physiology and plasticity. Therefore there is high demand for a reliable human skeletal cell line to fill the gap between understanding the pathophysiological mechanisms and the development of therapeutic strategies for human neuromuscular disorders. Nevertheless, although the use of an immortalized cell line has many advantages over primary cultures, the process of immortalization is known to modify many physiological parameters ranging from differentiation and secretion, to the expression of specific protein isoforms. For this reason, we characterized the EC coupling machinery and Ca^{2+} homoeostasis of HMCL-7304-derived myotubes. We chose to verify the levels of expression of the transcripts encoding the main components of skeletal muscle EC coupling, as well as their main isoforms and compared them with the levels found in biopsies from human skeletal muscle fibres from normal individuals. Transcripts encoding RyR1, CSQ1 and SERCA1 were significantly down-regulated as was RyR3, an isoform that is thought to be more abundantly expressed in developing muscles. On the other hand, Ca$_v$1.1 was expressed to similar levels in both mature fibres and myotubes and produced large Ca^{2+} currents, as shown in patch–clamp measurements. These results are in contrast with what occurs during skeletal muscle development, where components of the SR appear at an earlier stage of development compared with the transverse tubules containing the DHPR L-type Ca^{2+} channel [29–31]. Interestingly, the relative mRNA expression of HMCL-7304-derived myotubes was either similar

to that of mature biopsies (SERCA2) or up-regulated (CSQ2). Thus it seems that the HMCL-7304 cell line has more of the characteristics of slow-twitch than that of fast-twitch muscle. This is confirmed further by the predominant expression of slow myosin compared with fast myosin in differentiated HMCL-7304 myotubes. There are several possible reasons for this observation: (i) either satellite stem cells are, by default, slow-twitch-like and it is the influence of innervation or electrical activity that enables them to become fast or slow [32], (ii) the immortalization procedure 'selects' satellite stem cells that have a 'slow muscle' phenotype, and/or (iii) as reported in hindlimb muscles of adult rats, the satellite cells contained within fast or slow twitch fibres are intrinsically different subpopulations [33] so that the HMCL-7304 cell line that originated from dorsal muscles resembles more a slow-twitch muscle from which it originated.

Two noticeable differences in the physiological characteristics of human cultured myotubes and mature fibres are that human (as opposed to rodent) -derived primary myotubes do not contract [34], and the timescale of the depolarization-induced Ca^{2+} transient occurs in hundreds of milliseconds in myotubes, whereas it lasts only a few milliseconds in mature fibres. Although the lack of contracture of myotubes derived from the immortalized human muscle cell line probably reflects the composition of the actomyosin contractile machinery, the slow Ca^{2+} transients observed in myotubes probably reflects the lower level of expression of SERCA1 and the absence of a highly organized micro-architecture. After Ca^{2+} release, cytosolic Ca^{2+} is rapidly removed and pumped back into the SR lumen by the SERCA, which is the main protein of non-junctional SR in skeletal muscle fibres [35]. Reduced SERCA1 expression levels as shown in the HMCL-7304 cell line have a significant impact

on the Ca^{2+}-removal kinetics, leading to deceleration of Ca^{2+} re-uptake compared with normal muscle fibres. Thus lack of mature subcellular architectural organization and reduction in SERCA1 expression may explain the slow Ca^{2+} removal after release in the HMCL-7304 cell line.

In mature fibres, four $Ca_v1.1$ subunits on the T-tubular face in square formation, referred to as tetrads, are directly opposite the four subunits of one RyR1 tetramer on the SR junctional membrane, to form the Ca^{2+}-release units [30]. In intact FDB fibres, the Ca^{2+} release units form double rows on each side of the Z line. The highly organized arrangement is characteristic of mature skeletal muscle and is probably one of the features allowing the extremely rapid Ca^{2+} release kinetics upon T-tubule membrane depolarization. As is evident by the 3D-SIM images, HMCL-7304 myotubes show distinct rows of $Ca_v1.1$ that overlap, at least in part, with RyR1 and we believe that these structures may represent the Ca^{2+}-release units of the HMCL-7304 myotubes. This conclusion is consistent with whole patch-clamp measurements showing that voltage-induced Ca^{2+} release is highly functional in these myotubes, indicating direct coupling between sarcolemmal DHPRs and RyR1 despite structural immaturity. HMCL-7304 myotubes exhibit Cd^{2+}-sensitive Ca^{2+} currents, having half-maximal current activation at -9 mV, a value that is comparable with obtained by others [36,37]. Parallel imaging revealed that the voltage-dependence of Ca^{2+} release ($V_{1/2}$) was -32 mV in the present study and -29.4 mV in non-immortalized primary human myotubes from control individuals [38], which is similar to the values (-26 mV) obtained on primary myotubes from wild-type mice [39]. Furthermore, the process of immortalization does not affect the pharmacological characteristics of RyR1 activation since the caffeine and 4-chloro-m-cresol dose–response curves of the HMCL-7304 cell line are similar to those of non-immortalized human myotubes [14,40] or RyR1 isolated from mature rodent muscles [41].

In conclusion, in the present study, we characterized a human muscle cell line derived from a 'normal' individual and show that it retains a pattern of expression of proteins involved in EC coupling similar to that of slow-twitch muscles. The ability to perform pharmacological and electrophysiological studies illustrates the potential use of such a biological tool to a variety of approaches from studying the effect of mutations and gene silencing to testing drugs and pharmacological agents aimed at correcting Ca^{2+} dysregulation as occurs in a variety of neuromuscular disorders including core myopathies.

AUTHOR CONTRIBUTION

Ori Rokach performed experiments and analysed data; Nina Ullrich performed electrophysiological experiments and analysed the data; Martin Rausch performed the 3D-SIM experiments; Vincent Mouly established the immortalized cell line; Haiyan Zhou designed experiments and analysed data; Francesco Muntoni designed experiments and analysed data; Francesco Zorzato performed the 3D-SIM experiments, took care of the conception and design of the experiments, collection and analysis of data, and drafting of the paper; Susan Treves took care of the conception and design of the experiments, collection and analysis of data, and drafting of the paper.

ACKNOWLEDGEMENTS

We thank Professor Vincenzo Sorrentino for kindly providing the polyclonal rabbit anti-RyR1 antibody.

FUNDING

REFERENCES

1   Ravenscroft, G., Nowak, K. J., Jackaman, C., Clément, S., Lyons, M. A., Gallagher, S., Bakker, A. J. and Laing, N. G. (2007) Dissociated flexor digitorum brevis myofiber culture system: a more mature muscle culture system. Cell Motil. Cytoskeleton **64**, 727–738

2   Calderon, J. C., Bolaños, P., Torres, S. H., Rodríguez-Arroyo, G. and Caputo, C. J. (2009) Different fibre populations distinguished by their calcium transient characteristics in enzymatically dissociated murine flexor digitorum brevis and soleus muscles. J. Muscle Res. Cell Motil. **30**, 125–137

3   Calderon, J. C., Bolaños, P. and Caputo, C. (2011) Kinetic changes in tetanic Ca^{2+} transients in enzymatically dissociated muscle fibres under repetitive stimulation. J. Physiol. **589**, 5269–5283

4   Lovering, R. M., Michaelson, L. and Ward, C. W. (2009) Malformed mdx myofibers have normal cytoskeletal architecture yet altered EC coupling and stress-induced Ca^{2+} signaling. Am. J. Physiol. Cell. Physiol. **297**, C571–C580

5   Brown, L. D., Rodney, G. G., Hernàdez-Ochoa, E. and Schneider, M. F. (2007) Ca^{2+} sparks and T-tubule reorganization in dedifferentiating adult mouse skeletal muscle fibers. Am. J. Physiol. Cell. Physiol. **292**, C1156–C1166

6   Yasin, R., Van Beers, G., Nurse, K. C., Al-Ani, S., Landon, D. N. and Thompson, E. J. (1977) A quantitative technique for growing human adult skeletal muscle in culture starting from mononucleated cells. J. Neurol. Sci. **32**, 347–359

7   Zuurveld, J. G. E. M., Oosterhof, A., Veerkamp, J. H. and van Moerkerk, H. T. B. (1985) Oxidative metabolism of cultured human skeletal muscle cells in comparison with biopsy material. Biochim. Biophys. Acta **844**, 1–8

8   Blau, H. M. and Webster, C. (1981) Isolation and characterization of human muscle cells. Proc. Natl. Acad. Sci. U.S.A. **78**, 5623–5627

9   Censier, K, Urwyler, A., Zorzato, F. and Treves, S. (1991) Intracellular calcium homeostasis in human primary muscle cells from malignant hyperthermia-susceptible and normal individuals: effect of overexpression of recombinant wild-type and Arg163Cys mutated ryanodine receptors. J. Clin. Invest. **15**, 1233–1242

10 Yaffe, D. and Saxel, O. (1977) Serial passaging and differentiation of myogenic cells isolated from dystrophic mouse muscle. Nature **270**, 725–727

11 Lorenzon, P., Grohovaz, F. and Ruzzier, F. (2000) Voltage- and ligand-gated ryanodine receptors are functionally separated in developing C2C12 mouse myotubes. J. Physiol. **525**, 499–507

12 McMahon, D. K., Anderson, P. A., Nassar, R., Bunting, J. B., Saba, Z., Oakeley, A. E. and Malouf, NN. (1994) C2C12 cells: biophysical, biochemical, and immunocytochemical properties. Am. J. Physiol. Cell. Physiol. **266**, C1795–C1802

13 Gutierrez-Martin, Y., Martin-Romero, F. J. and Henao, F. (2005) Store operated calcium entry in differentiated C2C12 skeletal muscle cells. Biochim. Biophys. Acta **1711**, 33–40

14 Ducreux, S., Zorzato, F., Muller, C., Sewry, C., Muntoni, F., Quinlivan, R., Restagno, G., Giraird, T. and Treves, S. (2004) Effect of ryanodine receptor mutations on interleukin-6 release and intracellular calcium homeostasis in human myotubes from malignant hyperthermia-susceptible individuals and patients affected by central core disease. J. Biol. Chem. **279**, 43838–43846

15 Treves, S., Vukcevic, M., Jeannet, P. Y., Levano, S., Girard, T., Urwyler, A., Fischer, D., Voit, T., Jungbluth, H., Lillis, S. et al. (2010) Enhanced excitation-coupled Ca^{2+} entry induces nuclear translocation of NFAT and contributes to IL-6 release from myotubes from patients with central core disease. Hum. Mol. Genet. **20**, 589–600

16 Zhu, C. H., Mouly, V., Cooper, R. N., Mamchaoui, K., Bigot, A., Shay, J. W., Di Santo, J. P., Butler-Browne, G. S. and Wright, W. E. (2007) Cellular senescence in human myoblasts is overcome by human telomerase reverse transcriptase and cyclin-dependent kinase 4: consequences in aging muscle and therapeutic strategies for muscular dystrophies. Aging Cell **6**, 515–523

17 Mamchaoui, K., Trollet, C., Bigot, A., Negroni, E., Chaouch, S., Wolff, A., Kandalla, P. K., Marie, S., Di Santo, J., St Guily, J. L. et al. (2011) Immortalized pathological human myoblasts: towards a universal tool for the study of neuromuscular disorders. Skeletal Muscle **1**, 34

18 Hashimoto, N., Kiyono, T., Wada, M. R., Shimizu, S., Yasumoto, S. and Ingagawa, M. (2005) Immortalization of human myogenic progenitor cell clone retaining multipotentiality. Biochem. Biophys. Res. Commun. **348**, 1383–1388

19 Shiomi, K., Kiyono, T., Okamura, K., Uezumi, M., Goto, Y., Yasumoto, S., Shimizu, S and Hashimoto, N. (2011) CDK4 and cyclin D1 allow human myogenic cells to recapture growth property without compromising differentiation potential. Gene Ther. **18**, 857–866

20 Philippi, S., Bigot, A., Marg, A., Mouly, V., Spuler, S. and Zacharias, U. (2012) Dysferlin-deficient immortalized human myoblasts and myotubes as a useful tool to study dysferlinopathy. PLoS Curr. **4**, RRN1298

21 Prosser, B. L., Hernandez-Ochoa, E. O., Zimmer, D. B. and Schneider, M. F. (2009) The Qγ component of intra-membrane charge movement is present in mammalian muscle fibres, but suppressed in the absence of S100A1. J. Physiol. **587**, 4543–4559

22 Barrett, S. D. (2002) Software for scanning microscopy. Proc. R. Microsc. Soc. **37**, 167–174

23 Mosca, B., Delbono, O., Messi, L. M., Bergamelli, L., Wang, Z. M., Vukcevic, M., Lopez, R., Treves, S., Nishi, M., Takeshima, H. et al. (2013) Enhanced dihydropyridine receptor calcium channel activity restores muscle strength in JP45/CASQ1 double knockout mice. Nat. Commun. **4**, 1541

24 Anderson, A. A., Treves, S., Biral, D., Betto, R., Sandonà, D., Ronjat, M. and Zorzato, F. (2003) The novel skeletal muscle sarcoplasmic reticulum JP-45 protein: molecular cloning, tissue distribution, developmental expression, and interaction with α1.1 subunit of the voltage-gated calcium channel. J. Biol. Chem. **278**, 39987–39992

25 Schermelleh, L., Heintzmann, R. and Leonhardt, H. (2010) A guide to super-resolution fluorescence microscopy. J. Cell Biol. **190**, 777–791

26 DeCaprio, J. A., Ludlow, J. W., Figge, J., Shew, J. Y., Huang, C. M., Lee, W. H., Marsilio, E., Paucha, E. and Livingston, D. M. (1988) SV40 large tumor antigen forms a specific complex with the product of the retinoblastoma susceptibility gene. Cell **54**, 275–283

27 Simon, L. V., Beauchamp, J. R., O'Hare, M. and Olsen, I. (1996) Establishment of long-term myogenic cultures from patients with Duchenne muscular dystrophy by retroviral transduction of a temperature-sensitive SV40 large T antigen. Exp. Cell Res **224**, 264–271

28 Zhou, H., Rokach, O., Feng, L., Munteanu, I., Mamchaoui, K., Wilmhurst, J. M., Sewry, C., Manzur, A. Y., Pillay, K., Mouly, V. et al. (2013) RyR1 deficiency in congenital myopathies disrupts excitation–contraction coupling. Hum. Mutat. **34**, 986–996

29 Franzini-Armstrong, C. and Jorgensen, A. O. (1994) Structure and development of E–C coupling units in skeletal muscle. Annu. Rev. Physiol. **56**, 509–534

30 Flucher, B. E., Andrews, S. B., Fleischer, S., Marks, A. R., Caswell, A. and Powell, J. A. (1993) Triad formation: organization and function of the sarcoplasmic reticulum calcium release channel and triadin in normal and dysgenic muscle *in vitro*. J. Cell Biol. **123**, 1161–1174

31 Al-Qusari, L. and Laporte, J. (2011) T-tubule biogenesis and triad formation in skeletal muscle and implication in human diseases. Skeletal Muscle **1**, 26

32 Nedachi, T., Fujita, H. and Kanzaki, M. (2008) Contractile C2C12 myotube model for studying exercise-inducible responses in skeletal muscle. Am. J. Physiol. Endocrinol. Metab. **295**, E1191–E1204

33 Kalhovde, J. M., Jerkovic, R., Sefland, I., Cordonnier, C., Calantibodiesria, E., Schiaffino, S. and Lømo, T. (2005) "Fast" and "slow" muscle fibres in hindlimb muscles of adult rats regenerate from intrinsically different satellite cells. J. Physiol. **562**, 847–857

34 Bandi, E., Jevsek, M., Mars, T., Jordana, M., Formaggio, E., Sciancalepore, M., Fumagalli, G., Grubic, Z., Ruzzier, F. and Lorenzon, P. (2008) Neural agrin controls maturation of the excitation–contraction coupling mechanism in human myotubes developed *in vitro*. Am. J. Physiol. Cell. Physiol. **294**, C66–C73

35 Periasamy, M. and Kalyanasundaram, A. (2007) SERCA pump isoforms: their role in calcium transport and disease. Muscle Nerve **35**, 430–442

36 Delbono, O. (1992) Calcium current activation and charge movement in denervated mammalian skeletal muscle fibres. J. Physiol. **451**, 187–203

37 Hernandez-Ochoa, E. O. and Schneider, M. F. (2012) Voltage clamp methods for the study of membrane currents and SR Ca^{2+} release in adult skeletal muscle fibers. Prog. Biophys. Mol. Biol. **108**, 98–118

38 Ullrich, N. D., Fischer, D., Kornblum, C., Walter, M. C., Niggli, E., Zorzato, F. and Treves, S. (2011) Alterations of excitation–contraction coupling and excitation coupled Ca^{2+} entry in human myotubes carrying *CAV3* mutations linked to rippling muscle. Hum. Mutat. **32**, 309–317

39 Chelu, M. G., Goonasekera, S. A., Durham, W. J., Tang, W., Lueck, J. D., Riehl, J., Pessah, I. N., Zhang, P., Bhattacharjee, M. B., Dirksen, R. T. and Hamilton, S. L. (2006) Heat- and anesthesia-induced malignant hyperthermia in an RyR1 knock-in mouse. FASEB. J. **20**, 329–330

40 Kaufmann, A., Kraft, B., Michalek-Sauberer, A., Weindlmayr, M., Kress, H. G., Steinboeck, F. and Weigl, L. G. (2012) Novel double and single ryanodine receptor 1 variants in two Austrian malignant hyperthermia families. Anesth. Analg. **114**, 1017–1025

41 Zorzato, F., Scutari, E., Tegazzin, V., Clementi, E. and Treves, S. (1993) Chlorocresol: an activator of ryanodine receptor-mediated Ca^{2+} release. Mol. Pharmacol. **44**, 1192–1201

2. RyR1 deficiency in congenital myopathies disrupts excitation-contraction coupling

The highly specialized architecture of skeletal muscle membranes allows ECC to occur within milliseconds and permits the interaction between the RyR1 and the DHPR. Upon membrane depolarization, RyR1 mediates the release of Ca^{2+} from the SR. In this publication we report abnormal distribution and expression of the RyR1 and the DHPR in patients with recessive RYR1 mutations leading to neuromuscular disorders. Histopathological sections from patients with heterozygous compound recessive RYR1 mutations, show a reduction in the expression of the RyR1 receptor and accumulation of the signal arising from the DHPR in areas surrounding the cores. Similar accumulations were observed in histopathological sections of muscles from patients with recessive homozygous mutations. The relative expression of the RYR1 mRNA extracted from muscles of patients with recessive RYR1 mutations is significantly lower compared to that of muscles from healthy individuals. Similar results were observed with the protein levels of the RyR1 in these patients. Unexpectedly, the expression of the 3 isoforms of InsP3R were increased significantly (*ITPR1-ITPR3*). A cellular model of reduced RyR1 expression was created by silencing the expression of RyR1, using siRNA in the HMCL- 7304 immortalized human muscle cell line (described in the previous paper). The increase of the 3 isoforms of the InsP3R receptors was also observed in this cellular model prompting us to hypothesize that InsP3R were trying to compensate for the reduced RyR1 expression. In order to test our hypothesis, we activated the RyR1 pharmacologically with 600 µM of 4-cmc and 60mM KCl in cells that were either pre-treated with Xestospongin (an inhibitor of InsP3R) or in control cells and in cells that were either treated with siRYR1 to silence the RyR1 or in control cells. Interestingly, RyR1 silencing significantly reduced Ca^{2+} release from the SR, which disproved our initial hypothesis for functional compensation from the InsP3R.

Moreover, addition of Xestospongin C in cells treated with siRyR1, did not reduce Ca^{2+} release from the SR. These studies **do not support** a hypothesis that InsP3R can compensate functionally for the absence of RyR1.

Author contribution: In the 2nd publication entitled "RyR1 deficiency in congenital myopathies disrupts excitation-contraction coupling" Haiyan Zhou performed the experiments in figures 1-3,5 and 6, while Ori Rokach performed experiments relate to figures 4 and 7.

RyR1 Deficiency in Congenital Myopathies Disrupts Excitation–Contraction Coupling

Haiyan Zhou,[1] Ori Rokach,[2] Lucy Feng,[1] Iulia Munteanu,[1] Kamel Mamchaoui,[3] Jo M. Wilmshurst,[4] Caroline Sewry,[1] Adnan Y. Manzur,[1] Komala Pillay,[5] Vincent Mouly,[2] Michael Duchen,[6] Heinz Jungbluth,[7,8,9] Susan Treves,[2,10]* and Francesco Muntoni[1]*

[1]Dubowitz Neuromuscular Centre, Institute of Child Health, University College London, London, UK; [2]Department of Anaesthesia and Biomedicine, Basel University and University Hospital Basel, Basel, Switzerland; [3]UM76 Université Pierre et Marie Curie, UMRS974 INSERM, UMR 7215 CNRS, Institut de Myologie AIM, Groupe hospitalier Pitié-Salpétrière, 47 bd de l'Hôpital, Paris, France; [4]Department of Paediatric Neurology, School of Child and Adolescent Health, University of Cape Town, Red Cross Children's Hospital, Cape Town, South Africa; [5]Department of Paediatric Pathology, School of Child and Adolescent Health, University of Cape Town, Red Cross Children's Hospital, Cape Town, South Africa; [6]Cell and Developmental Biology, University College London, London, UK; [7]Department of Paediatric Neurology, Evelina Children's Hospital, London, UK; [8]Clinical Neuroscience Division, IoP, King's College, London, UK; [9]Randall Division of Cell and Molecular Biophysics, Muscle Signalling Group King's College London, London, UK; [10]Department of Life Sciences, University of Ferrara, Ferrara, Italy

ABSTRACT: In skeletal muscle, excitation–contraction (EC) coupling is the process whereby the voltage-gated dihydropyridine receptor (DHPR) located on the transverse tubules activates calcium release from the sarcoplasmic reticulum by activating ryanodine receptor (RyR1) Ca^{2+} channels located on the terminal cisternae. This subcellular membrane specialization is necessary for proper intracellular signaling and any alterations in its architecture may lead to neuromuscular disorders. In this study, we present evidence that patients with recessive RYR1-related congenital myopathies due to primary RyR1 deficiency also exhibit downregulation of the alfa 1 subunit of the DHPR and show disruption of the spatial organization of the EC coupling machinery. We created a cellular RyR1 knockdown model using immortalized human myoblasts transfected with RyR1 siRNA and confirm that knocking down RyR1 concomitantly downregulates not only the DHPR but also the expression of other proteins involved in EC coupling. Unexpectedly, this was paralleled by the upregulation of inositol-1,4,5-triphosphate receptors; functionally however, upregulation of the latter Ca^{2+} channels did not compensate for the lack of RyR1-mediated Ca^{2+} release. These results indicate that in some patients, RyR1 deficiency concomitantly alters the expression pattern of several proteins involved in calcium homeostasis and that this may influence the manifestation of these diseases.

Hum Mutat 34:986–996, 2013. © 2013 Wiley Periodicals, Inc.

KEY WORDS: ryanodine receptor; dihydropyridine; RYR1; congenital myopathies

Introduction

The precise regulation of intracellular calcium homeostasis is critical for normal skeletal muscle development and function. Excitation–contraction (EC) coupling requires the correct assembly, distribution, and interaction of a number of proteins residing in the sarcoplasmic reticulum (SR), the organelle of striated muscle dedicated to calcium homeostasis. Two key elements involved in calcium release are the voltage-gated dihydropyridine receptor (DHPR; MIM #114208), located on the transverse tubules, and the ryanodine receptor (RyR1; MIM #180901), the principal calcium release channel of skeletal muscle situated in the terminal cisternae of the SR [Nakai et al., 1996]. The predicted structure of the RyR1 suggests that the calcium release pore is located in the C-terminal domain of the protein, whereas the N-terminal domain constitutes the foot structure that interacts with DHPR [Dulhunty and Pouliquin, 2003; Ramachandran et al., 2009; Van Petegem, 2012]. The direct physical interaction between DHPR and RyR1 is essential for skeletal muscle EC coupling and any alterations in the subcellular distribution of proteins or membranes involved EC coupling can lead to impaired muscle function [Oddoux et al., 2009; Pan et al., 2002].

Disturbance of calcium homeostasis due to defects in RyR1 is the underlying feature of the malignant hyperthermia susceptibility (MIM #145600) trait, a pharmacogenetic reaction to volatile anesthetics and muscle relaxants, and a wide range of

congenital myopathy phenotypes, including dominantly inherited central core disease (CCD; MIM #117000) and recessively inherited multiminicore disease (MIM #255320) with or without opthalmoplegia [Jungbluth et al., 2002; 2005; Quane et al., 1993; Zhou et al., 2006; 2007], subgroups of centronuclear myopathy, congenital fiber type disproportion, and the King-Denborough Syndrome [Clarke et al., 2010; Dowling et al., 2011; Jungbluth et al., 2007; Wilmshurst et al., 2010]. Although dominantly inherited *RYR1*-related congenital myopathies have been extensively studied and are usually attributed to RyR1 channels that are either "leaky" or show impaired calcium conductance [Dirksen and Avila, 2002; Treves et al., 2008], the pathogenesis of recessively inherited *RYR1*-related myopathies is not well understood, though a decrease in RyR1 protein content has been reported in muscle biopsies from some patients [Wilmshurst et al., 2010; Zhou et al., 2007]. Besides mutations in the *RYR1*, substitutions in other genes linked to neuromuscular disorders, encoding proteins involved in EC coupling have so far been reported only for *CACNA1*, the gene encoding the alfa 1 subunit of the DHPR ($Ca_v1.1$) in patients with malignant hyperthermia [Monnier et al., 1997; Pirone et al., 2010; Toppin et al., 2010]. We recently reported that a patient with periodic paralysis who harbored recessively inherited *RYR1* mutations [Zhou et al., 2010] with no *CACNA1S* mutation, had a marked reduction of RyR1 protein and a disruption of RyR1/$Ca_v1.1$ colocalization, indicating potential secondary effects of certain *RYR1* mutations on key proteins of the EC coupling machinery.

In the present investigation, we extended these findings and report abnormal expression and distribution of $Ca_v1.1$ in muscle biopsies from a number of patients with recessive *RYR1* mutations with reduced RyR1 content. Mimicking RyR1 depletion in human myotubes using a *RYR1* siRNA knockdown approach caused a decrease in $Ca_v1.1$ with a concomitant upregulation of inositol-1,4,5-trisphosphate receptors (IP3R; MIM #147265). These results provide new insights into the pathogenesis of recessive *RYR1*-related myopathies with primary RyR1 deficiency.

Materials and Methods

Muscle Biopsies

Studies on muscle biopsies from patients were approved by the author's Institutional Ethical Committee and conducted under the Declaration of Helsinki. Patients were encoded to protect their confidentiality, and written informed consent obtained. Routine histopathological studies were performed according to standard procedures. All patients presented in this study have a clear clinical and histological diagnosis of a congenital myopathy, and were molecularly diagnosed as having *RYR1* mutations. Control muscle biopsies were from donors with no neuromuscular diseases. RNA samples were studied in nineteen patients and nine controls; immunohistochemical studies were performed in four patients and three controls; Western blot studies were performed in two patients and three controls.

Molecular Genetics

The genetic information of all patients was taken from the genetic reports. The *RYR1* nucleotide numbering is based on transcript variant NM_00540.2, where the nucleotide numbering reflects cDNA numbering with +1 corresponding to the A of the ATG translation initiation codon in the reference sequence, according to journal guidelines (www.hgvs.org/mutnomen). The initiation codon is

codon 1. The variants reported have been submitted to the Leiden RYR1 locus specific database (http://www.lovd.nl/RYR1).

Immortalization and Culture of Skeletal Muscle Cell Line

Human satellite cells were derived from the skeletal muscle biopsy of a 19-year-old female donor with no neuromuscular disorder. Skeletal muscle cell line immortalization was performed as previously described [Mamchaoui et al., 2011; Zhu et al., 2007]. Briefly, cultured cells were double transfected by recombinant retroviruses containing the telomerase (hTERT) cDNA and Cdk4 cDNA, followed by clonal selection of myogenic lines. Immortalized myoblasts were maintained in skeletal muscle cell growth medium (Promo-Cell, Heidelberg, Germany) in low oxygen atmosphere (5% O_2 and 5% CO_2) at 37°C.

Immunofluorescence

All cryosections from muscle biopsies were cut at a thickness of 8 μm for immunohistochemistry. Sections were incubated with primary antibodies at room temperature for 1 hr, washed in 0.1 M PBS pH 7.2 and incubated with secondary antibody conjugated to Alexa 488 and biotinylated secondary antibody for 1 hr at room temperature, followed by thorough rinsing in PBS. After washing, muscle sections were incubated with streptavidin conjugated to Alexa 594 for 15 min at room temperature then washed and mounted using Hydromount mounting medium (National Diagnostics, Georgia, USA). Images were digitally captured using Metamorph software. For immunofluorescence on myotubes, glass coverslip grown cells were fixed for 30 min in 3.7% paraformaldehyde in PBS; cells were rinsed with PBS and permeabilized with 1% Triton X-100 in PBS for 30 min. After incubation with blocking buffer (1% blocking buffer, Roche, in PBS) for 60 min at room temperature, slides were processed as described above. The primary antibodies used for immunohistochemistry were mouse anti-RyR1 monoclonal antibody (1:500; Abcam, Cambridge, UK), goat anti- $Ca_v1.1$ polyclonal antibody (1:200; Santa Cruz, Texas, USA), and rabbit anti-ß-tubulin (1:20; Santa Cruz, Texas, USA).

cDNA Synthesis and Quantitative Real-Time PCR

Total RNA was extracted from muscle biopsies using the RNeasy kit (Qiagen, Crawley, UK); 500 ng of each RNA sample was used for first-strand cDNA synthesis with Superscript III reverse transcription kit (Invitrogen, Paisley, UK). Quantitative real-time PCR products of *RYR1*, *CACNA1S*, and *DES* were amplified with the TaqMan universal PCR Master Mix (Applied Biosystems, Leusden, Netherlands). Samples were incubated in a 25 μl reaction mix according to manufacturer's instructions. Quantitative real-time PCR was performed using Applied Biosystem fast 7500 Real Time PCR System using the recommended program: activation at 50°C for 2 min and 95°C for 10 min, 40 cycles of 95°C for 15 sec and 60°C for 1 min. Quantification was based on the comparative ΔΔCt method. One of the samples treated with negative control siRNA was used to calibrate the data and to analyze results. For *ITPR1*, *ITPR2*, and *ITPR3* quantitative real-time PCR samples were amplified with MESA Blue qPCR kit (Eurogentec, Seraing, Belgium). Gene specific qPCR primers, including *ITPR1*, *ITPR2*, *ITPR3*, *GAPDH*, and *DES*, were commercially available from Qiagen. Samples were incubated in a 25 μl reaction mix according to manufacturer's instructions. Quantitative real-time PCR was performed using Applied Biosystem fast 7500 Real Time PCR System using the recommended program: activation at 95°C for 5 min, 40 cycles of 95°C for 3 sec, and 60°C

for 1 min. Quantification was based on concurrent standard curves produced from serial dilutions of control cDNA from untreated cultured myotubes. *DES* and *GAPDH* were used as internal reference genes. The expression of *ITPRs* in cultured myotubes or muscle biopsies were normalized by DES or GAPDH, and calibrated by taking the ratio of one of the control samples as 1.0. Total RNA was extracted from human myotubes using Trizol (Invitrogen, Lucerne, Switzerland) and cDNA synthesized with the High Capacity cDNA synthesis kit from Applied Biosystem and the following primers: MYH 1-Myosin heavy chain, forward: 5′ GGG AGA CCT AAA ATT GGC TCA A 3′, reverse: 5′ TTG CAG ACC GCT CAT TTC AAA 3′; TNNT1—Troponin T1, forward: 5′ TGA TCC CGC CAA AGA TCC C 3′, reverse: 5′ TCT TCC GCT GCT CGA AAT GTA 3′; DAG1—Dystroglycan 1, forward: 5′ AGC AAA GGA TTG ACC TCC TGC 3′, reverse: 5′ CCA CCG GCA CTA ATT TCA TGT T 3′; Desmin, forward: 5′ AAC CAG GAG TTT CTG ACC ACG 3′, reverse: 5′ TTG AGC CGG TTC ACT TCG G 3′; GAPDH, forward: 5′ CTG GGC TAC ACT GAG CAC C 3′, reverse: 5′AAG TGG TCG TTG AGG GCA ATG 3′. As well as the ITPR primers described above. Transcript levels were normalized to GAPDH expression levels.

Western Blotting

Total protein was extracted from cells lysates or frozen skeletal muscle sections in sampling buffer consisting of 75 mM Tris–HCl, 1% SDS, and cocktail of protease inhibitor (Roche, Burgess Hill, UK). Protein concentration was quantified by the BCA protein assay kit (Pierce, Rockford, IL, USA). Thirty micrograms of proteins were loaded and separated using NuPAGE Precast gels (3%–8% Tris–acetate; Invitrogen) and then transferred electrophoretically to nitrocellulose membrane (GE Healthcare, Buckinghamshire, UK). The membrane was blocked with 5% goat serum (Sigma, Dorset, UK) in PBS buffer with 0.5% Tween-20 (PBS-T) and then probed with primary antibodies at room temperature for 1 hr or 4°C overnight. After washing in PBS-T, membranes were incubated with HRP-antimouse or HRP-antirabbit IgG (the Jackson Laboratory, West Grove, PA, USA; 1:50,000) for 1 hr at room temperature. Immunoreactivity was visualized using enhanced chemiluminescence detection kit (GE Healthcare). Semi-quantification of the bands was performed by densitometric analysis and data was processed using the Image J software.

The primary antibodies used in this study include mouse monoclonal anti-RyR1 (Abcam; 1:2,500), rabbit anti-Ca$_v$1.1 (Santa Cruz; 1:1,000), mouse monoclonal-antidesmin (DAKO, Glostrup, Denmark; 1:2,000), mouse monoclonal anti-IP3R III (BD, Devon UK; 1:1,000), mouse monoclonal anti-SERCA2 antibody (Abcam; 1:1,000), mouse monoclonal anti-α-actinin 2 (Sigma; 1:20,000), and mouse monoclonal anti-β-tubulin (Sigma; 1:4,000).

*RYR*1 Knockdown by siRNA

Immortalized myoblasts obtained as described above (immortalization and culture human skeletal muscle cell line) were seeded on 30 mm diameter plates at a density of 5–8 × 10^5 cells per well in order to be confluent by the next day. *RYR1* siRNA (Santa Cruz Biotechnology) was transfected using lipofectamine 2000 in OptiMEM medium following the manufacturer's recommendations (Invitrogen). A series of concentrations [10, 30, and 50 nM] of siRNA were tested and cells treated with the same concentrations of negative siRNA were used as control. The transfection medium was changed to differentiation medium (PromoCell) 6 hr after transfection and changed thereafter every 2 days; cells visibly started to

fuse 4–5 days after transfection/differentiation, and myotubes were collected at day 7.

Intracellular Calcium Measurements

Myotubes, mock transfected or transfected with 50 nM siRNA, were either untreated or treated with 1 µM Xestsospongin C (Sigma chemicals, St. Gallen, Switzerland) for 40 min during fura-2 (final concentration was 5 µM) loading. Cells were rinsed one time with Krebs-Ringer and then coverslips were mounted onto a 37°C thermostated chamber which was continuously perfused with Krebs-Ringer medium; individual cells were stimulated with the indicated agonists (60 mM KCl, 600 µM 4-chloro-*m*-cresol, 100 µM ATP) made up in Krebs-Ringer containing no added Ca^{2+} plus 100 µM La^{3+} in order to monitor changes in the cytoplasmic calcium concentration due to release from intracellular stores, by means of a 12-way 100 mm diameter quartz micromanifold computer-controlled microperfuser (ALA Scientific Instruments, Farmingdale, NY, USA), as previously described [Ducreux et al., 2004]. On-line measurements were recorded using a fluorescent Axiovert S100 TV inverted microscope (Carl Zeiss GmbH, Jena, Germany) equipped with a 20× water-immersion FLUAR objective (0.17 NA), filters (BP 340/380, FT 425, BP 500/530) and attached to a Cascade 125+ CCD camera. Changes in the free cytosolic calcium concentration were analyzed using MetaMorph (Molecular Devices) imaging system and the average pixel value for each cell was measured as previously described [Ducreux et al., 2004; Treves et al., 2010].

Statistical Analysis

Statistical analysis was performed using the Student's *t*-test for comparison of two samples or the ANOVA test for comparison of multiple data, followed by the Bonferroni's post hoc test. GraphPad Prism 5 and Origin softwares were used for statistical analysis and graph design.

Results

RyR1 and DHPR Expression and Distribution in Skeletal Muscle Biopsies from Patients Carrying *RYR*1 Mutations

Figure 1 shows immunohistochemical staining on skeletal muscle biopsies from three patients carrying recessive *RYR1* mutations, one patient carrying a dominant *RYR1* mutation and one control individual. A summary of the clinical and histopathological features and genetic details of the patients is given in Supp. Table S1. Patient 1 carried the heterozygous mutations p.R109W+p.M485V in one allele and the missense plus nonsense mutations p.D708N+p.R2241X in the other allele; patient 2 carried the heterozygous p.E879K mutation in one allele and the splice site mutation c.3381+1G>A in the other allele. Patient 3 carried the dominant *RYR1* mutation p.G4638D and patient 4 carried the homozygous missense mutation p.R3772Q. No additional mutations were found after screening the entire *RYR1* coding region of each patient. Biopsies from patients 3 and 4, where histopathology showed typical central or eccentric cores on NADH staining, showed the same patterns of distribution of DHPR and RyR1 in a rim around the core area (Fig. 1). On the other hand, a segregated distribution of RyR1 and DHPR was observed in muscle sections from patients 1 and 2, in whom histopathology showed the characteristic multi-mini cores on NADH staining, there was distinct aggregation of the DHPR in some of the muscle fibers in associated with reduction of RyR1 staining.

83
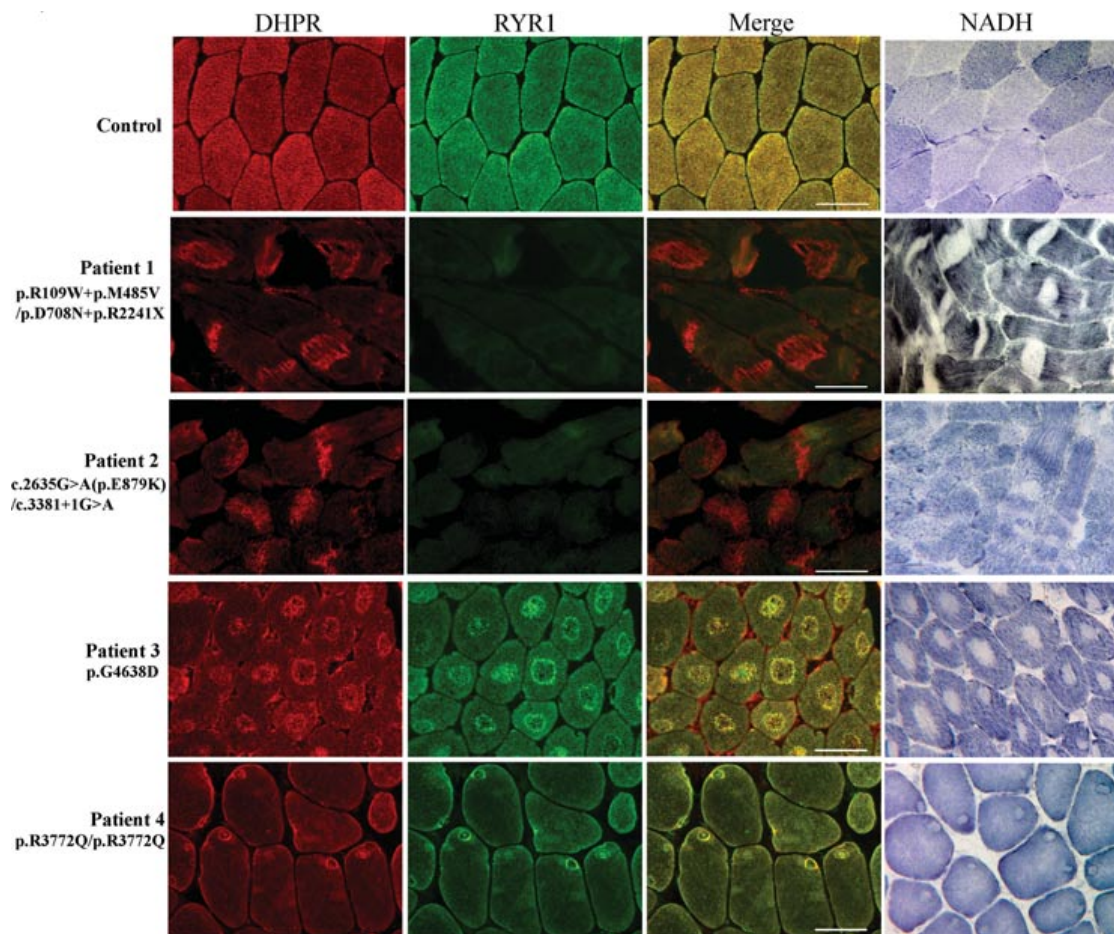
Figure 1. Protein expression of RyR1 and DHPR in muscle biopsy of patients with different *RYR1* mutations. Double staining of RyR1 and DHPR, and NADH staining in muscle biopsies of patients with congenital myopathy and *RYR1* mutations. NADH staining was performed in non-serial sections from RyR1/DHPR double staining. Scale bar = 25 μm.

*RYR*1 but Not *CACNA1S* Transcript is Reduced in Skeletal Muscle from Patients Carrying Recessive *RYR*1 Mutations

To investigate changes in *RYR1* expression at the transcriptional level, we performed quantitative real-time PCR of *RYR1* in patient's muscle biopsies, using *DES* as the skeletal muscle specific reference gene. RNA samples extracted from muscle biopsies of 19 patients with confirmed *RYR1* mutations were collected for this study. Patients were arranged into three groups according to the types of mutations. *RYR1*-AD group consisted of six patients carrying dominant *RYR1* mutations; *RYR1*-R1 group included four patients with recessive homozygous or compound heterozygous missense mutations; and *RYR1*-R2 group included nine patients carrying heterozygous recessive mutations in which one allele contained a missense mutation, and the other a loss of function mutation. We also included biopsies from nine normal control individuals in the control group. The relative expression of *RYR1* was 0.89 ± 0.07 in the control group, 0.83 ± 0.10 in the *RYR1*-AD group, 0.61 ± 0.07 in the *RYR1*-R1 group and 0.57 ± 0.06 in the *RYR1*-R2 group (Fig. 2A). Significant reduction of *RYR1* mRNA transcripts was observed in *RYR1*-R1 and *RYR1*-R2 groups, where patients were affected by recessive mutations on both alleles, compared with control group ($P = 0.0035$ between *RYR1*-R2 and control; $P = 0.044$ between *RYR1*-R1 and

control). No difference was observed in patients carrying dominant *RYR1* mutations (*RYR1*-AD) compared with control group. *CACNA1S* mRNA was also measured by quantitative real-time but no significant difference was observed in its transcription level in muscle biopsies between mutation groups and controls (Fig. 2B).

We further investigated the effects of RyR1 depletion by performing RyR1 knockdown experiments on an immortalized human muscle cell line, using *RYR1* siRNA. Seven days after transfection and differentiation, once visible multinucleated myotubes appeared, *RYR1* mRNA was quantified by real-time PCR. As shown in Figure 3A the *RYR1* transcript was reduced in a siRNA concentration-dependent manner. The relative expression of *RYR1* mRNA was: 0.47 ± 0.09 for the 10 nM siRYR1 group; 0.31 ± 0.03 for the 30 nM siRYR1 group and 0.23 ± 0.03 for the 50 nM siRYR1 group compared with the control group (1.0 ± 0.0). In the same samples, the relative expression of *CACNA1S* (Fig. 3B) and *DES* (Fig. 3C) were not significantly changed.

Downregulation of RyR1 by siRNA did not affect myotube differentiation; indeed mean myotube diameter as well as the relative expression of differentiation-related markers such as dystroglycan 1 (DAG), myosin heavy chain 1 (MHC1), troponin T1 (TNNT1), and desmin (DES) [Galbiati et al., 1999; Trendelensburg et al.,

84
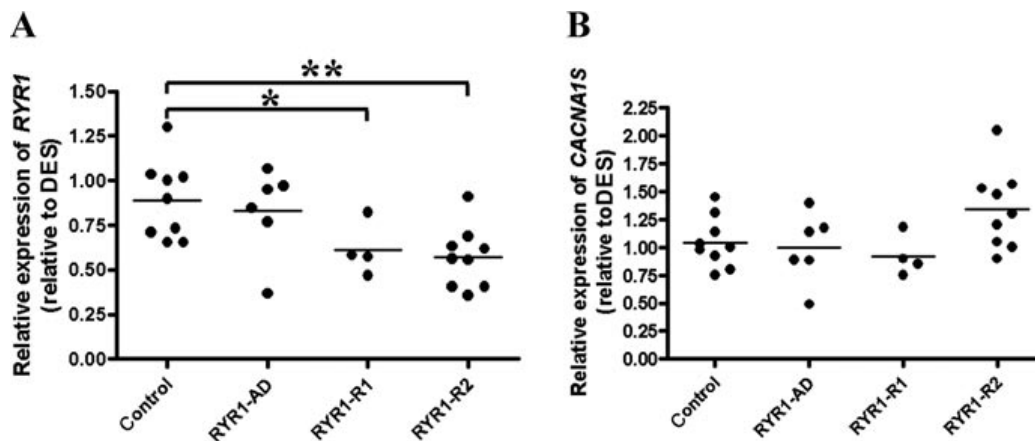
Figure 2. Quantitative reverse transcriptional real-time PCR of *RYR1* and *CACNA1S* in skeletal muscle biopsies from patients carrying different *RYR1* mutations. The relative content of *RYR1* and *CACNA1S* mRNA was assessed by real-time PCR using $\triangle\triangle Ct$ method and using *DES* as muscle specific reference gene. The relative expression of *RYR1* and *CACNA1S* to *DES* in one of the control individuals was set as 1.0, and was used to calibrate the values of all other samples. Each symbol represents an individual and the bar indicates mean relative expression. ANOVA was used for the statistical analysis of the values in different groups, followed by the Bonferroni post statistics test. **A:** Relative expression of *RYR1* transcript in muscle biopsies. **B:** Relative expression of *CACNA1S* transcript in muscle biopsies. $^{*}P < 0.05$, $^{**}P < 0.01$.
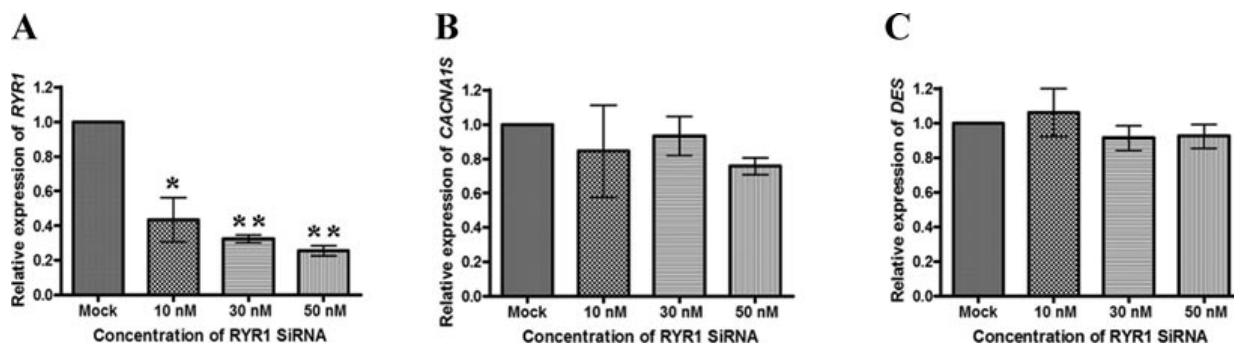
Figure 3. *RYR1*, *CACNA1S*, and DES mRNA expression in myotubes treated with *RYR1* siRNA. The relative quantification of *RYR1* (**A**), *CACNA1S* (**B**), and *DES* (**C**) mRNA was performed by quantitative real-time PCR. The value was obtained from three independent transfection experiments of myotubes treated with *RYR1* siRNA at concentrations of 10, 30, and 50 nM. The data are presented as mean $\pm$ SEM, $N = 3$. ANOVA was used for the statistical analysis of the values in the *RYR1* siRNA-treated myotubes to negative control siRNA, followed by Bonferroni post statistics test. The relative expression of target genes in control siRNA-treated myotubes was set as 1.0, and was used to normalize the values in the *RYR1* siRNA-treated myotubes. $^{*}P < 0.05$, $^{**}P < 0.01$.

2009] were similar in control and *RYR1* siRNA transfected myotubes (Fig. 4).

RyR1 Deficiency Affects Ca$_{v}$1.1 Content

We next assessed if the decrease in mRNA in siRNA transfected immortalized cells was paralleled by a decrease in protein content. Figure 5A shows a representative western blot performed seven days after treatment and Figure 5B shows the mean ($\pm$SEM) protein content in control versus siRNA-treated myotubes. As shown desmin and tubulin content were not affected by *RYR1* siRNA but there was a >50% decrease in RyR1, Ca$_{v}$1.1, SERCA2, and α-actinin content as assessed by western blotting in myotubes transfected with 50 nM *RYR1* siRNA. Unexpectedly, the relative content of IP3RIII, the other intracellular Ca^{2+} release channel of ER membranes was increased by approximately twofold.

The protein content of Ca$_{v}$1.1, SERCA2, α-actinin2, and IP3RIII were also assessed in the muscle biopsies from patients with RyR1 deficiency due to recessive mutations. Western blotting was performed on protein extracted from the muscle biopsies of two patients and three normal controls. The immunohistochemical staining of RyR1 and DHPR of patient 2 was shown in Figure 1; the double staining of RyR1 and DHPR in patient 5 has been previously reported [Zhou et al., 2010], with similar distribution pattern as shown in Figure 1.

Representative blots from patients and controls are shown in Figure 5C. There was a significant reduction of both RyR1 and DHPR proteins in the samples from the patients compared with controls ($N = 3$) (Fig. 5D). Significant upregulation of IP3R III (approximately twofold) was also observed in patients' muscle biopsies compared with the controls (Fig. 5D). However, no changes in SERCA2 and α-actinin 2 protein was observed in the patients' muscle biopsies samples.

85
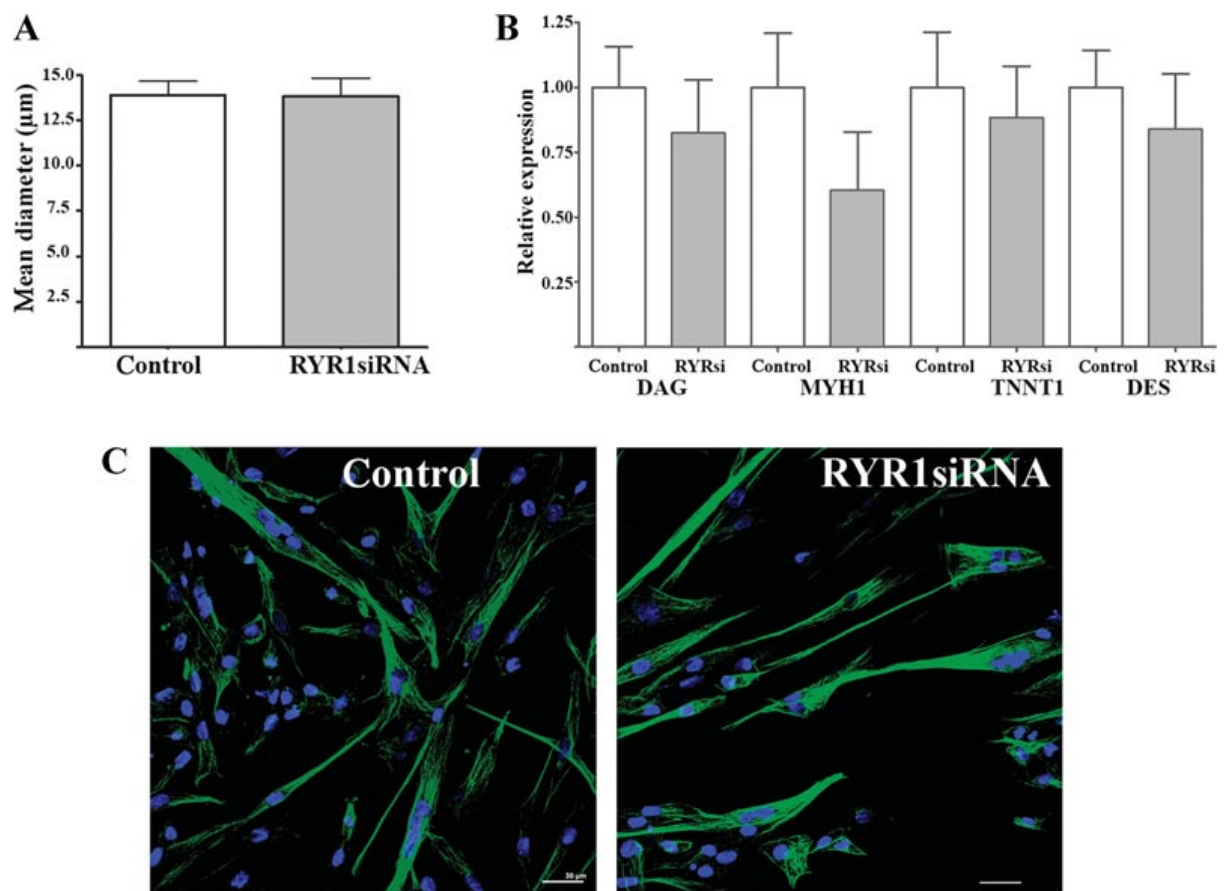
Figure 4. Downregulation of RyR1 by *RYR1* siRNA transfection does not affect myotube differentiation: Cells were transfected with 50 nM *RYR1* siRNA, differentiated for 5 days and then stained with β-tubulin and DAPI, the diameter of myotubes with >3 nuclei were measured and averagedconsidered. **A**: Mean ($\pm$SE) myotube diameter (μm) of 30 transfected and 30 mock transfected myotubes. (**B**: Relative mRNA expression of differentiation-related markers; *Dystroglycan* 1 (*DAG*), *Myosin heavy chain 1* (*MYH1*), *Troponin T1* (*TNNT1*), and *Desmin* (*DES*) normalized to *GAPDH* expression as internal control ($N = 6$). **C**: Immunofluorescentce of transfected (RYR1siRNA) or mock transfected (control) myotubes stained with anti- β tubulin (green) and DAPI and observed with a Nikon A1R confocal microscope with a 40$\times$ NeoFluar objective (1.4 NA). Bar indicates 30 μm.

All Three Types of *ITPRs* Transcripts are Upregulated in *RYR*1 Knockdown Myotubes and in Skeletal Muscles from Patients with Primary RyR1 Deficiency

The transcripts of all three isoforms of Inositol-1,4,5- Triphosphate Receptor (IP3R) genes (*ITPR1*, *ITPR2*, and *ITPR3*) were quantified by real-time RT-PCR in myotubes treated by *RYR1* siRNA. Significant upregulation of all three isoforms of ITPRs was observed in the *RYR1* knocked-down group compared with the control group (Fig. 6A). We then analyzed *ITPRs* transcripts in skeletal muscle from controls (N = 7), from patients with dominant *RYR1* mutations (N = 5) and from patients with heterozygous recessive *RYR1* mutations and RyR1 protein deficiency (N = 6). To ensure that the observed alterations were not due to heterogeneous tissue composition of the biopsies due to variable degrees of fibrosis or connective tissue accumulation, we used both the ubiquitous housekeeping gene *GAPDH* and muscle specific *DES* gene as internal reference genes. Irrespective of whether the analysis was made using *GAPDH* (Fig. 6B) or *DES* (Fig. 6C), patients with recessive *RYR1* mutations showed significant upregulations of all three IP3R transcripts, compared with

the control group. No significant differences in *ITPR1*, *ITPR2*, and *ITP3R* expression were observed between the group of patients harboring dominant *RYR1* mutations and the control group, except for a patient carrying the dominant mutation p.R4861C, who showed unusually high levels of *ITPRs* expression. Interestingly, although this mutation was identified as de novo and was not found in either parent, the case was initially considered a recessive core myopathy because of the severe clinical features of the patient and the abnormality observed in parent's muscle biopsy [Manzur et al., 1998]. Unfortunately, the muscle biopsy failed western blotting RyR1 protein quantification due to sampling problems. In order to rule out the presence of other allelic mutations, we performed genomic analysis of the entire coding region and exon/intron boundaries of the *RYR1* gene; no other pathogenic variants were identified in this patient suggesting that in this patient the p.R4861C mutation is responsible for the pathological phenotype.

Taken together these results confirm that RyR1 deficiency induced in vitro as well as RyR1 protein deficiency occurring in vivo due to recessive *RYR1* mutations cause the upregulation of *ITPRs* transcripts.

991
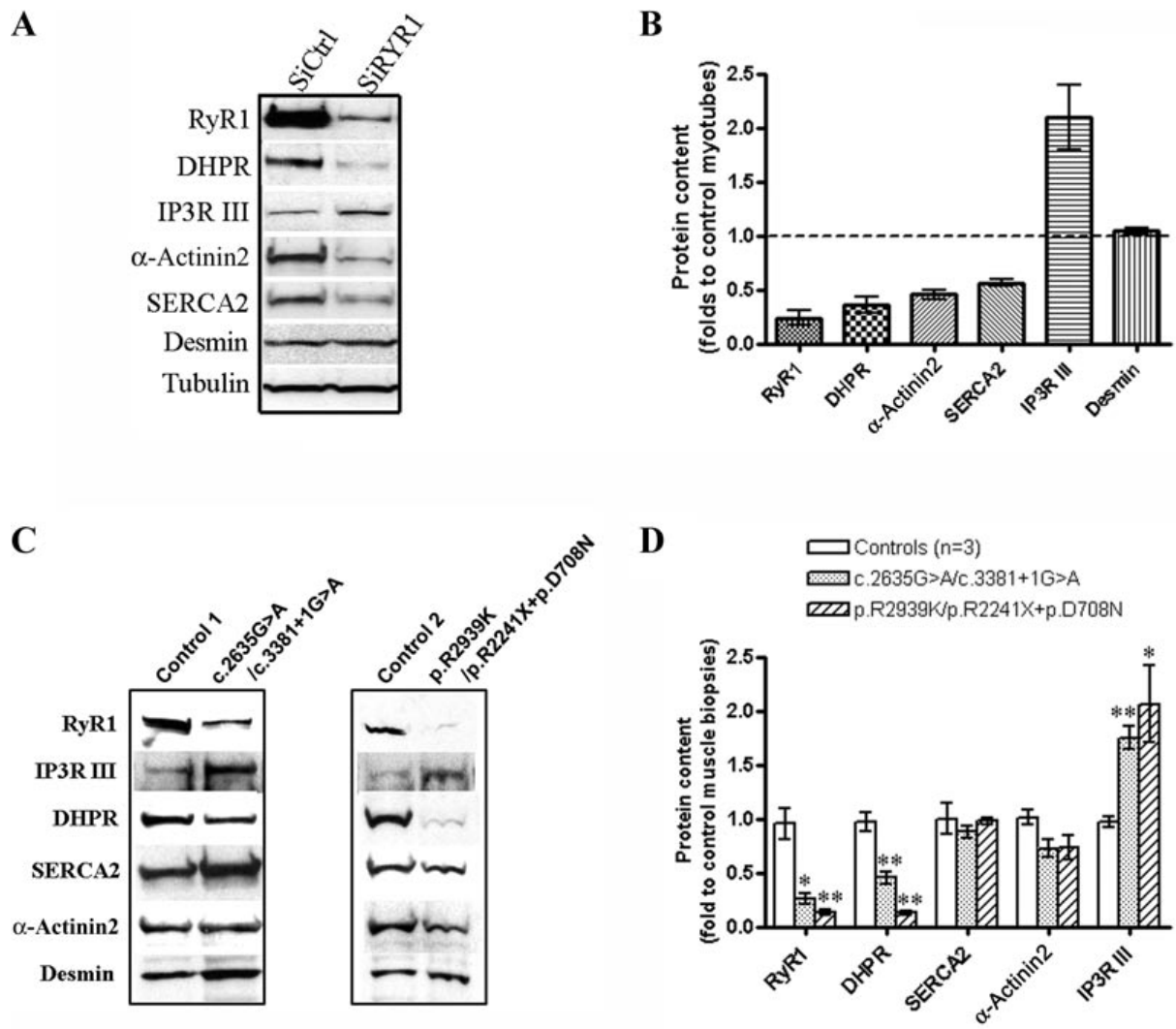
Figure 5. RyR1, DHPR, and other SR protein in *RYR1* siRNA-treated myotubes and muscle biopsies from patients with RyR1 deficiency due to recessive *RYR1* mutations. **A**: Representative western blots of RyR1, DHPR, IP3R-III, α-actinin 2, SERCA 2, desmin, and β-tubulin in human myotubes treated by *RYR1* siRNA. **B**: Semi-quantification of proteins in *RYR1* siRNA-treated myotubes. The expression of proteins was normalized to tubulin. Protein content in *RYR1* siRNA-treated group was compared with the control group. **C**: Representative western blots of RyR1, DHPR, IP3R-III, α-actinin 2, SERCA 2, and desmin in muscle biopsies from two patients (patient 2 and 5 in Supp. Table S1) with recessive RYR1 mutations. **D**: Semi-quantification of proteins in two patients, with RyR1 deficiency due to recessive *RYR1* mutations, and three controls. The expression of proteins was normalized by desmin.

Changes in Intracellular Ca²⁺ Homeostasis in *RYR1* Knocked-Down Myotubes

Using the human muscle cell line we assessed how downregulation of RyR1 by siRNA affects calcium homeostasis. Besides the resting [Ca^{2+}] and the size ionomycin sensitive Ca^{2+} stores, we measured several parameters, including the response (expressed as area under the curve, which more accurately reflects the total amount of Ca^{2+} released) of myotubes to KCl-induced depolarization, to pharmacological activation of RyR1 with 4-chloro-m-cresol and to ATP stimulation (which measures Ca^{2+} release via IP3R) in control cells, control cells treated with the IP3R inhibitor Xestospongin C and in RYR1 siRNA-treated cells (± Xestospongin C). This approach allows us to evaluate if the decrease in Ca^{2+} released due to downregulation of RyR1 could be compensated by upregulation of IP3R-mediated Ca^{2+} release. Figure 7 shows that RyR1 activation either directly by the addition of 600 µM 4-chloro-m-cresol or indirectly, by the addition of 60 mM KCl induces a large Ca^{2+} release that is independent of IP3Rs since the same amount of Ca^{2+} was released whether cells had been pre-treated or not with Xestospongin C. Downregulation of *RYR1* by 50 nM siRNA caused a threefold decrease of Ca^{2+} release by 4-cmc and KCl that was unaffected by Xestospongin C. Addition of 100 µM ATP (1) caused the release of approximately 50% of the Ca^{2+} compared with the release obtained by RyR1 activation, (2) was inhibited by Xestospongin C and importantly, (3) was unaffected by downregulation of *RYR1*. Downregulation of RyR1 affected neither the resting [Ca^{2+}] nor the total amount of ionomycin-induced Ca^{2+}-release, indicating no significant effect on the size of the intracellular

87
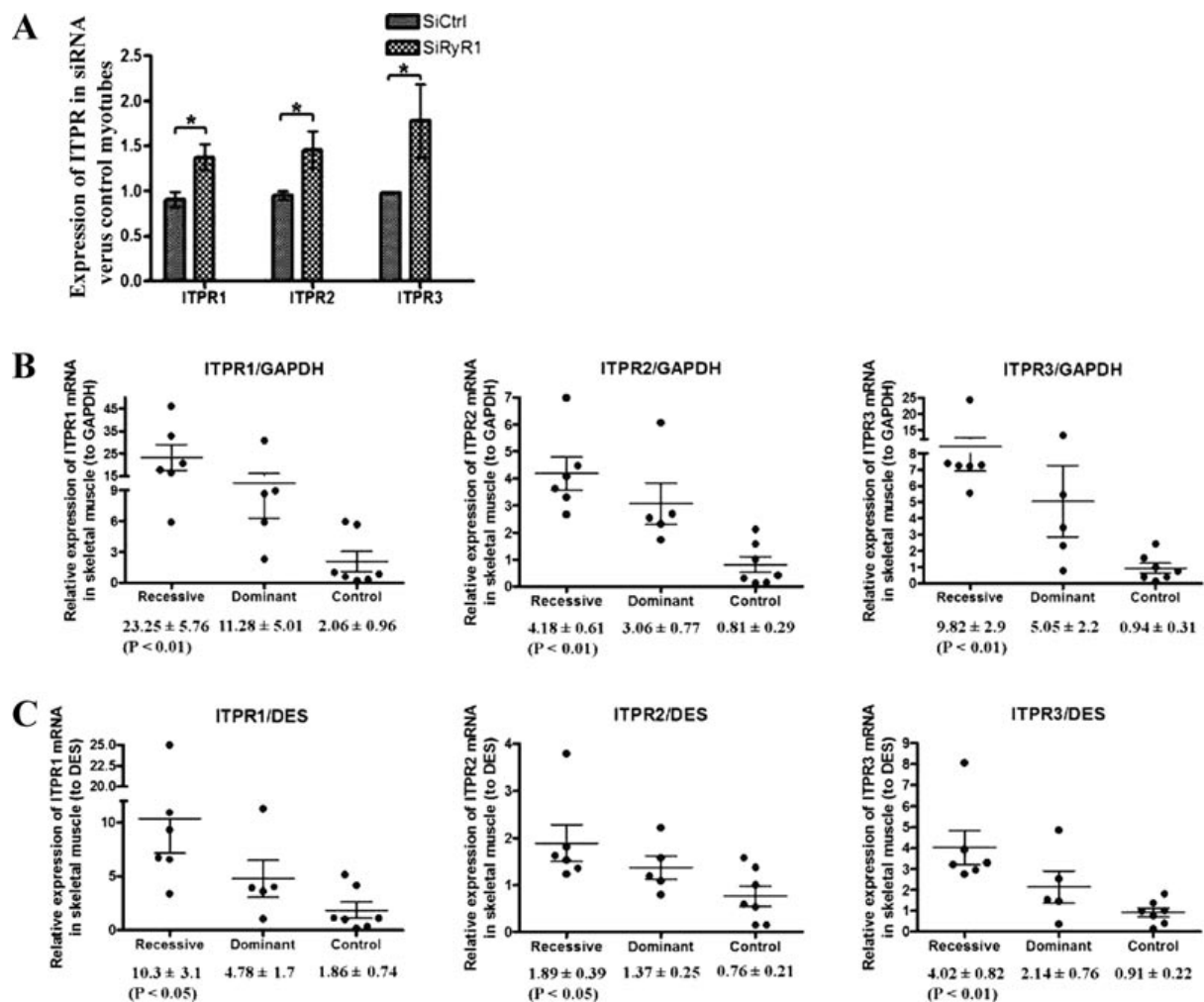
Figure 6. The expression of *ITPR1, ITPR2,* and *ITPR3* mRNA in RYR1 siRNA-treated myotubes and skeletal muscle biopsies from patients with different *RYR1* mutations. **A**: The relative expression of *ITPRs* mRNA in cultured myotubes treated with siRNA was measured by quantitative reverse transcript real-time PCR. Data are presented as mean ± SEM. *N* = 4 samples per group. *$P < 0.05$. **B**: The relative expression of *ITPRs* mRNA measured by quantitative real-time PCR in skeletal muscle biopsies from controls (*N* = 7), patients with dominant *RYR1* mutations (*N* = 5) and patients with complex recessive *RYR1* mutations with RyR1 protein deficiency (*N* = 6). *GAPDH* was used as general internal control gene. **C**: The relative expression of *ITPRs* mRNA measured by quantitative real-time PCR in skeletal muscle biopsies by using *DES* as muscle-specific internal control gene.

Ca^{2+} stores. These results indicate that upregulation of IP3R does not functionally compensate the decreased Ca^{2+}-release due to the lower levels of RyR1 protein content.

Discussion

RYR1-related disorders with mainly dominant inheritance and normal RyR1 protein expression have been extensively studied at the functional level, whereas the mechanisms underlying *RYR1*-related myopathies with recessive inheritance and RyR1 deficiency remain only partially understood. Functional studies of common dominant *RYR1* mutations associated with CCD indicate two principal mechanisms associated with disturbed function of the mutant RyR1 channel, namely presence of a 'leaky channels' associated with reduction of SR calcium stores [Lynch et al., 1999], or "uncoupled" channels with muscle weakness resulting from a reduced capacity

of RyR1 to transport Ca^2 [Avila et al., 2001]. In the present study, we report that recessive *RYR1* mutations associated with RyR1 deficiency are also responsible for EC uncoupling by negatively affecting DHPR-RyR1 colocalization in skeletal muscle. Indeed, this kind of EC uncoupling was initially reported in two animal models of *RYR1*-related disorders, the sporadic zebrafish *relatively relaxed* mutant with marked reduction of functional RyR1 protein [Hirata et al., 2007], and in *Ryr1* knockout (dyspedic) mice which do not express any ryanodine receptor 1 [Takeshima et al., 1994]. In dyspedic myotubes cultured from *Ryr1* knockout mice, there is no EC coupling, whereas introduction of exogenous RyR1 restores EC coupling and increases the density of the L-type Ca^{2+} current toward normal [Nakai et al., 1996]. The dependence of physiological EC coupling on correct mechanical coupling is also indicated by ultrastructural studies demonstrating the importance of a tight alignment of RyR tetramers on the junctional face membrane and of DHPR molecules (a tetrad) on the opposing T-tubule membrane [Block et al., 1988].
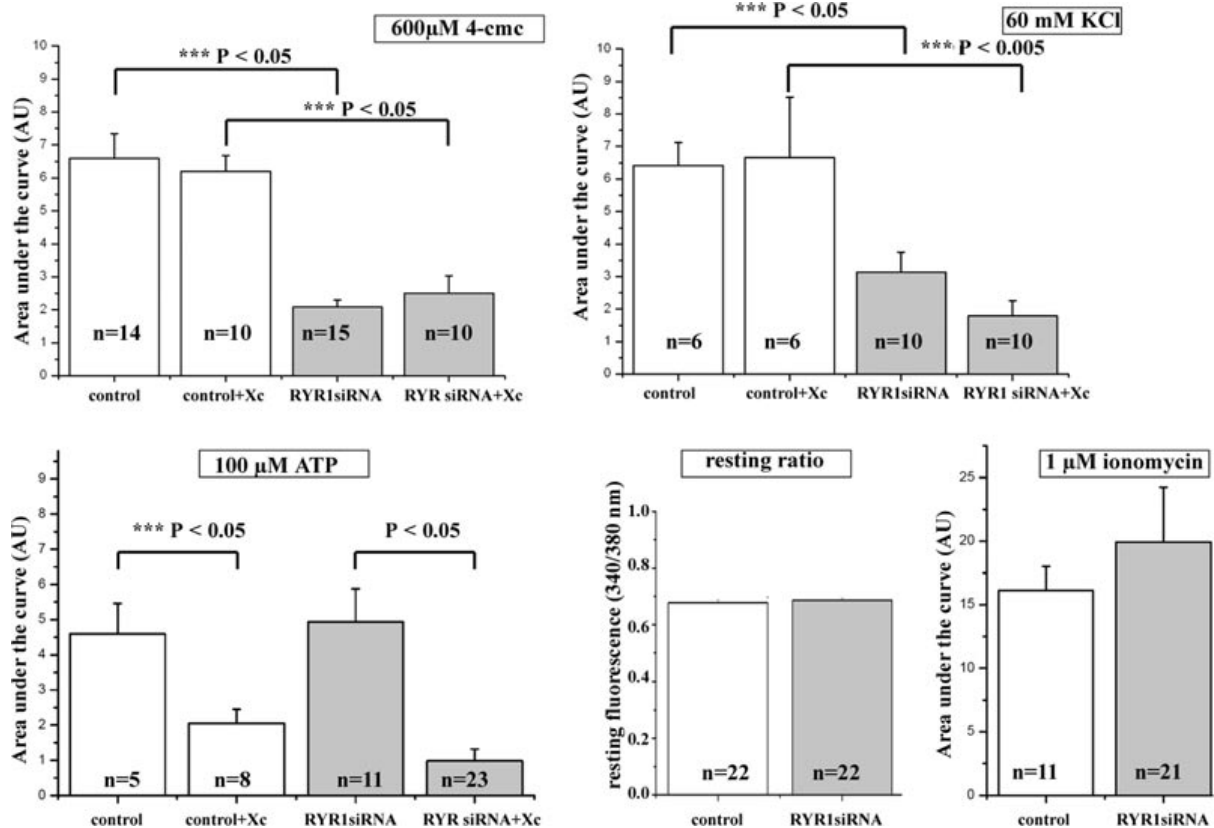
Figure 7. Analysis of calcium regulation in a human muscle cell line after transfection with *RYR1* siRNA. Cells were transfected with 50 nM RYR1 siRNA or mock transfected as described in the *Materials and Methods* section and were either untreated or treated with 1 μM Xestospongin C during the 40 min of fura-2 loading. Myotubes were stimulated with the indicated agonist in Krebs-Ringer containing no added Ca^{2+} plus 100 μM La^{3+} and the total amount of calcium released was calculated using Origin software by calculating the total transient, i.e. the area under the curve. Resting [Ca^{2+}] is presented as fluorescence ratio (340/380 nm) (au) before cell stimulation in Krebs-Ringer containing 2 mM Ca^{2+}; the total amount of rapidly releasable Ca^{2+} present in the SR/ER stores was obtained by calculating the area under the curve after exposing cells to 1 μM ionomycin in the Krebs-Ringer containing no added Ca^{2+} plus 0.5 mM EGTA. For details see *Materials and Methods* section. All results are expressed as mean value ($\pm$SEM) of the indicated number of cells. White bars mock transfected cells, grey bars cells transfected with *RYR1* siRNA. Statistical analysis was performed using Student's *t*-test.

Interestingly, depletion of RyR1 in vitro by siRNA in an immortalized human muscle cell line caused a decrease of $Ca_v1.1$ content, suggesting that proper alignment between the two calcium channels is required for the stability of the complex. Diminishment of $Ca_v1.1$ content has also been reported in dyspedic mouse skeletal muscle [Buck et al., 1997] and in one previous immunohistochemical study on core myopathies, in which a patient exhibiting virtual absence of RyR1 showed focal accumulation of DHPR within or around the cores [Herasse et al., 2007]. The loss of DHPR/RyR1 colocalization strongly suggests a physical EC uncoupling in patients with some recessive *RYR1* mutations. We suggest that the characteristic staining pattern of $Ca_v1.1$ may be a useful immunohistochemical indicator to select patients for *RYR1* sequencing, currently still very costly and time consuming due to the large size of the gene.

Aside the downregulation of $Ca_v1.1$, we observed downregulation of SERCA2 and alfa-actinin in RyR1 knocked-down myotubes. This is in contrast to the upregulation of SERCA reported in dyspedic myotubes [Eltit et al., 2010; 2011] and to the lack of changes in SERCA2 and alfa-actinin protein levels in the patient's biopsies. Opposing effects on SERCA2 expression have been reported in C_2C_{12} cells transfected with two different *RYR1* mutations. Vega

et al. (2011) reported that transfection with the *RYR1* Y523S MH-linked mutation caused an increase in SERCA2 expression whereas transfection of C2C12 cells with the CCD-linked I4897T *RYR1* mutation caused its downregulation. Furthermore, they also reported that the expression of a particular mutant affects the degree of myotube differentiation, in that C2C12 cells transfected with the RyR1 cDNA harboring the I4897T mutation were similar to control myotubes in size and fusion index 8 days after differentiation, whereas cells transfected with the RyR1 cDNA harboring the Y523S substitution were larger than control myotubes [Vega et al., 2011]. We did not find any significant differences in size and in the expression of differentiation-related markers such as dystroglycan 1, troponin T1, myosin heavy chain, and desmin [Galbiati et al., 1999; Trendelenburg et al., 2009] in RYR1siRNA transfected and control cells. Thus, knocking down a protein in vitro does not mimic all aspects of what happens in vivo in muscles of patients harboring recessive mutations causing RyR1 depletion and further experiments are required to understand the mechanisms involved in the reciprocal regulation of SR proteins.

In the present study, we demonstrate that in human skeletal muscle under conditions of RyR1 deficiency, IP3R are upregulated. In

89

cultured mouse skeletal muscle cells IP3R predominantly expressed around the nuclear envelope, are mainly associated with slow Ca^{2+} transients and appear to be involved in the regulation of gene expression [Jaimovich et al., 2000; Jaimovich and Carrasco, 2002]. The IP3/IP3R-induced calcium signal plays little or no substantial role in skeletal muscle EC coupling under physiological conditions [Posterino and Lamb, 1998] and as shown in the present study, upregulation of IP3R in RyR1-deficient states does not compensate for the physical collapse of the EC coupling machinery. Nevertheless, the IP3/IP3R pathway may be involved in slow calcium release leading to activation of expression of certain genes and the present study indicates the possible existence of a complex interplay of RyR1 and IP3R signaling pathways.

In conclusion, our results demonstrate upregulation of an alternative calcium regulating system via IP3R in recessive *RYR1*-related myopathies with RyR1 deficiency, and indicate the potential importance of the IP3R signaling cascade in the pathophysiology of these neuromuscular disorders. Future studies aimed at determining the role of the IP3R system in RyR1-deficient congenital myopathies and its correlation with disease progression could provide further insight into the pathogenesis of this condition.

Acknowledgments

References

Avila G, O'Brien JJ, Dirksen RT. 2001. Excitation–contraction uncoupling by a human central core disease mutation in the ryanodine receptor. Proc Natl Acad Sci USA 98:4215–4220.

Block BA, Imagawa T, Campbell KP, Franzini-Armstrong C. 1988. Structural evidence for direct interaction between the molecular components of the transverse tubule/sarcoplasmic reticulum junction in skeletal muscle. J Cell Biol 107:2587–2600.

Buck ED, Nguyen HT, Pessah IN, Allen PD. 1997. Dyspedic mouse skeletal muscle expresses major elements of the triadic junction but lacks detectable ryanodine receptor protein and function. J Biol Chem 272:7360–7367.

Clarke NF, Waddell LB, Cooper ST, Perry M, Smith RL, Kornberg AJ, Muntoni F, Lillis S, Straub V, Bushby K, Guglieri M, King MD, et al. 2010. Recessive mutations in RYR1 are a common cause of congenital fiber type disproportion. Hum Mutat 31:E1544–E1550.

Dirksen RT, Avila G. 2002. Altered ryanodine receptor function in central core disease: leaky or uncoupled Ca(2+) release channels? Trends Cardiovasc Med 12:189–197.

Dowling JJ, Lillis S, Amburgey K, Zhou H, Al-Sarraj S, Buk SJ, Wraige E, Chow G, Abbs S, Leber S, Lachlan K, Baralle D, et al. 2011. King-Denborough syndrome with and without mutations in the skeletal muscle ryanodine receptor (RYR1) gene. Neuromuscul Disord 21:420–427.

Ducreux S, Zorzato F, Muller C, Sewry C, Muntoni F, Quinlivan R, Restagno G, Girard T, Treves S. 2004. Effect of ryanodine receptor mutations on interleukin-6 release and intracellular calcium homeostasis in human myotubes from malignant hyperthermia-susceptible individuals and patients affected by central core disease. J Biol Chem 279:43838–43846.

Dulhunty AF, Pouliquin P. 2003. What we don't know about the structure of ryanodine receptor calcium release channels. Clin Exp Pharmacol Physiol 30:713–723.

Eltit JM, Li H, Ward CW, Molinski T, Pessah IN, Allen PD, Lopez JR. 2011. Orthograde dihydropyridine receptor signal regulates ryanodine receptor passive leak. Proc Natl Acad Sci USA 108:7046–7051.

Eltit JM, Yang T, Li H, Molinski TF, Pessah IN, Allen PD, Lopez JR. 2010. RyR1-mediated Ca²⁺ leak and Ca²⁺ entry determine resting intracellular Ca²⁺ in skeletal myotubes. J Biol Chem 285:13781–13787.

Galbiati F, Volonté D, Engelman JA, Scherer PE, Linsanti MP. 1999. Targeted downregulation of caveolin-3 is sufficient to inhibit myotube formation in differentiating C2C12 myoblasts. J Biol Chem 274: 30315–30321.

Herasse M, Parain K, Marty I, Monnier N, Kaindl AM, Leroy JP, Richard P, Lunardi J, Romero NB, Ferreiro A. 2007. Abnormal distribution of calcium-handling proteins: a novel distinctive marker in core myopathies. J Neuropathol Exp Neurol 66:57–65.

Hirata H, Watanabe T, Hatakeyama J, Sprague SM, Saint-Amant L, Nagashima A, Cui WW, Zhou W, Kuwada JY. 2007. Zebrafish relatively relaxed mutants have a ryanodine receptor defect, show slow swimming and provide a model of multi-minicore disease. Development 134:2771–2781.

Jaimovich E, Carrasco MA. 2002. IP3 dependent Ca²⁺ signals in muscle cells are involved in regulation of gene expression. Biol Res 35:195–202.

Jaimovich E, Reyes R, Liberona JL, Powell JA. 2000. IP(3) receptors, IP(3) transients, and nucleus-associated Ca(2+) signals in cultured skeletal muscle. Am J Physiol Cell Physiol 278:C998–C1010.

Jungbluth H, Muller CR, Halliger-Keller B, Brockington M, Brown SC, Feng L, Chattopadhyay A, Mercuri E, Manzur AY, Ferreiro A, Laing NG, Davis MR, et al. 2002. Autosomal recessive inheritance of RYR1 mutations in a congenital myopathy with cores. Neurology 59:284–287.

Jungbluth H, Zhou H, Hartley L, Halliger-Keller B, Messina S, Longman C, Brockington M, Robb SA, Straub V, Voit T, Swash M, Ferreiro A, et al. 2005. Minicore myopathy with ophthalmoplegia caused by mutations in the ryanodine receptor type 1 gene. Neurology 65:1930–1935.

Jungbluth H, Zhou H, Sewry CA, Robb S, Treves S, Bitoun M, Guicheney P, Buj-Bello A, Bonnemann C, Muntoni F. 2007. Centronuclear myopathy due to a de novo dominant mutation in the skeletal muscle ryanodine receptor (RYR1) gene. Neuromuscul Disord 17:338–345.

Lynch PJ, Tong J, Lehane M, Mallet A, Giblin L, Heffron JJ, Vaughan P, Zafra G, MacLennan DH, McCarthy TV. 1999. A mutation in the transmembrane/luminal domain of the ryanodine receptor is associated with abnormal Ca²⁺ release channel function and severe central core disease. Proc Natl Acad Sci USA 96:4164–4169.

Mamchaoui K, Trollet C, Bigot A, Negroni E, Chaouch S, Wolff A, Kandalla PK, Marie S, Di SJ, St Guily JL, Muntoni F, Kim J, et al. 2011. Immortalized pathological human myoblasts: towards a universal tool for the study of neuromuscular disorders. Skelet Muscle 1:34.

Manzur AY, Sewry CA, Ziprin J, Dubowitz V, Muntoni F. 1998. A severe clinical and pathological variant of central core disease with possible autosomal recessive inheritance. Neuromuscul Disord 8:467–473.

Monnier N, Procaccio V, Stieglitz P, Lunardi J. 1997. Malignant-hyperthermia susceptibility is associated with a mutation of the alpha 1-subunit of the human dihydropyridine-sensitive L-type voltage-dependent calcium-channel receptor in skeletal muscle. Am J Hum Genet 60:1316–1325.

Nakai J, Dirksen RT, Nguyen HT, Pessah IN, Beam KG, Allen PD. 1996. Enhanced dihydropyridine receptor channel activity in the presence of ryanodine receptor. Nature 380:72–75.

Oddoux S, Brocard J, Schweitzer A, Szentesi P, Giannesini B, Brocard J, Faure J, Pernet-Gallay K, Bendahan D, Lunardi J, Csernoch L, Marty I. 2009. Triadin deletion induces impaired skeletal muscle function. J Biol Chem 284:34918–34929.

Pan Z, Yang D, Nagaraj RY, Nosek TA, Nishi M, Takeshima H, Cheng H, Ma J. 2002. Dysfunction of store-operated calcium channel in muscle cells lacking mg29. Nat Cell Biol 4:379–383.

Pirone A, Schredelseker J, Tuluc P, Gravino E, Fortunato G, Flucher BE, Carsana A, Salvatore F, Grabner M. 2010. Identification and functional characterization of malignant hyperthermia mutation T1354S in the outer pore of the Cavalpha1S-subunit. Am J Physiol Cell Physiol 299:C1345–C1354.

Posterino GS, Lamb GD. 1998. Investigation of the effect of inositol trisphosphate in skinned skeletal muscle fibres with functional excitation–contraction coupling. J Muscle Res Cell Motil 19:67–74.

Quane KA, Healy JM, Keating KE, Manning BM, Couch FJ, Palmucci LM, Doriguzzi C, Fagerlund TH, Berg K, Ording H. 1993. Mutations in the ryanodine receptor gene in central core disease and malignant hyperthermia. Nat Genet 5:51–55.

Ramachandran S, Serohijos AW, Xu L, Meissner G, Dokholyan NV. 2009. A structural model of the pore-forming region of the skeletal muscle ryanodine receptor (RyR1). PLoS Comput Biol 5:e1000367.

Takeshima H, Iino M, Takekura H, Nishi M, Kuno J, Minowa O, Takano H, Noda T. 1994. Excitation–contraction uncoupling and muscular degeneration in mice lacking functional skeletal muscle ryanodine-receptor gene. Nature 369:556–559.

Toppin PJ, Chandy TT, Ghanekar A, Kraeva N, Beattie WS, Riazi S. 2010. A report of fulminant malignant hyperthermia in a patient with a novel mutation of the CACNA1S gene. Can J Anaesth 57:689–693.

Trendelensburg AU, Meyer A, Rohner D, Boyle J, Hatakeyama S, Glass DJ. 2009. Myostatin reduced Akt/TORC1/p70S6K signaling, inhibiting myoblast differentiation and myotube size. Am J Physiol Cell Physiol 296:C1258–C1270.

Treves S, Jungbluth H, Muntoni F, Zorzato F. 2008. Congenital muscle disorders with cores: the ryanodine receptor calcium channel paradigm. Curr Opin Pharmacol 8:319–326.

Treves S, Vukcevic M, Griesser J, Franzini-Armstrong C, Zhu MX, Zorzato F. 2010. Agonist-activated Ca2+ influx occurs at stable plasma membrane and endoplasmic reticulum junctions. J Cell Sci 123:4170–4181.

Van Petegem F. 2012. Ryanodine receptors: structure and function. J Biol Chem 287:31624–31632.

Vega AV, Ramos-Mondragon R, Calderon-Rivera A, Zarain-Herzberg A, Avila G. 2011. Calcitonin gene-related peptide restores disrupted excitation–contraction coupling in myotubes expressing central core disease mutations in RyR1. J Physiol 589:4649–4669.

Wilmshurst JM, Lillis S, Zhou H, Pillay K, Henderson H, Kress W, Muller CR, Ndondo A, Cloke V, Cullup T, Bertini E, Boennemann C, et al. 2010. RYR1 mutations are a common cause of congenital myopathies with central nuclei. Ann Neurol 68:717–726.

Zhou H, Jungbluth H, Sewry CA, Feng L, Bertini E, Bushby K, Straub V, Roper H, Rose MR, Brockington M, Kinali M, Manzur A, et al. 2007. Molecular mechanisms and phenotypic variation in RYR1-related congenital myopathies. Brain.

Zhou H, Lillis S, Loy RE, Ghassemi F, Rose MR, Norwood F, Mills K, Al-Sarraj S, Lane RJ, Feng L, Matthews E, Sewry CA, et al. 2010. Multi-minicore disease and atypical periodic paralysis associated with novel mutations in the skeletal muscle ryanodine receptor (RYR1) gene. Neuromuscul Disord 20:166–173.

Zhou H, Yamaguchi N, Xu L, Wang Y, Sewry C, Jungbluth H, Zorzato F, Bertini E, Muntoni F, Meissner G, Treves S. 2006. Characterization of recessive RYR1 mutations in core myopathies. Hum Mol Genet 15:2791–2803.

Zhu CH, Mouly V, Cooper RN, Mamchaoui K, Bigot A, Shay JW, Di Santo JP, Butler-Browne GS, Wright WE. 2007. Cellular senescence in human myoblasts is overcome by human telomerase reverse transcriptase and cyclin-dependent kinase 4: consequences in aging muscle and therapeutic strategies for muscular dystrophies. Aging Cell 6:515–523.

91

Supp. Table S1. Summary of clinical and histopathological features of the *RYR1*-related patients

Patient	Clinical features	Muscle histopathology	*RYR1* Mutations	Exons affected	References
1	Neonatal hypotonia and prolonged ventilation; feeding difficulties; delayed motor milestones and muscle weakness.	Wide variation in fibre size; rod-like structures; core-like area in NADH; type I fibre predominance.	1. p.R109W + p.M485V 2. p.D708N+ p.R2241X	14 + 38 18 + 41	Zhou et al. 2006
2	Hypotonia; feeding difficulties; facial weakness; delayed motor milestones; low head control.	Abnormal variation in fibre size; multi internal nuclei; core-like area in NADH; type I fibre predominance.	1. p.E879K 2. c.3381+1G>A	21 25	This study
3	Facial weakness; scoliosis; malignant hyperthermia.	Central cores; type I fibre predominance.	p.G4638D	95	Zhou et al. 2007
4	Proximal weakness; clubfeet; malignant hyperthermia.	Eccentric cores in NADH; type I fibre uniformity.	p.R3772Q (homozygous)	79	Zhou et al. 2007
5	Neonatal hypotonia; proximal muscle weakness; independent walking at 7 years old.	Increased internal and central nuclei; type I fibre predominance; increase in connective tissues.	1. p.L2059fs 2. p.V4842M	38 101	Wilmhurst et al. 2010
6	Reduced fetal movement; neonatal hypotonia; feeding difficulty; proximal muscle weakness; non-ambulant but no major health issues at young adult.	Increased central and internal nuclei; type I fibre predominance.	1. I2781fs+p.H3981Y 2. p.V4842M	53 + 87 101	WIlmhurst et al. 2010
7	Neonatal hypotonia; proximal and axial muscle weakness; frequent respiratory tract infection; non-ambulant and fragile at 8 years old.	Increased central and internal nuclei; type I fibre predominance; 'moth-eaten' fibre.	1. I2781fs+p.H3981Y 2. p.V4842M	53 + 87 101	Wilmhurst et al. 2010

3. Epigenetic changes as a common trigger of muscle weakness in congenital myopathies

Congenital myopathies have been defined by their predominant histopathological features into Central Core Disease (CCD), Multi-minicore Disease (MmD), Central Nuclear Myopathy (CNM), Congenital Fiber Type Disproportion (CFTD) and Nemaline Myopathy (NEM). These diseases are characterized clinically by muscle weakness, atrophy and no cardio-respiratory involvement. The aim of this project was to investigate the causes of the decreased RyR1 expression in muscles from patients with recessive RYR1 mutations. We first performed KCl-dependent Ca^{2+} release curves in myotubes from patients and controls and our results showed that the dose response curves and peak Ca^{2+} released were similar in myotubes from healthy individuals and patients with recessive RYR1 mutations. This was surprising since RyR1 protein expression was significantly decreased in patients. This discrepancy led us to reason that epigenetic mechanism might be involved. Primarily, we postulated that microRNAs predicted to bind the 3' untranslated region of RYR1 (miR22 and miR124) and cause its down-regulation may be involved. We therefore determined the levels of miR22 and miR124 together with muscle specific microRNAs (miR1, miR133 and miR206) and found that they were also significantly decreased. miR22, miR124, miR1 and miR206 are also predicted to bind the 3' UTR of HDAC4 and miR124 is predicted to bind the 3' UTR of HDAC5. As discussed in the paper, studies have also shown that miR22 regulates the expression of HDAC4 and inhibition of miR22 potentiates HDAC4 expression levels [146]. Consequently we also measured the expression levels of HDAC4 and HDAC5 in muscle biopsies and found that they were very high in patients with recessive RYR1 mutations, compared to healthy individuals. Over-expression of class II HDACs is tightly linked to increased methylation of DNA CpG islands and vis-versa [147, 148]. DNA methylation in the CpG rich regions of the RYR1 was measured, and our results show that the methylation level of the RYR1 CpG island III was significantly higher in patients with recessive RYR1 mutations, compared to controls. In order to confirm the pathological mechanism linking HDAC and miRs expression we over-expressed HDAC4/HDAC5 and silenced

RYR1 using siRNA in mouse FDB fibers. Our results support the observations in patients, that overexpression of HDAC4 and HDAC5 leads to a decrease of RYR1 expression and to a decreased expression level of muscle specific microRNAs, while silencing RYR1 resulted in higher expression levels of HDAC4 and HDAC5.

We also investigated if similar changes were occurring in the muscles of patients with other congenital muscle disorders such as Nemaline myopathy and similar results were obtained. These results indicate that a common epigenetic pathophysiological pathway is activated in some congenital myopathies and that these mechanisms contribute to the phenotype of muscle weakness and atrophy. HDACs inhibitors or DNMT inhibitors may thus improve the muscle function of these patients and therefore improve the patient's quality of life. Future studies aimed in this direction will be undertaken in the laboratory.

Author contribution: In the 3rd publication entitled "Epigenetic changes as a common trigger of muscle weakness in congenital myopathies", Ori Rokach performed all the experiments in figures 2, 3_{c-d}, 4_{c-e}, 6, 7, 8_a, 9, sup1, sup2, sup3 and shares the contribution with Susan Treves for the experiment presented in figures 1_{a-b}, 4_{a-b} and 8_{b-c}. Haiyan Zhou performed the western blot of figure 1_c. Figure 3_{a-b} and 5 were performed by Roberto Gambari and Alessia Finotti.

OXFORD

ORIGINAL ARTICLE

Epigenetic changes as a common trigger of muscle weakness in congenital myopathies

Ori Rokach[1], Marijana Sekulic-Jablanovic[1], Nicol Voermans[2], Jo Wilmshurst[3], Komala Pillay[4,5], Luc Heytens[6], Haiyan Zhou[7], Francesco Muntoni[7], Mathias Gautel[8], Yoram Nevo[9], Stella Mitrani-Rosenbaum[10], Ruben Attali[10], Alessia Finotti[11], Roberto Gambari[11], Barbara Mosca[12], Heinz Jungbluth[13,14,†], Francesco Zorzato[1,12,†] and Susan Treves[1,12,†,*]

[1]Department of Biomedicine and Anesthesia, Basel University Hospital, Basel, Switzerland, [2]Department of Neurology, Roadboud University Medical Center, Nijmegen, The Netherlands, [3]Department of Paediatric Neurology and Child Health, [4]Department of Paediatric Pathology, NHLS, Cape Town, South Africa, [5]Department of Paediatrics and Child Health, University of Cape Town, Red Cross Children's Hospital, Cape Town, South Africa, [6]Department of Anesthesiology and Neurology, Antwerp University Hospital, Antwerp, Belgium, [7]Dubowitz Neuromuscular Centre and MRC Centre for Neuromuscular Diseases, Institute of Child Health, London, UK, [8]Randall Division of Cell and Molecular Biophysics and Cardiovascular Division, King's College London, London, UK, [9]The Unit of Neuropediatrics and Child Development, Division of Pediatrics, [10]Goldyne Savad Institute of Gene Therapy, Hadassah Hebrew University Medical Center, Jerusalem, Israel, [11]Department of Life Sciences, Section of Biochemistry and Molecular Biology, [12]Department of Life Sciences, General Pathology Section, University of Ferrara, Ferrara, Italy, [13]Department of Paediatric Neurology, Neuromuscular Service, Evelina Children's Hospital, St. Thomas' Hospital, London, UK and [14]Department of Basic and Clinical Neuroscience, Institute of Psychiatry, Psychology and Neuroscience (IoPPN), King's College London, London, UK

*To whom correspondence should be addressed at: LAB 408, Department of Biomedizin and Anesthesia, Hebelstrasse 20, 4031 Basel, Switzerland. Tel: +41 612652373; Fax: +41 612653702; Email: susan.treves@unibas.ch

Abstract

Congenital myopathies are genetically and clinically heterogeneous conditions causing severe muscle weakness, and mutations in the ryanodine receptor gene (RYR1) represent the most frequent cause of these conditions. A common feature of diseases caused by recessive RYR1 mutations is a decrease of ryanodine receptor 1 protein content in muscle. The aim of the present investigation was to gain mechanistic insight into the causes of this reduced ryanodine receptor 1. We found that muscle biopsies of patients with recessive RYR1 mutations exhibit decreased expression of muscle-specific microRNAs, increased DNA methylation and increased expression of class II histone deacetylases. Transgenic mouse muscle fibres over-expressing HDAC-4/HDAC-5 exhibited decreased expression of RYR1 and of muscle-specific miRNAs, whereas acute knock-down of RYR1 in mouse muscle fibres by siRNA caused up-regulation of HDAC-4/HDAC-5. Intriguingly, increased class II HDAC expression and decreased ryanodine receptor protein and miRNAs expression were also observed in muscles of patients with nemaline myopathy, another congenital neuromuscular disorder. Our results indicate that a common

95

pathophysiological pathway caused by epigenetic changes is activated in some forms of congenital neuromuscular disorders.

Introduction

Congenital myopathies constitute a genetically and phenotypically broad spectrum of disorders characterized clinically by muscle weakness and atrophy, joint contractures, spinal deformities and variable cardiorespiratory involvement. Congenital myopathies have been historically defined by their most predominant histopathological feature, with major entities being central core disease (CCD), multi-minicore disease (MmD), nemaline myopathy (NM) and congenital fibre type disproportion (CFTD) (1–4). Their severe complications require patients to receive continual medical attention, resulting in a substantial individual, familial, and social disease burden. Each congenital myopathy can be caused by mutations in more than one gene, and mutations in the same gene can cause different pathological phenotypes. The prime examples are ryanodine receptor 1 (RYR1)-related myopathies, caused by mutations in the gene encoding the RyR1, the calcium release channel of the skeletal muscle sarcoplasmic reticulum. Physiologically, activation of the RyR1 leads to release of calcium from the sarcoplasmic reticulum, leading to muscle contraction by a process called excitation–contraction coupling (ECC) (5). Excitation–contraction coupling occurs at the triad, a structure made up of two membrane compartments: the transverse tubules containing the voltage-gated dihydropyridine receptors and the sarcoplasmic reticulum terminal cisternae containing the RyR1. ECC requires the proper distribution and assembly of sarcoplasmic reticulum proteins, and tight regulation of calcium homeostasis is critical for proper muscle function. Indeed, mutations in *RYR1* lead to calcium dysregulation and are the underlying cause of several neuromuscular disorders. While most dominant mutations associated with CCD and malignant hyperthermia susceptibility are missense (6), recessive mutations associated with the pathological phenotypes of MmD, centronuclear myopathy (CNM) and CFTD (1–4) are often compound heterozygous, with one allele presenting a nonsense, intronic splice site or a frameshift mutation, and the other allele presenting a missense mutation (3,4). As to their mode of action, dominant missense mutations affect the biophysical properties of the RyR Ca^{2+} channel (6), whereas for recessive mutations, the mechanism is still elusive, though a common finding is the low levels of RyR1 and of other SR proteins in biopsied muscles (2–4,7). Intriguingly, this decrease occurs only in mature muscle and not in other tissues expressing RyR1 such as B-lymphocytes (8).

Because of their heterogeneity, one of the major aims of research in congenital myopathies is to find a common target in order to develop a pharmacological tool to help improve muscle function and thus quality of life in this group of patients. In fact, though the number of patients with a given genetic form of a disease is small (1:3000), the number of patients suffering from inheritable congenital myopathies worldwide is ~286 million (9) with CCD accounting for 16% of cases, nemaline rod myopathy for 20%, CNM for 14% and multicore myopathy for 10% (http://www.muscular-dystrophy.org/research/patient_registries) (1). Thus, discovering a common target downstream of the primary genetic defect could potentially benefit a large number of patients. The findings of the present investigation indicate that common epigenetic changes consequent to the primary genetic defect are activated in different congenital myopathies.

Results

Calcium homeostasis in myotubes from patients with mutations leading to decrease RyR1 content

Our first approach was to study calcium homeostasis in myotubes derived from biopsies of four patients initially diagnosed as having MmD, three of whom carry recessive *RYR1* mutations and one carrying the heterozygous mutation p.G297D but who exhibited reduced RyR1 protein on western blot. Subsequent whole-exome sequencing later revealed that the patient also harboured two compound heterozygous *NEB* mutations and is therefore identified as NEM UK06 in Figure 1. Figure 1 shows that the resting fura-2 fluorescence ratio (340/380 nm) as well as the KCl-dependent calcium release curves were not different, except for patient Minicore UK 07, who showed a significantly reduced sensitivity to KCl (EC_{50} for KCl was 55.3 ± 8.2 in myotubes from Minicore UK07 compared with 13.9 ± 8.4 in myotubes from controls) (Fig. 1A and B). The KCl-dependent calcium release curve for patient Minicore UK08 (dotted trace with asterisk symbol Fig. 1B) had also been previously reported to be similar to that of control myotubes (10). These results were surprising as western blots of muscle biopsies from all four patients showed a very large reduction of RyR1 protein content (Fig. 1C) leading us to expect a large effect on calcium homeostasis in myotubes. Because of these reasons, we hypothesized that the mechanism leading to reduced RyR1 expression is only operative in more mature tissues, such as myofibres, and not in cultured myotubes, even though the latter express the main protein components of the ECC machinery (7).

Epigenetic down-regulation of the ryanodine receptor 1

We focussed the next series of experiments on epigenetic mechanisms that may be responsible for regulating RyR1 expression levels and in particular on the content of microRNAs (miRs). These endogenous ~22 nucleotide small non-coding RNAs are known to control gene expression by repressing translation or enhancing RNA degradation. Because of the limited amount of biological material available from patients, we decided to measure the expression levels of a selected group of muscle-specific miR transcripts, namely miR-1, miR-133, miR-206, and the muscle enriched miR-486 (11–13). miR-22 and miR-124 were also measured as bioinformatics analysis showed that the 3′ UTR of the *RYR1* gene contains binding sites for these two miRs. As controls, we selected miR-126 and miR-221 that are reported to be expressed in many different tissues (14,15). We analysed muscle biopsies from 5–9 controls, from 4–5 patients with CCD with dominant *RYR1* mutations and from 12–16 patients with mutations leading to a decrease of RyR1 protein expression with pathological features of either MmD or CNM. The latter patients are categorized as 'Minicore', and in addition to muscle weakness, they show decreased RyR1 protein in their muscle biopsy, and all have the following common pathological features: several minicores and increased number of internal nuclei in their muscle biopsy as well as a myopathic face often accompanied by ophthalmoplegia (16). All but patients Minicore NL01, UK02, UK05 and UK09 harboured recessive *RYR1* mutations (see Supplementary Material, Table S1 for patient's diagnosis, genotypic and phenotypic characteristics). Figure 2 shows that the relative contents of miR-22, miR-124, miR-1 and miR-133 were reduced to almost undetectable
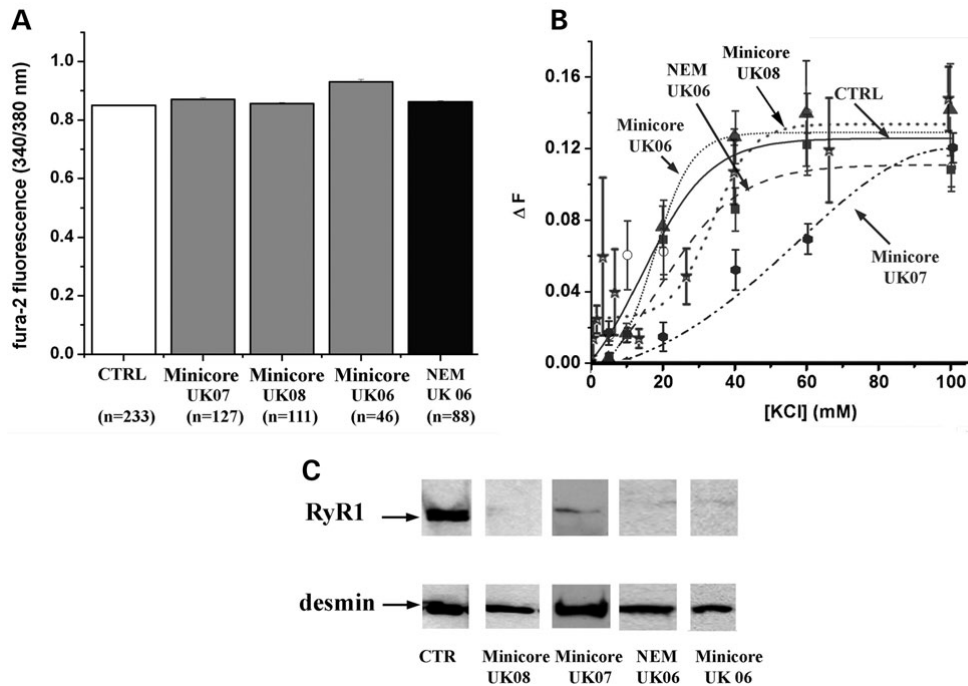
Figure 1. Myotubes from Minicore patients harbouring recessive *RYR1* mutations do not show alterations of the resting [Ca^{2+}] nor decreased Ca^{2+} release after *in vitro* stimulation. (**A**) Fura-2-loaded myotubes were imaged in Krebs Ringer solution containing 2 mм Ca^{2+}. No difference in the resting [Ca^{2+}]$_i$ was observed between controls (white bar), cells from patients with recessive mutations (grey bars) or a patient initially diagnosed as MmD carrying the heterozygous p.G297D *RYR1* mutation but who also carries two compound heterozygous *NEB* mutations (black bar). Bars represent the mean (± SEM) fluorescence (340/380 nm) from the indicated number of cells. (**B**) KCl-dependent peak Ca^{2+} release in Krebs Ringer containing 100 μм La^{3+}. Each point represents the mean (±SEM) increase in fura-2 fluorescence ratio (340/380 nm) of at least 10 myotubes. The data were analysed through Bolzmann equation using Origin 6.0. (**C**) Western blot analysis of total protein extracts from muscle biopsies shows major decrease in RyR1 protein expression in Minicore patients. Desmin served as loading control.

levels in biopsies from >60% of Minicore patients with decreased RyR1 protein expression, whereas the reduction was not as consistent in biopsies from CCD patients. Our results also indicate that the observed changes in miRs are specific to some muscle transcripts and not caused by a more global defect in the miR-synthesizing machinery, as miR-206, miR486 as well as miR-126 and miR-221 were not decreased (Fig. 2 and Supplementary Material, Fig. S1).

RYR1 methylation

The results obtained so far point to a potential role of regulation of skeletal muscle gene expression by additional factors. We next verified whether changes of DNA methylation occur within the *RYR1* gene. This experiment is essential as methylation-dependent expression of the *RYR1* gene was not unexpected considering the presence of several CpG-rich regions. Genomic DNA was extracted from biopsies of four controls and four Minicore patients, and the methylation of CpG regions was studied using the methyl-sensitive HpaII and the methyl-insensitive MspI restriction enzymes. After cleavage of genomic DNA, quantitative real-time PCR was performed and compared with a control PCR amplifying a proximal *RYR1* gene region lacking HpaII/MspI cleavage sites (see schematic representation in Fig. 3A). The results obtained clearly indicate that the CpG-III region of the *RYR1* gene (from nucleotide 6790 to nucleotide 7035) of all the Minicore patients analysed is hypermethylated compared with that of controls (Fig. 3B) suggesting that *RYR1* mutations are associated with deep changes in the pattern of DNA methylation. Additionally,

we analysed biopsies from Minicore patients and controls for DNA methyltransferase (DNM) expression and found that in the former group DNMT1 and DNMT2 are significantly up-regulated (Fig. 3C), whereas the expression of DNMT3 did not vary significantly between controls and patients (results not shown).

HDAC expression levels in muscle biopsies of patients with minicores with recessive RYR1 mutations

The levels of expression of HDAC-4 and HDAC-5 in muscle biopsies from controls and patients were subsequently determined for the following reasons: (i) class II histone deacetylases (HDACs) can be recruited in association with DNA methylation, (ii) these enzymes repress transcription by deacetylating core histones (17), (iii) they affect myogenesis by binding to the muscle transcription factor mef2 (18), (iv) they are predominantly expressed in those tissues expressing mef2, that is skeletal muscle, heart and brain (18) and (v) HDAC-4 is a target of miR-22 whose down-regulation potentiates HDAC-4 expression (19). Figure 4A shows a representative western blot of total muscle homogenate stained with anti-HDAC-4 and HDAC-5 antibodies; the bottom lane shows a loading control of the same blot stripped and probed with anti-myosin heavy chain (MHC) antibodies recognizing all MHC isoforms. The control biopsy shows low levels of class II HDACs (Lane 1 Fig. 4A), whereas samples from the Minicore patients contain abnormally high levels of HDAC-4 and HDAC-5. Figure 4B shows the relative content of HDAC-4 and HDAC-5 normalized for MHC content in biopsies from all the available
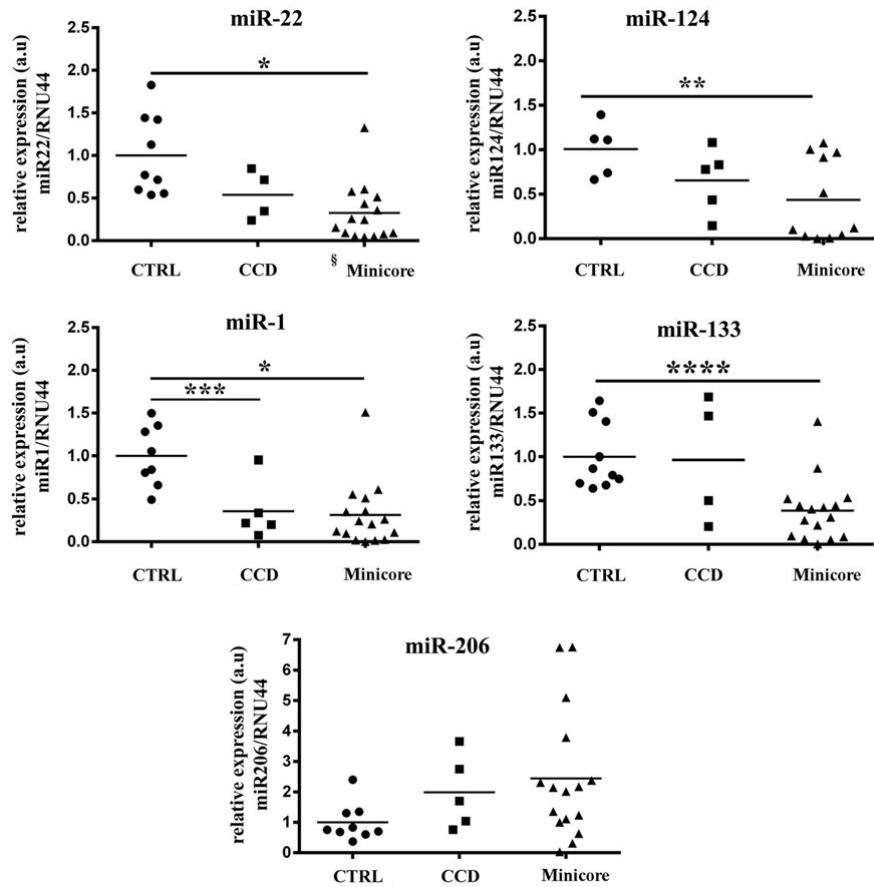
Figure 2. Muscle-specific miR expression levels differ in biopsies from patients with dominant and recessive *RYR1* mutations. Each symbol represents the mean relative expression of the indicated miR from a single patient normalized to RNU44 content and to the muscle-specific housekeeping genes (*DES/ACTN2*). Control healthy individuals, circles; CCD with dominant *RYR1* mutations, squares; Minicore, triangles. Statistical analysis was performed using ANOVA and Bonferroni multiple comparison test (95% confidence interval). miR-22 $^*P < 0.0005$, CTRL $n = 9$, CCD $n = 4$, Minicore $n = 15$; miR-124 $^{**}P < 0.05$, CTRL and CCD $n = 5$, Minicore $n = 12$; miR-1 $^*P < 0.0005$, $^{***}P < 0.009$, CTRL $n = 8$, CCD $n = 5$, Minicore $n = 16$; miR133 $^{****}P < 0.002$, CTRL $n = 10$, CCD $n = 4$, Minicore $n = 16$; miR-206; no statistical significance change between groups. CTRL $n = 9$, CCD $n = 5$, Minicore $n = 16$. Statistical analysis was performed using ANOVA and Bonferroni multiple comparison test (95% confidence interval).

patients. Biopsies from patients with recessive compound heterozygous *RYR1* mutations, with a non-sense, intronic splice site or a frameshift mutation in one allele and a missense mutation in the other allele show a 6- to 15-fold increase in class II HDAC content, and the increase in HDAC-4 expression was also detectable at the transcriptional level (Fig. 4D). Interestingly, HDAC-4 was not detectable in any of the myotube cultures (Fig. 4C) supporting the observed lack of effect of the mutations on the ECC characteristics of myotubes from the Minicore patients (Fig. 1). Figure 4E shows a photomicrograph taken by confocal microscopy on a sample from Minicore SA06; as can be seen, though the vast majority of HDAC-4 is distributed throughout the muscle fibre, the amount co-localizing with nuclei is higher in the patient's biopsy than in the control biopsy. Analysis of two Minicore patients and two controls confirmed that the percentage of HDAC-4 co-localizing with nuclei is ∼10 times higher in muscles from Minicore patients than that from controls (9.2 ± 3.8% versus 1.1 ± 0.3%, respectively). We also compared HDAC-4 and HDAC-5 up-regulation and *RYR1* hypermethylation in the samples of the four Minicore patients and found a positive correlation between high HDAC-4/5 levels and hypermethylation of the studied *RYR1* CpG-III gene sequence (Fig. 5A and B).

Effect of HDAC4/5 over-expression and RYR1 silencing in mouse muscle fibres

To demonstrate a causative link between *RYR1* mutations and the above-described epigenetic changes, we manipulated gene expression by creating transgenic intact adult mouse skeletal muscle *flexor digitorum brevis* (FDB) fibres by either (i) over-expressing HDAC-4 and HDAC-5 or (ii) knocking down RyR1 by siRNA silencing. When compared with acute transfection with an empty plasmid, acute over-expression of HDAC-4 and HDAC-5 directly recapitulates the effects observed in muscle biopsies from Minicore patients (Fig. 6). That is, acute over-expression of HDAC-4 and HDAC-5 in mouse FDB fibres decreases *RYR1* transcript expression by ∼70% (Fig. 6) and RyR1 protein content by 75% (Supplementary Material, Fig. S3), down-regulates muscle-specific miRs and down-regulates the expression of myomesin-1, a muscle-specific gene whose expression is regulated by the transcription factor mef2 (20,21) (Fig. 6). No changes were observed in mef2, miR-126, miR-221 and miR-486 expression (Supplementary Material, Table S2). On the other hand, silencing *RYR1* for 8 days with siRYR1 significantly increased HDAC-4 and HDAC-5 expression levels but did not change the expression of muscle-specific miRs (Fig. 7).
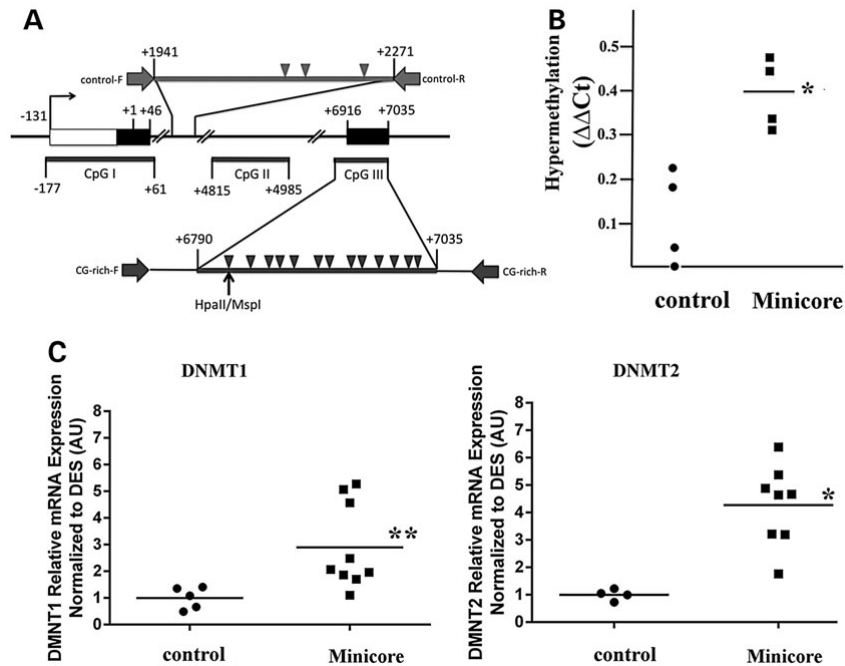
Figure 3. The *RYR1* is hypermethylated, and DNA methyltransferases 1 and 2 are up-regulated in muscles from Minicore patients. (**A**) Schematic representation showing the location of the CpG region III within the *RYR1* gene, the position of the CpG sites (indicated by arrowheads) and the location of the 5′ CCGG 3′ HpaII/MspI site (arrowed); the location of the internal control region lacking HpaII/MspI sites is also shown, as well as the location of the PCR primers used to amplify the DNA. (**B**) Hypermethylation of CpG region III of the *RYR1*. Each symbol represents the mean relative methylation value from a patient (CTRL $n = 4$; Minicore $n = 4$). Experimental details are outlined in Materials and Methods. (**C**) DNA methyltransferase 1 (DNMT1) and DNMT2 are significantly up-regulated in muscles of Minicore patients. Each symbol represents the mean relative expression of DNMT1 (CTRL $n = 5$; Minicore $n = 9$) and DNMT2 (CTRL $n = 4$, Minicore $n = 8$) from a single patient normalized to the muscle-specific housekeeping gene *DES* (*$P < 0.02$, **$P < 0.025$, Student's t-test).

Increasing class II HDAC expression does not affect mef2 expression

Having established that down-regulation of *RYR1* causes an increase in HDAC-4/5 expression, we reasoned that this elevation could lead to downstream effects on mef2, a master trans-activator of skeletal muscle gene expression (22). Mef2 is sequestered by class II HDACs resulting in blockage of mef2-dependent gene transcription (23), and the *RYR1* and miR-1/miR-133 genes contain intragenic mef2-dependent enhancer sequences that regulate their transcription in muscle (24,25). We therefore examined the patient's muscle biopsies for: (i) mef2 content, to ascertain that there was no compensatory up-regulation of its expression owing to the increased expression of HDAC-4/5 and (ii) myomesin a protein that is transcriptionally regulated by mef2 (20,21). Figure 8 shows that the transcript levels of MEF2A, MEF2C and MEF2D are not significantly different between controls and biopsies from patients. On the other hand, myomesin-1 protein levels normalized to MHC are significantly decreased (by ~50% in biopsies isolated from patients with minicores (Fig. 8B and C).

HDAC-4/5 are also up-regulated in other congenital myopathies

To verify whether these observed effects (that is increased levels of HDACs, decreased levels of RyR1 and decreased levels of muscle-specific miRs) are specific for congenital myopathies owing to recessive *RYR1* mutations or a more general response occurring in patients with other congenital myopathies, we analysed biopsies from 11 patients with NM harbouring mutations in *KBTBD13*,

ACTA1 or *NEB* (NEM 6, NEM3 and NEM2, respectively). A similar decrease in muscle-specific miR-22, miR-133 and miR-1s was observed (Supplementary Material, Fig. S2). We also tested the muscle biopsies from the patients with NM for RyR1 content and HDAC-4 and HDAC-5 expression. Surprisingly, RyR1 protein content was significantly reduced (control versus NEM was $100 \pm 27.9\%$ versus $0.03 \pm 0.02\%$, $P < 0.01$, Student's t-test), and HDAC-4 and HDAC-5 protein levels were significantly increased (Supplementary Material, Fig. S2).

Discussion

Here, we identify a novel pathophysiological mechanism occurring in skeletal muscles of patients with congenital myopathies whereby activation of a cascade of events leads to the down-regulation of muscle-specific genes. We report that recessive compound heterozygous *RYR1* mutations are accompanied by the following changes in skeletal muscle: (i) hypermethylation of the *RYR1* gene, (ii) a 6- to 15-fold increase in class II HDAC expression and (iii) reduction in muscle-specific miRs. Our results represent a major advancement in the field as to date the mode of action of recessive *RYR1* mutations identified in patients with MmD, CNM and CFTD has been elusive and the functional characterization of cells harbouring such mutations has failed to yield a mechanism compatible with the disease phenotype (8,10,26). A regular finding in muscle biopsies of patients with recessive *RYR1* mutations has been a reduced expression level of RyR1 protein and transcript (2–4,26–28). This reduction appears to be muscle-specific and has not been observed in other tissues
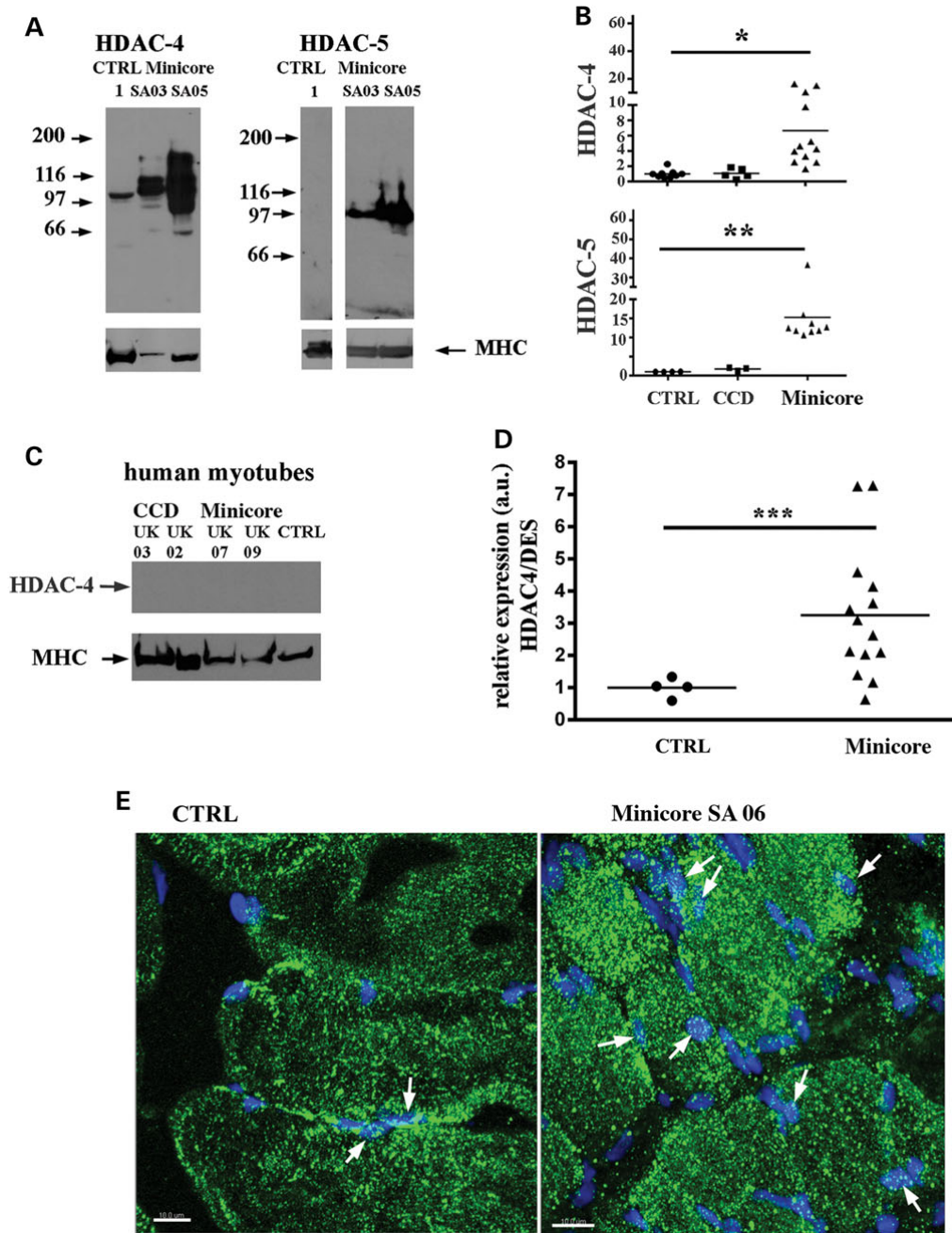
Figure 4. Class II HDACs are significantly up-regulated in muscle biopsies from patients with Congenital Muscle Disorders. (**A**) Western blot analysis of biopsies from a control muscle (Lane 1) and Minicore patients (Minicore SA03 and Minicore SA05). Fifty micrograms of total muscle protein extracts were separated on a 6% SDS–PAGE, blotted onto nitrocellulose and probed with anti-HDAC-4 and HDAC-5 antibodies. Lower portion of the figure, loading control; the same blot was probed with anti-MHC recognizing all isoforms. (**B**) Quantification of HDAC-4 and HDAC-5 normalized to MHC in muscle biopsies of controls (circles), CCD patients (squares) and Minicore patients (triangles). HDAC-4 *$P < 0.001$, CTRL $n = 9$, CCD $n = 5$, Minicore $n = 12$; HDAC-5**$P < 0.01$ CTRL, $n = 4$, CCD $n = 3$, Minicore $n = 9$; ANOVA and Bonferroni multiple comparison test were performed. Each symbol represents results from a single patient. (**C**) No HDAC-4 protein is detectable in myotubes. (**D**) HDAC-4 transcript levels as assessed by qPCR in muscle biopsies from controls and Minicore patients ***$P < 0.02$, CTRL $n = 4$, Minicore $n = 14$; statistical analysis performed using Student *t*-test. (**E**) Confocal microscopy showing distribution of HDAC-4 in a muscle biopsy from a control (left panel) and Minicore patient. Arrows indicate co-localization of HDAC-4 and DAPI. Bar indicates 10 µm.

ectopically expressing RYR1, such as B-lymphocytes (8). Because of these results, we set out to test the hypothesis whereby the mechanism leading to reduced RyR1 muscle expression may be epigenetically regulated and the schematic representation depicted in Figure 9 summarizes the results of the present study. The key point is that RYR1 mutations are accompanied by an
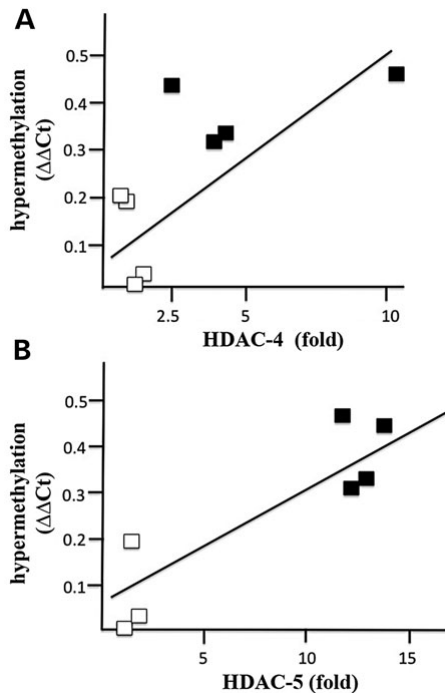
Figure 5. Correlation between DNA methylation and HDAC-4/HDAC-5 expression and up-regulation of DNA methyltransferases in muscles of patients with Minicore. The data shown in this figures were obtained from biopsies from four control individuals (empty squares) and from biopsies from four Minicore patients (filled squares) (Minicore NL02, Minicore NL03; Minicore SA03, Minicore SA05). (**A**) Correlation between HDAC-4 and *RYR1* hypermethylation (correlation coefficient $r = 0.4695$). (**B**) Correlation between HDAC-5 and *RYR1* hypermethylation (correlation coefficient $r = 0.7925$).

increased expression of class II HDACs. We are aware that an increase in HDAC expression has been reported in other conditions, including denervation, muscle atrophy, ALS and Huntington's disease (29–34). However, we would like to point out that (i) such high levels of expression of class II HDACs have not been reported in any other human neuromuscular abnormalities investigated so far; (ii) such an increase of HDAC is specific because the signal to background ratio of our set of data is 6–16 times greater than that reported in other muscle disorders and (iii) over-expression of HDAC-4 and HDAC-5 in mouse FDB fibres results in the down-regulation of RYR1 and of muscle-specific miRs. High levels of HDACs not only lead to chromatin condensation thereby decreasing gene transcription (21,35,36), but also sequester mef2 (23,37–39). In this context, it should be pointed out that there is no compensatory up-regulation of mef2 in muscles from the patients, so that up-regulation of HDACs would lead to the down-regulation of mef2-dependent proteins. That this is the case is supported by the fact that RYR1, myomesin and muscle-specific miRs containing mef2-dependent binding domains (21,24,25) are significantly down-regulated in the muscles of Minicore patients. Though few studies have focussed on the mechanisms regulating RYR1 expression, the 5′ region of the human and porcine RYR1 gene contains, aside a mef2-binding domain (24), consensus sequences for the transcription factor SP1, for muscle-specific promoter elements as well as for a number of transcriptional activators (40). SP1 is a zinc finger transcription factor that binds to CG-rich regions present in many promoters.

In fibroblasts, SP1 interacts with HDAC-2 leading to the transcriptional silencing of the human telomerase reverse transcriptase (hTERT) gene in normal somatic cells (41). Whether SP1 can also interact with class II HDACs and whether this interaction is modified by CpG methylation also leading to repression of RYR1 gene transcription remains to be investigated.

Interestingly, the 3′ UTR of HDAC-4 and that of HDAC-5 have binding sites for miR-22/mir-124/miR-1/miR-206 and miR-206, respectively, and HDAC-4 is a target of miR-22 whose down-regulation potentiates its expression (19). Thus, it follows that a decrease of miR-22, miR-124 and miR-1 activates a pathological loop leading to the further up-regulation of class II HDACs (Fig. 9). This mechanism is compatible with and gives mechanistic insight to two previous observations: (i) other muscle-specific genes besides the RYR1 are down-regulated in patients with congenital myopathies owing to RYR1 mutations (7) and (ii) the RYR1 was reported to be imprinted in some patients with MmD because of epigenetic factors (42). The former observation is likely due to the sequestration of mef2 by class II HDACs (37–39). The latter observations on the other hand can be explained by the finding that the DNA methyltransferases DNMT1 and DNMT2 are over-expressed in muscle biopsies of Minicore patients, bringing about RYR1 hypermethylation. DNMT1 is a maintenance methyltransferases preserving methylation patterns but also has *de novo* activity (43). DNMT2 on the other hand is thought to participate in the recognition of damaged DNA and mutation repair (44). In fact, the two observations are mechanistically linked as hypermethylation goes hand in hand with HDAC activation and gene down-regulation (23,24,35,36,45); furthermore, DNA damage can activate DNA-methylation via activation of DNMT1 (46), resulting in a pathological loop that will ultimately shut down gene transcription of mef2-dependent genes.

As to the role miRs in neuromuscular diseases, this is still unclear: over-expression of miR-22 is sufficient to cause cardiomyocyte hypertrophy (47) and several miRs are up-regulated in muscular dystrophies (48–50) but depending on the disease, some miRs may appear to be down-regulated (50). Interestingly, a recent study demonstrated that mice lacking miR-133 develop an adult onset CNM in type-2 fibres, and this is accompanied by impaired mitochondrial function, fast to slow myofiber conversion and disarrangement of triads (51), histopathological changes very similar to those observed in recessive human RYR1-related myopathies. Though in the paper the authors conclude that this is principally due to the dysregulation of dynamin-2, one of miR-133′s targets, the similarities between the phenotype of the miR-133a knockout mice and that of patients with RYR1 mutations is striking and is indicative of a common pathophysiological pathway.

The main point emerging from our studies is that epigenetic factors are central culprits in recessive RYR1-linked myopathies. Our results also show that these factors are likely to also play a major role in other congenital muscle diseases such as NM. In support of a role of epigenetics, moderate exercise has been shown to improve the muscle function of some patients with congenital myopathies (52,53) and there is increasing evidence that physical activity influences DNA methylation in humans (53,54). Taken together our results suggest that a common pathophysiological mechanism is activated in skeletal muscles of patients with some congenital myopathies. The presence of mutations in muscle-specific genes (in this case RYR1) activates factors that lead to the up-regulation of DNMs and of class II HDACs, the master regulator of chromatin structure. Though the primary mechanism causing HDAC up-regulation is at the moment unclear, our data provide the proof of concept that
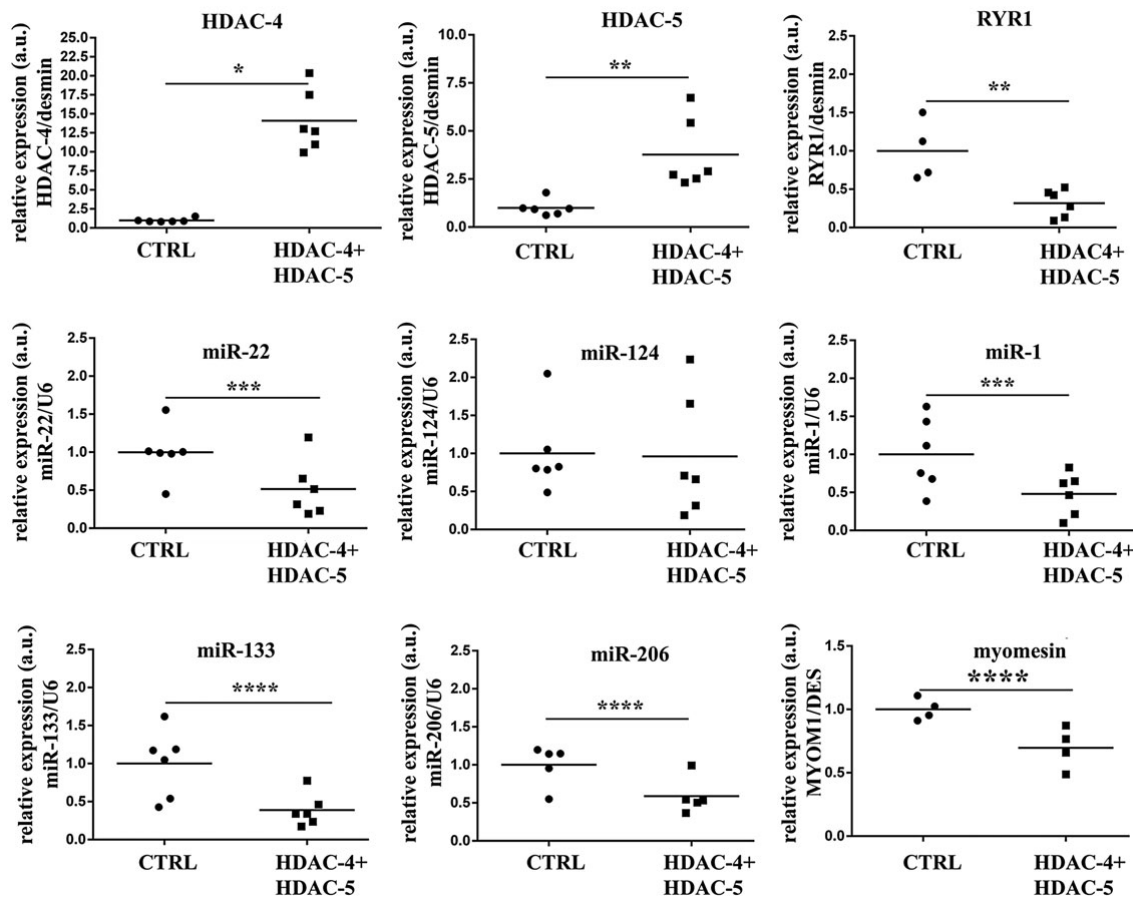
Figure 6. *In vivo* over-expression of HDAC-4 and HDAC-5 causes down-regulation of RYR1 and of muscle-specific miRs. Each symbol shows the mean triplicate relative expression value of the indicated transcript normalized to the indicated gene. Circles, control FDB fibres mock transfected with the empty pIRES2-dsRed2 plasmid; squares, FDB fibres transfected with a plasmid encoding mouse HDAC-4 and HDAC-5. HDAC-4; *P < 0.0001, n = 6; HDAC-5 **P < 0.005, n = 6; RYR1 **P < 0.005, CTRL n = 4, HDAC-4 and 5 n = 6; miR-22 and miR-1; ***P < 0.045, n = 6; miR-133 ****P < 0.035, n = 6; miR-206 ****P < 0.035, n = 5; Myomesin ****P < 0.035, n = 4; miR-124 was quantified and no significance change was observed. Statistical analysis was performed using the Student's t-test.

DNM and HDAC are potential pharmacological targets to treat a wide range of inherited neuromuscular conditions with different genetic backgrounds that as a common feature lead to a decrease in RyR1.

Materials and Methods

Quantitative PCR

Total RNA was extracted using Trizol (Life Technologies, #15596018). cDNA was synthesized with the High Capacity cDNA synthesis kit or Taqman microRNA Reverse Transcription kit (Applied Biosystems, #4366596). Transcript levels were quantified using Syber-Green reagent on an Applied Biosystem platform (7500 fast real-time PCR system); levels of expression from triplicate replicas were averaged and normalized to the content of the muscle-specific gene desmin (*DES*). In the case of human samples, because of the limited amount of biological material, not all biopsies could be investigated for all genes. The sequences of the primers used for qPCR are listed in Supplementary Material, Table S3.

MicroRNA determination

Quantification of selected miRs was performed using TaqMan master mix no-UNG 2 (Life Technologies, # PN 4427788) and the following miR assays (Life Technologies, # PN 4427975): miR-22, miR124a, miR-133a, miR-1, miR-206, miR-486-3p, miR-221 and miR-126. Each reaction was performed in triplicate, and the results from each muscle sample were analysed and averaged. In human muscle biopsies, miR expression levels were normalized to RNU44 and to the muscle-specific genes *DES* and Actinin2 (*ACTN2*) that show similar Ct values in patients and healthy individuals. In mouse FDBs, miR expression levels were normalized to U6 snRNA. In the case of human samples, because of the limited amount of biological material, not all biopsies could be investigated for all microRNAs.

DNA methylation

Total genomic DNA was isolated using the GeneElute mammalian genomic DNA Miniprep kit (Sigma Genosys). DNA methylation
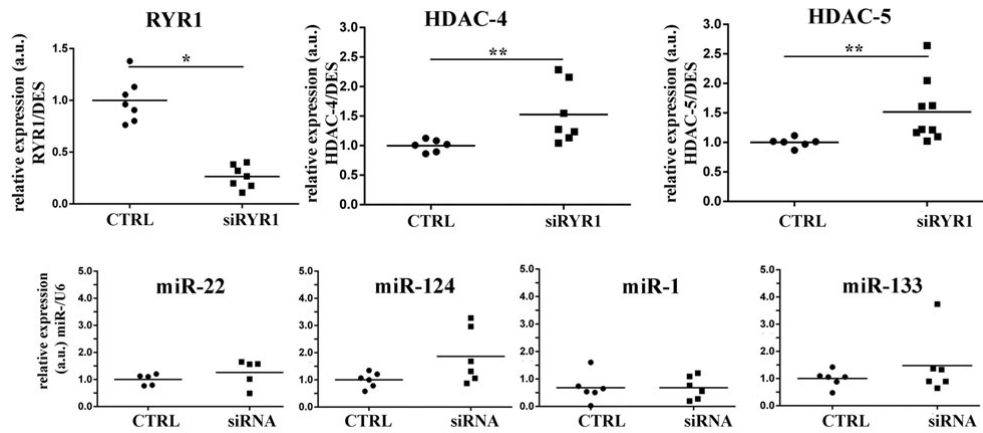
Figure 7. Down-regulation of RYR1 by siRNA leads to up-regulation of HDAC-4 and HDAC-5. Each symbol shows the mean triplicate value relative expression level of the indicated transcript normalized to U6 snRNA (miR expression) or *DES* (RYR and *HDAC* expression), in fibres isolated from a single mouse. Circles, control (mock) transfection with a scrambled siRNA; squares FDB transfected with siRYR RNA (see Materials and Methods for details). RYR1 *$P < 0.0001$, $n = 7$; HDAC-4 **$P < 0.04$, CTRL $n = 6$, siRYR1 $n = 7$. HDAC-5; **$P < 0.04$, CTRL $n = 6$, siRYR1 $n = 9$. miR-22, miR-133, miR-124 and miR-1 show no statistical difference. Statistical analysis was performed using the Student's t-test.
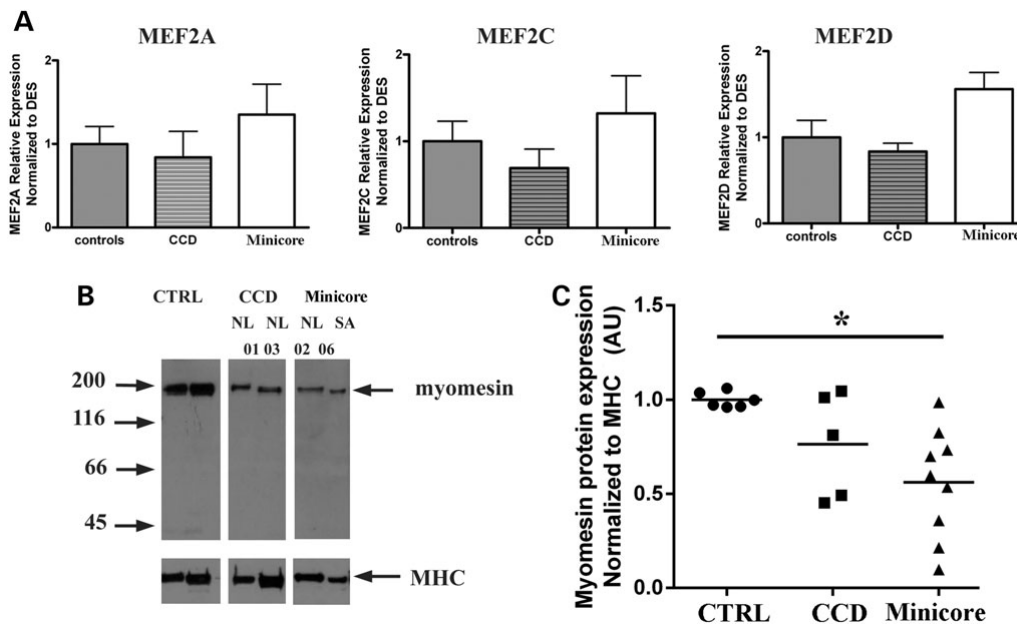
Figure 8. Increased expression of HDAC-4/HDAC-5 leads to a decrease in the content of myomesin, without affecting mef2. (**A**) mef2A, mef2C and mef2D transcript levels are similar in muscle biopsies of patients and controls (expression levels normalized to *DES*). (**B**) Representative western blot showing that the protein content of myomesin is lower in patients with Minicore compared with healthy individuals (letters and numbers refer to patient no.; see Supplementary Material, Table S1); (**C**). Quantification of myomesin protein content in muscle biopsies: controls, circles ($n = 6$); CCD, squares ($n = 5$); Minicore, triangles ($n = 9$). *$P < 0.02$. Statistical analysis was performed using ANOVA and Bonferroni multiple comparison test (95% confidence interval).

was assessed by PCR amplification of genomic DNA digested with the methyl-sensitive HpaII and MspI restriction enzymes (55) (see schematic representation in Fig. 3A). Restriction enzyme digestion reactions were carried out overnight at 37°C, with HpaII or MspI (New England BioLabs), in final volume of 20 μl. The primers used for PCR amplification are listed in Supplementary Material, Table S3 as: Human RYR1 CG-rich (F and R) amplifying the CpG-III region of the *RYR1* gene and Human

RYR1 Control (F and R), amplifying a control region of the *RYR1* gene lacking HpaII/MspI sites (see Fig. 3A). To determine the extent of DNA methylation, the ΔCt values were first obtained comparing the CpG-III and control PCRs of HpaII digestions, and then the ΔΔCt values were generated using as reference the samples exhibiting the higher ΔCt. Higher ΔΔCt values indicate higher extent of DNA methylation at the CpG-III RyR1 MspI/HpaII cleavage sites.
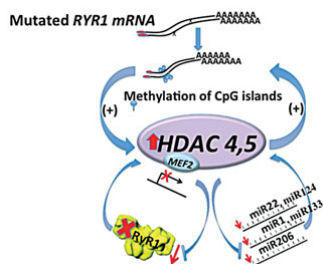
Figure 9. Cartoon depicting how mutations in *RYR1* lead to a decrease in RyR1 content thereby leading to weak muscles. Mutations lead to DNA hypermethylation and HDAC-4/HDAC-5 over-expression. This causes mef2 sequestration thereby inhibiting transcription of genes regulated by mef2, including the *RYR1* and muscle-specific miRs. A decrease in RyR1 would severely affect muscle excitation–contraction coupling because this calcium channel is a central player in this mechanism, releasing the calcium necessary for muscle contraction from the sarcoplasmic reticulum.

Electrophoresis and immunoblotting

Total muscle proteins were extracted in 10 mM Hepes pH 7.0, 150 mM NaCl, 1 mM EDTA and anti-protease (Roche, # 11873580001). Protein concentration was determined using Protein Assay Kit II (Bio-Rad Laboratories) using BSA as a standard. SDS–PAGE, protein transfer on to nitrocellulose membranes and immunostaining were performed as described previously (2,8). The following primary antibodies were used: mouse anti-RyR1 (Ryanodine 1 Receptor, Thermo Scientific, # MA3-925), mouse anti-MHC (MHC, Millipore, #05-716), Rabbit anti-HDAC-4 (Histone Deacetylase 4, Cell Signaling, #2072) and rabbit anti- HDAC-5 (Histone Deacetylase 5, Abcam #1439), and rat anti-myomesin was a generous gift of Prof. Mathias Gautel, King's College, London, UK (56). Secondary peroxidase conjugates were Protein G–peroxidase (Sigma, #P8170) and peroxidase-conjugated goat anti-mouse IgG (Sigma, #A2304). The immunopositive bands were visualized by chemiluminescence using the Super Signal West Dura kit (Thermo Scientific). In order to perform statistical analysis, the intensity of the immunopositive bands was determined using ImageJ/FIJI. The intensity values were normalized to the intensity of the indicated muscle-specific housekeeping protein. The value (arbitrary units) obtained from the patient's biopsies were divided by the mean value obtained from control biopsies and are expressed as 100%.

Mouse muscle fibre electroporation and isolation

The procedure was as described by DiFranco *et al.* (57). Briefly, 8- to 14-week-old mice were anaesthetized using isofluorane, and 7.5 µl of 2 mg/ml Hyaluronidase in RNase-free Tyroide's Buffer (Sigma Fine Chemicals, #H3506) was injected under the footpad. The mice were left 1 h under supervision, and subsequently, the following constructs were injected into the footpad: pCMV6-HDAC4 (Origene #MR211598) and pCMV6-HDAC5 (Origene # MC202550) whereas control mice (mock transfected) received 20 µg of pIRES2-dsRed2 plasmid (Clonetech #632420). For siRNA silencing experiments, 6 nmol of RNA either specific for the RYR1 (Ambion; siRNA RyR1-#4390771) or a scrambled siRNA sequence (Negative control 2-#4390845) were used. siRNA-transfected FDBs were also injected with lipofectamine RNAiMAX (Invitrogen, #13778-030). Ten minutes post-injection, FDBs were electroporated using acupuncture needles placed parallel and perpendicular to the long axis of the foot (with 1 cm distance), and twenty pulses (100v/cm, 20 ms duration and 1 Hz of frequency) were given. Six to ten days post–transfection, the mice were sacrificed and FDBs were isolated by enzymatic dissociation at 37°C for 60 min in Krebs Ringer solution no Ca^{2+} (pH 7.4), containing 0.2% collagenase I (Sigma Fine Chemicals, C-0130). Enzymatic digestion was terminated by washing the muscle with Tyrode's solution (pH 7.4), and single fibres were isolated and total protein extracts prepared or RNA was extracted and analysed by qPCR.

Ca^{2+} measurements

Primary skeletal muscle cultures and cell imaging were performed as previously described (58).

Confocal microscopy and immunofluorescence

Biopsies were embedded for pathological examination and sliced using a cryostat (10 µm thickness). Cryosections were fixed with methanol: acetone (1:1) for 30 min and then incubated in the following solutions for 90 min at room temperature: blocking solution (Roche, #115000694011), rabbit anti-HDAC-4 (Cell Signaling, #2072) and Alexa Fluor 647-conjugated anti-Rabbit IgG (Life Technologies, #A21245). Nuclear staining was performed using DAPI (Invitrogen, #D21490), and slides were mounted with mounting medium (Sigma, #1000-4) and sealed hermetically with 1.5-mm-thick coverslip. A Nikon A1R Confocal microscope was used for 3D image acquisition with a 40× oil objective (N.A. = 1.3). Images were analysed using threshold co-localization function in ImageJ2/FIJI program.

Compliance with ethical standards

All procedures performed in studies involving human participants were in accordance with the ethical standards of the institutional and/or national research committee and with the 1964 Helsinki declaration and its later amendments or comparable ethical standards. This study was approved by the Ethikkommission beider Basel (permit No. EK64/12); all subjects gave written informed consent to carry out this work.

All applicable international, national and/or institutional guidelines for the care and use of animals were followed. All procedures performed in studies involving animals were in accordance with the ethical standards of the institution or practice at which the studies were conducted. Experiments on mouse muscles were approved by the local Cantonal Veterinary authorities (permit No. 2658).

Statistical analysis and graphical software

Statistical analysis was performed using the Student's *t*-test; means were considered statistically significant when the *P*-value was < 0.05. When more than two groups were compared, analysis was performed using the ANOVA test followed by the Bonferroni *post hoc* test using the statistical package included in GraphPad Prism 6.0 software. Origin 6 was used to generate dose–response curves. Images were assembled using Adobe Photoshop CS (version 8.0).

Supplementary Material

Supplementary Material is available at *HMG* online.

Acknowledgements

Funding

References

1. Maggi, L., Scoto, M., Cirak, S., Robb, S.A., Klein, A., Lillis, S., Cullup, T., Feng, L., Manzur, A.Y., Sewry, C.A. *et al.* (2013) Congenital myopathies–clinical features and frequency of individual subtypes diagnosed over a 5-year period in the United Kingdom. *Neuromuscul. Disord.*, **23**, 195–205.

2. Zhou, H., Jungbluth, H., Sewry, C.A., Feng, L., Bertini, E., Bushby, K., Straub, V., Roper, H., Rose, M.R., Brockington, M. *et al.* (2007) Molecular mechanisms and phenotypic variation in RYR1-related congenital myopathies. *Brain*, **130**, 2024–2036.

3. Wilmshurst, J.M., Lillis, S., Zhou, H., Pillay, K., Henderson, H., Kress, W., Müller, C.R., Ndondo, A., Cloke, V., Cullup, T. *et al.* (2010) RYR1 mutations are a common cause of congenital myopathies with central nuclei. *Ann. Neurol.*, **68**, 717–726.

4. Clarke, N.F., Waddell, L.B., Cooper, S.T., Perry, M., Smith, R.L., Kornberg, A.J., Muntoni, F., Lillis, S., Straub, V., Bushby, K. *et al.* (2010) Recessive mutations in RYR1 are a common cause of Congenital Fiber Type disproportion. *Hum. Mutat.*, **31**, E1544–E1550

5. Franzini-Armstrong, C. and Protasi, F.G. (1997) Ryanodine receptors of striated muscles: a complex channel capable of multiple interactions. *Physiol. Rev.*, **77**, 699–729.

6. Treves, S., Jungbluth, H., Muntoni, F. and Zorzato, F. (2008) Congenital muscle disorders with cores: the ryanodine receptor calcium channel paradigm. *Curr. Opin. Pharmacol.*, **8**, 319–326.

7. Zhou, H., Rokach, O., Feng, L., Munteanu, I., Mamchaoui, K., Wilmshurst, J.M., Sewry, C., Manzur, A.Y., Pillay, K., Mouly, V. *et al.* (2013) RYR1 deficiency in congenital myopathies disrupts excitation-contraction coupling. *Hum. Mutat.*, **34**, 986–996.

8. Attali, R., Aharoni, S., Treves, S., Rokach, O., Becker-Cohen, M., Fellig, Y., Straussberg, R., Do, T., Daana, M., Mitrani-Rosenbaum, S. and Nevo, Y. (2013) Variable myopathic presentation in a single family with novel skeletal RYR1 mutation. *PLoS One*, **8**, e69296. doi:10.1371/journal. pone. 0069296.

9. Emery, A.E. (1991) Population frequencies of inherited neuromuscular diseases—a world survey. *Neuromuscul. Disord.*, **1**, 19–29.

10. Zhou, H., Yamaguchi, N., Xu, L., Wang, Y., Sewry, C., Jungbluth, H., Zorzato, F., Bertini, E., Muntoni, F., Meissner, G. and Treves, S. (2006) Characterization of recessive RYR1 mutations in core myopathies. *Hum. Mol. Genet.*, **16**, 2791–2803.

11. Chen, J.F., Mandel, E.M., Thomson, J.M., Wu, Q., Callis, T.E., Hammond, S.M., Conlon, F.L. and Wang, D.Z. (2006) The role of microRNA-1 and microRNA-133 in skeletal muscle proliferation and differentiation. *Nat. Genet.*, **38**, 228–233.

12. Kim, H.K., Lee, Y.S., Sivaprasad, U., Malhotra, A. and Dutta, A. (2006) Muscle-specific microRNA miR-206 promotes muscle differentiation. *J. Cell. Biol.*, **174**, 677–687.

13. Small, E.M., O'Rourke, J.R., Moresi, V., Sutherland, L.B., McAnally, J., Gerard, R.D., Richardson, J.A. and Olson, E.N. (2010) Regulation of PI3-kinase/Akt signaling by muscle enriched microRNA-486. *Proc. Natl Acad. Sci. USA.*, **107**, 4218–4223.

14. Wang, M., Zhao, C., Shi, H., Zhang, B., Zhang, L., Zhang, X., Wang, S., Wu, X., Yang, T., Huang, F. *et al.* (2014) Deregulated microRNAs in gastric cancer tissue-derived mesenchymal stem cells: novel biomarkers and a mechanism for gastric cancer. *Br. J. Cancer.*, **110**, 1199–1210.

15. Sun, X., Wang, Z.M., Song, Y., Tai, X.H., Ji, W.Y. and Gu, H. (2014) MicroRNA-126 modulates the tumor microenvironment by targeting calmodulin-regulated spectrin-associated protein 1 (Camsap1). *Int. J. Oncol.*, **44**, 1678–1684.

16. Jungbluth, H., Sewry, C. and Muntoni, F. (2011) Core myopathies. *Semin. Pediatr. Neurol.*, **18**, 239–249.

17. Workmann, J.L. and Kingston, R.E. (1998) Alteration of nucleosome structure as a mechanism of transcriptional regulation. *Annu. Rev. Biochem.*, **67**, 545–579.

18. Lu, J., McKinsey, T.A., Zhang, C.L. and Olson, E.N. (2000) Regulation of skeletal myogenesis by association of the mef2 transcription factor with class II Histone deacetylases. *Mol. Cell.*, **6**, 233–244.

19. Zhang, J., Yang, Y., Yang, T., Liu, Y., Li, A., Fu, S., Wu, M., Pan, Z. and Zhou, W. (2010) microRNA-22, downregulated in hepatocellular carcinoma and correlated with prognosis, suppresses cell proliferation and tumourigenicity. *Br. J. Cancer*, **103**, 1215–1220.

20. Potthoff, M.J., Arnold, M.A., McAnally, J., Richardson, J.A., Bassel-Duby, R. and Olson, E.N. (2007) Regulation of skeletal muscle sarcomere integrity and postnatal muscle function by Mef2c. *Mol. Cell Biol.*, **27**, 8143–8151.

21. Hinits, Y. and Hughes, S.M. (2007) Mef2s are required for thick filament formation in nascent muscle fibres. *Development*, **134**, 2511–2519.

22. Naya, F.J. and Olson, E. (1999) MEF2: a transcriptional target for signaling pathways controlling skeletal muscle growth and differentiation. *Curr. Opin. Cell Biol.*, **11**, 683–688.

23. McKinsey, T.A., Zhang, C.L., Lu, J. and Olson, E.N. (2000) Signal-dependent nuclear export of a histone deacetylase regulates muscle differentiation. *Nature*, **408**, 106–111.

24. Schmoelzl, S., Leeb, T., Brinkmeier, H., Brem, G. and Brenig, B. (1996) Regulation of tissue-specific expression of the skeletal muscle ryanodine receptor gene. *J. Biol. Chem.*, **271**, 4763–4769.

25. Liu, N., Williams, A.H., Kim, Y., McAnally, J., Bezprozvannaya, S., Sutherland, L.B., Richardson, J.A., Bassel-Duby, R. and Olson, E.N. (2007) An intragenic MEF2-dependent enhancer directs muscle-specific expression of microRNAs 1 and 133 Mef2 and myomesin. *Proc. Natl Acad. Sci. USA*, **104**, 20844–20849.

26. Zhou, H., Lillis, S., Loy, R.E., Ghassemi, F., Rose, M.R., Norwood, F., Mills, K., Al-Sarraj, S., Lane, R.J., Feng, L. *et al.* (2010) Multiminicore disease and atypical periodic paralysis associated with novel mutations in the skeletal muscle ryanodine receptor (RYR1) gene. *Neuromuscul. Disord.*, **20**, 166–173.

27. Monnier, N., Marty, I., Faure, J., Castiglioni, C., Desnuelle, C., Sacconi, S., Estournet, B., Ferreiro, A., Romero, N., Laquerriere, A. *et al.* (2008) Null mutations causing depletion of the type 1 ryanodine receptor (RYR1) are commonly associated with recessive structural congenital myopathies with cores. *Hum. Mutat.*, **29**, 670–678.

28. Bevilacqua, J.A., Monnier, N., Bitoun, M., Eymard, B., Ferreiro, A., Monges, S., Lubieniecki, F., Taratuto, A.L., Laquerrière, A., Claeys, K.G. *et al.* (2011) Recessive RYR1 mutations cause unusual congenital myopathy with prominent nuclear internalization and large areas of myofibrillar disorganization. *Neuropathol. Appl. Neurobiol.*, **37**, 271–284.

29. Bongers, K.S., Fox, D.K., Ebert, S.M., Kunkel, S.D., Dyle, M.C., Bullard, S.A., Dierdorff, J.M. and Adams, C.M. (2013) Skeletal muscle denervation causes skeletal muscle atrophy through a pathway that involves both Gadd45a and HDAC4. *Am. J. Physiol. Endocrinol. Metab.*, **98**, 4089–4096.

30. Bruneteau, G., Simonet, T., Bauché, S., Mandjee, N., Malfatti, E., Girard, E., Tanguy, M.L., Behin, A., Khiami, F., Sariali, E. *et al*. (2013) Muscle histone deacetylase 4 upregulation in amyotrophic lateral sclerosis: potential role in reinnervation ability and disease progression. *Brain*, **136**, 2359–2368.

31. Mielcarek, M., Landles, C., Weiss, A., Bradaia, A., Seredenina, T., Inuabasi, L., Osborne, G.F., Wadel, K., Touller, C., Butler, R. *et al*. (2013) HDAC4 reduction: a novel therapeutic strategy to target cytoplasmic huntingtin and ameliorate neurodegeneration. *PLOS Biol.*, **11**, e1001717.

32. Cohen, T.J., Waddell, D.S., Barrientos, T., Lu, Z., Feng, G., Cox, G.A., Bodine, S.C. and Yao, T.P. (2007) The histone deacetylase HDAC4 connects neural activity to muscle transcriptional reprogramming. *J. Biol. Chem.*, **282**, 33752–33759.

33. Consalvi, S., Saccone, V., Giordani, L., Minetti, G., Mozzetta, C. and Puri, P.L. (2011) Histone deacetylase inhibitors in the treatment of muscular dystrophies: epigenetic drugs for genetic diseases. *Mol. Med.*, **17**, 457–465.

34. Falkenberg, K.J. and Johnstone, R.W. (2014) Histone deacetylases and their inhibitors in cancers, neurological dieases and immune disorders. *Nature Rev. Drug. Discov.*, **13**, 673–691.

35. Wang, Z., Qin, G. and Zhao, T.C. (2014) HDAC4: mechanism of regulation and biological functions. *Epigenomics*, **6**, 139–150.

36. Baylin, S.B., Esteller, M., Rountree, M.R., Bachmanm, K.E., Schuebelm, K. and Herman, J.G. (2001) Aberrant patterns of DNA methylation, chromatin formation and gene expression in cancer. *Hum. Mol. Genet.*, **10**, 687–692.

37. Lu, J., McKinsey, T.A., Nicolm, R.L. and Olson, E.N. (2000) Signal dependent activation of the MEF2 transcription factor by dissociation from histone deacytlases. *Proc. Natl Acad. Sci. USA*, **97**, 4070–4075.

38. Miska, E.A., Karlsson, C., Langley, E., Nielesen, S.J., Pines, J. and Kouzaridesm, T. (1999) HDAC4 deacetylase associates with and represses the MEF2 transcription factor MEF2 transcription factor. *EMBO J.*, **18**, 5099–5107.

39. Wang, A.H., Bertos, N.R., Vezmar, M., Pelletier, N., Crosato, M., Heng, H.H., Th'ng, J., Han, J. and Yang, X.L. (1999) HDAC4, a human histone deacetylase related to yeast HDA1, is a transcriptional corepressor. *Mol. Cell. Biol.*, **19**, 7816–7827.

40. Phillips, M.S., Fujii, J., Khanna, V.K., DeLeon, S., Yokobata, K., DeJong, P. and MacLennan, D.H. (1996) The structural organization of the human skeletal muscle ryanodine receptor (RYR1) gene. *Genomics*, **34**, 24–41.

41. Won, J., Yim, J. and Kim, T.K. (2002) Sp1 and Sp3 recruit histone deacetylase to repress transcription of human telomerase reverse transcriptase (hTERT) promoter in normal human somatic cells. *J. Biol. Chem.*, **277**, 38230–38238.

42. Zhou, H., Brockington, M., Jungbluth, H., Monk, D., Stanier, P., Sewry, C.A., Moore, G.E. and Muntoni, F. (2006) Epigenetic allele silencing unveils recessive *RYR1* mutations in core myopathies. *Am. J. Hum. Gen.*, **79**, 859–868.

43. Denis, H., Ndlovu, M.N. and Fuks, F. (2011) Regulation of mammalian DNA methyltransferases: a route to new mechanisms. *EMBO Reports*, **12**, 647–656.

44. Subramaniam, D., Thombre, R.T., Dhar, A. and Anant, S. (2014) DNA methyltransferases: a novel target for prevention and therapy. *Front. Oncol.*, **4**. doi:10.3389/fonc.2014.00080.

45. Newell-Price, J., Clark, A.J. and King, P. (2000) DNA methylation and silencing of gene expression. *Trends. Endocrinol. Metab.*, **11**, 142–148.

46. Cuozzo, C., Porcellini, A., Angrisano, T., Morano, A., Lee, B., Di Pardo, A., Messina, S., Iuliano, R., Fusco, A., Santillo, M.R. *et al*. (2007) DNA damage, homology-directed repair, and DNA methylation. *PLOS Genet*, **3**, e110.

47. Huang, Z.P., Chen, J., Seok, H.Y., Zhang, Z., Kataoka, M., Hu, X. and Wang, D.Z. (2013) MicroRNA-22 regulates cardiac hypertrophy and remodeling in response to stress. *Circ. Res.*, **112**, 1234–1243.

48. Eisenberg, I., Eran, A., Nishinom, I., Moggio, M., Lamperti, C., Amatom, A.A., Lidov, H.G., Kang, P.B., North, K.N., Mitrani-Rosenbaum, S. *et al*. (2007) Distinctive patterns of microRNA expression in primary muscle disorders. *Proc. Natl Acad. Sci. USA*, **104**, 17016–17021.

49. Dmitriev, P., Stankevicins, L., Ansseau, E., Petrov, A., Barat, A., Dessen, P., Robert, T., Turki, A., Lazar, V., Labourer, E. *et al*. (2013) Defective regulation of microRNA target genes in myoblasts from fascioscapulohumeral dystrophy patients. *J. Biol. Chem.*, **288**, 34989–35002.

50. Chen, J.F., Callis, T.E. and Wang, D.Z. (2009) microRNAs and muscle disorders. *J. Cell Sci.*, **122**, 13–20.

51. Liu, N., Bezprozvannaya, S., Shelton, J.M., Frisard, M.I., Hulver, M.W., McMillan, R.P., Wu, Y., Voelker, K.A., Grange, R.W., Richardson, J.A., Bassel-Duby, R. and Olson, E.N. (2011) Mice lacking microRNA 133a develop dynamin 2-dependent centronuclear myopathy. *J. Clin. Invest.*, **121**, 3258–3268.

52. Vosin, S., Eynon, N., Yan, X. and Bishop, D.J. (2014) Exercise training and DNA methylation in humans. *Acta. Physiol.*, doi:10.1111/apha.12414.

53. Ling, C. and Rönn, T. (2014) Epigenetic adaptation to regular exercise in humans. *Drug Discov. Today*, **19**, 1015–1018.

54. Barrès, R., Yan, J., Egan, B., Treebak, J.T., Rasmussen, M., Fritz, T., Caidahl, K., Krook, A., O'Gorman, D.J. and Zierath, J.R. (2012) Acute exercise remodels promoter methylation in human skeletal muscle. *Cell Metabol.*, **15**, 405–411.

55. Lee, W.H., Isaacs, W.B., Bova, G.S. and Nelson, W.G. (1997) CG island methylation changes near the GSTP1 gene in prostatic carcinoma cells detected using the polymerase chain reaction: a new prostate cancer biomarker. *Cancer Epidemiol. Biomarkers Prev.*, **6**, 443–450.

56. Obermann, W.M.J., Gautel, M., Steiner, F., van der Ven, P.F., Weber, K. and Fürst, D.O. (1996) The structure of the sarcomeric M band: localization of defined domains of myomesin, M-protein and the 250 kD carboxy-terminal region of titin by immunoelectron microscopy. *J. Cell Biol.*, **134**, 1441–1453.

57. DiFranco, M., Quinonez, M., Capote, J. and Vergara, J. (2009) DNA transfection of mammalian skeletal muscles using *in vivo* electroporation. *J. Vis. Exp.*, pii: 1520. doi:10.3791/1520.

58. Ducreux, S., Zorzato, F., Müller, C., Sewry, C., Muntoni, F., Quinlivan, R., Restagno, G., Girard, T. and Treves, S. (2004) Effect of ryanodine receptor mutations on interleukin-6 release and intracellular calcium homeostasis in human myotubes from malignant hyperthermia-susceptible individuals and patients affected by central core disease. *J Biol. Chem.*, **279**, 43838–43846.

106

SUPPLEMENTARY FIGURES

Supplementary Figure 1: Expression levels of non-muscle specific miR are not changed in patients with Congenital Muscle Disorders. Controls, circles; CCD patients, squares; Minicore patients, triangles. Each symbol represents the mean triplicate value from a single patient normalized to RNU44 content and to the muscle specific housekeeping genes (*DES/ACTN2*). **miR126**, **miR221** and **miR486** were quantified and no significant changes were observed between the groups. Statistical analysis was performed using ANOVA and Bonferroni multiple comparison test (95% Confidence interval).
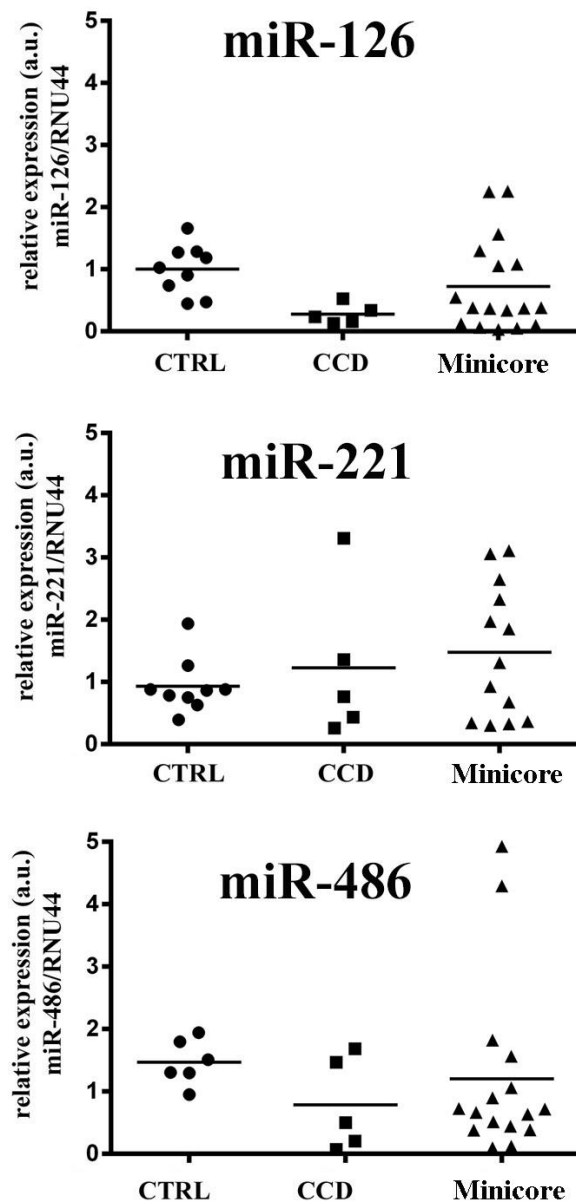
Supplementary Figure 2: Muscle-specific miRs are down-regulated and HDAC-4 and HDAC-5 are up-regulated in patients with Nemaline myopathy. For miRs, each symbol represents the mean triplicate value from a single patient normalized to RNU44 content and to the muscle specific housekeeping genes *DES/ACTN2*. For HDAC-4 and HDAC-5 the intensity of the immunopositive band obtained by Western blot was normalized to the intensity of the immunopositive MHC band. Controls, squares, Nemaline patients, diamonds. **miR22** *p<0.003, CTRL and NEM n=9; **miR133**, ** p<0.0007, CTRL n=10 NEM, n=11; **miR1**;***p<0.0015, CTRL n=8, NEM n=10; **HDAC4** ****p<0.045, CTRL n=9, NEM n=4; **HDAC5** ****p<0.045, CTRL n=4, NEM n=4. **miR124** and **miR206** were quantified and no statistical significance was observed. Statistical analysis performed using Student's *t* test.
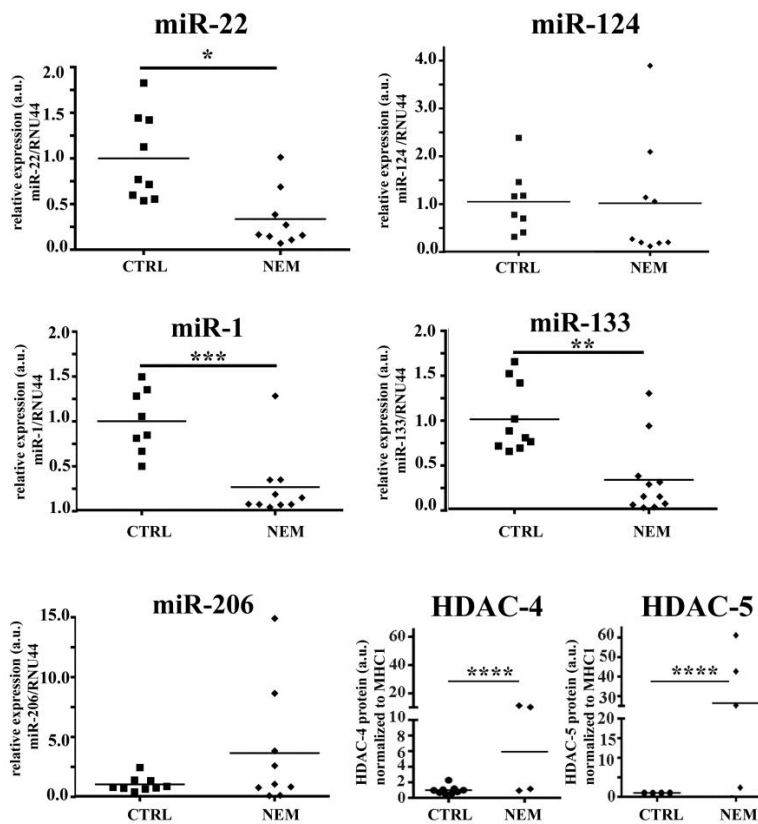
Supplementary Figure 3: **Over-expression of HDAC-4 and HDAC-5 in mouse FDB fibers significantly decreases RyR1 protein content.** Total homogenates prepared from mouse FDB fibers isolated from footpads eletroporated with an empty plasmid (CTRL) or with plasmids encoding HDAC-4 and HDAC-5 (HDAC) were isolated 6-10 days post-transfection. Proteins were separated on a 6% SDS PAG, transferred onto nitrocellulose and probed with mouse anti-RyR1 Abs (70 µg protein), with rabbit anti-HDAC-4 and rabbit anti-HDAC-5 Abs (20 µg) or with anti-MHC (20 µg) followed by peroxidase conjugated anti-mouse or anti-rabbit antibodies. The immunopositive bands were visualized by chemiluminescence using the Super Signal West Dura kit (Thermo Scientific).

In order to perform statistical analysis, the intensity of the immunopositive RyR1 band in CTRL and HDAC over-expressing muscle homogenates were compared. HDAC-over-expression resulted in a significant decrease of the RyR1 protein (% RyR1 protein remaining was 24.02 ± 9.42 % (n=6; p< 0.0025 Student t test).
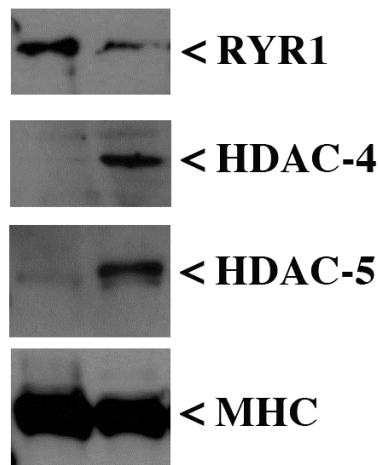
Supplementary Table I: Genotypes/phenotypes/ clinical details of patients enrolled in the present study

Code N° (Country)	Neurological Diagnosis	Identified *RYR1* mutation	Comment (and reference if available)
CCD NL 01 (The Netherlands)	CCD dominant Classical CCD phenotype	*RYR1* heterozygous c.13940T>C (p.L4647P)	Difficulties in sports in childhood, mild proximal weakness, ambulant, Achilles contractures. At present, ambulance normal; active in sports, clinically no signs of polyneuropathy. EMG focused on peripheral nerves: no signs of polyneuropathy. Muscle biopsy (age 32): type 1 predominance, increased variation in fibre diameter, many central cores, Z-band streaming.
CCD NL 02 (The Netherlands)	CCD dominant Classical CCD phenotype	*RYR1* heterozygous c.13940T>C (p.L4647P)	Difficulties in sports in childhood, mild proximal weakness, ambulant, Achilles contracture. EMG: both signs of myopathy and axonal polyneuropathy. Muscle biopsy (age 60): type 1 predominance (100%), increased variation in fibre diameter, cores in all cells, partly central cores, partly multiminicores, also abundance of fibres with nemaline rods. Uncle of patient above: T07-16076; he also has distal weakness, related to an axonal polyneuropathy most likely due to a MFN mutation. This is probably not relevant since the biopsy was taken from a proximal muscle.
CCD NL 03 (The Netherlands)	CCD dominant Classical CCD phenotype	*RYR1* heterozygous c.13940T>C (p.L4647P)	Muscle biopsy (age 61): Myopathy with central cores and cores with nemaline rods. Complete type 1 predominance. Muscle ultrasound and MR (2008): myopathic changes (back, abdominal, lower legs). Also distal weakness due to axonal polyneuropathy, most likely secondary to *MFN2* mutation (HMSN2). This is probably not relevant since the biopsy was taken from a proximal muscle. Father of patient below: T07-16076; brother of patient above: T08-10960.
CCD UK 01 (UK)	CCD dominant Classical CCD phenotype	*RYR1* heterozygous c.14680G>C (p.A4894P)	Typical dominant CCD family with clinical features of proximal weakness pronounced in the hip girdle, congenital dislocation of the hips and scoliosis, and central cores on muscle biopsy (56).
CCD UK 02 (UK)	King-Denborough syndrome with central cores	Screening of entire *RYR1* coding did not reveal any variation	Mild proximal weakness with dysmorphic facial features, short stature, scoliosis and multiple contractures. Typical central cores on muscle biopsy. A muscle biopsy performed at 9 months of age had shown increased fibre size variability but no other changes. A repeat muscle biopsy performed at 7 years of age from the quadriceps demonstrated increased variability in fibre size and type 1 predominance with clear central areas suggestive of central core disease (CCD) (57). This patient is likely to have a TTN mutation but this awaits confirmation
Minicore NL 01 (The Netherlands)	MmD	Heterozygous *RYR1* c.11905C>A (p.Q3969K) in exon 86. Second mutation not found yet	Developmental delay (milestones 4- 5 months delay at age 2 years) and generalized muscle weakness. Facial weakness (open mouth). Axial hypotonia with head lag and slipping through. Gowers sign positive. Hypermobility. Ambulant at latest follow-up at age 6. Biopsy (age 2): increase of central and internal nuclei, type 1 predominance (67%), on EM several minicores and disruption of Z-lines.
Minicore NL 02 (The Netherlands)	Congenital myopathy; few minicores	Compound heterozygous *RYR1* c.12629A>G (p.K4210R) c.14723A>G (p.D4908G)	Mild proximal muscle weakness since childhood, distal joint hypermobility. Muscle biopsy (age 14): Congenital myopathy; predominance of type 1 fibres (90%); mild myopathic features (increase of internal nuclei). Minicores on EM
Minicore NL 03 (The Netherlands)	Congenital myopathy; increase of internal nuclei, no fibre type 1 predominance, multiminicores	Compound heterozygous *RYR1*: c.4711A>G (p.I1571V); c.10097G>A (p.R3366H) c.11798A>G (p.Y3933C); c.14545G>A (p.V4849I).	Mild muscle weakness in childhood, gradual increase of muscle weakness. CK 441– 1962 U/l. Neurological examination (age 50): mild vertical ophthalmoplegia when looking upwards. Neckflexion, extension 4. Elbow extension and flexion 5. Hands 4. Hip- and kneeflexion 4 Can walk on heels, not on toes. Positive Gowers. No joint hypermobility Muscle biopsy (age 28): Fibre type 1 predominance, hypertrophic fibres, mild increase of endomysial connective tissue. Several cores in type 1-fibres, also at the peripheral zones of the cells. Increase of internal nuclei.
Minicore Bel 01	MmD MHS clinical	Compound heterozygous	Female patient, fourth decade. Delayed motor milestones as a child, moderate

Patient	Diagnosis	Genetics	Clinical description
(Belgium)	myopathy	*RYR1* p.I1571V + p.R3366H + p.Y3933C + p.V4849I	non-progressive weakness as an adult (difficulty mounting stairs), no ophthalmoplegia. Normal CK. Western blot demonstrates reduction of RYR1 expression by 50%. Muscle biopsy shows fatty infiltration, fibrosis, necrotic fibres, centralization of nuclei in numerous fibres and almost type 1 fibre 'uniformity'. EM shows multiple core-like myofibrillar alterations corresponding to 'multi-minicore type lesions, focal loss of striations, rods in atrophic fibres. Conclusion: "Multi-minicore disease + rods".
Minicore UK 01 (UK)	MmD with Ophthalmoplegia and atypical periodic paralysis	Compound heterozygous *RYR1* Het c.8816G>A (p.R2939K) + Het c.6721C>T (p.R2241X) and Het c.2122G>A (p.D708N) Last two - on the same allele; WT allele is not expressed.	Hypotonia at birth, respiratory impairment and feeding difficulties, delayed motor development, reduced walking distance, difficulties with overhead tasks, exercise-induced myalgia and muscle stiffness prompted by cold, from the age of 18 started experiencing repeated episodes of severe paralysis initially affecting the legs and then rapidly spreading to the upper limbs lasting up to several days (25).
Minicore UK 02 (UK)	MmD with Ophthalmoplegia	*RYR1* variant only Het p.P1787L, found to date. This variant is likely non-pathogenic.	Presentation with hypotonia and subsequent motor developmental delay. Marked facial weakness with external ophthalmoplegia and mild to moderate proximal weakness in both shoulder and hip girdle. Ambulant. Muscle biopsy with type 1 predominance and minicores.
Minicore UK 03 (UK)	Recessive myopathy related CNM	Compound *RYR1* heterozygous c.13513G>C; (pD4505H) + heterozygous c.10687-10C>T	Severe early-onset with marked hypotonia, generalized weakness, extraocular muscle involvement, respiratory impairment and features of centronuclear myopathy on muscle biopsy.
Minicore UK 05 (UK)	MmD with bulbar palsy	Het c.13513 G>C; p. (p.D4505H)	Born prematurely at 37+6 weeks. Polyhydramnios and feeding difficulties at birth, drooling, failure to thrive, nasogastric tube, pectus carinatum, scoliosis, hypotonia with antigravity power, distinctive facial features, neurogenic EMG in bulbar muscles.
Minicore UK 06 (UK)	MmD	Compound *RYR1* heterozygous c.338 l+l+ G>A + c.2635 G>A (p.E879K)	Hypotonia; feeding difficulties; facial weakness; delayed motor milestones; low head control. Muscle biopsy: Abnormal variation in fiber size; multi internal nuclei; core-like area in NADH; type 1 fiber predominance.
Minicore UK 07 (UK)	MmD	Compound *RYR1* heterozygous c.5030A>G (p.A1677S) + c.11752A>C (p.T3918P)	Born prematurely at 35+3 weeks. Congenital proximal muscle weakness, abnormal eye movement, recurrent respiratory infections, dependency at night. Muscle biopsy: abnormal variation in fiber size; population of small fibers some central nuclei, NADH-TR staining showed some core-like areas in a few fibers.
Minicore UK 08 (UK)	MmD	Compound *RYR1* heterozygous c. 4729G>A (p.A1577S)+c. 6178G>T (p.G2060C)	Muscle weakness, hypotonia and feeding difficulties followed by delayed motor milestones. Bilateral talipes. Muscle biopsy: mild variation in fiber size, an increase in internal nuclei. Oxidative enzyme staining revealed multiple focal areas devoid of stain, as well as some single cores of moderate size and some peripheral aggregation of stain. Patient Family 1 (10).
Minicore UK 09 (UK)	MmD +Ophthalmoplegia	*RYR1* variant only: Het p.P1787L + This variant is likely non-pathogenic. Homozygous MYH2 mutation	Early onset with developmental delay. Mild to moderate proximal weakness with more pronounced facial weakness and almost complete external ophthalmoplegia. Muscle biopsy with marked type 1 predominance and occasional unevenness of stain. MYH2 –related myopathy with features of MmD.
Minicore SA 02 (South Africa)	Congenital myopathy with central nuclei	Compound Het RYR1 c.8342_8343delTA (p.I2781R fsX49) + c.11941C>T (p.H3981Y) + c.10348-6C>G + c.14524G>A (p.V4842M)	Patient 2 [3]. This girl now into her second decade was profoundly weak with external ophthalmoplegia, marked myopathic facies, respiratory compromise and feeding difficulties. She was admitted for recurrent chest infections and required supplemental gastrostomy feeding in the first 5 years of life. She has not acquired independent ambulation but can sit unaided. She underwent spinal rod insertion for progressive scoliosis. She remains stable with occasional lower respiratory chest infections.

Patient code	Diagnosis	Mutation	Clinical description
Minicore SA 03 (South Africa)	Congenital myopathy with central nuclei	Compound Het RYR1 c. 6175_6187del13; (p.L2059Sfs X2) + c.10348-6C>G+ c.14524G>A (p.V4842M)	Patient 3 (3). This young man is now 22 years of age he was symptomatic from birth with myopathic facies, external ophthalmoplegia and proximal weakness. His power appeared to improve with time and he acquired independent ambulation. He has not demonstrated any deterioration in his motor capacity, if anything he has improved with time.
Minicore SA 05 (South Africa)	Congenital myopathy with central nuclei	Compound Het RYR1 c.8342_8343delTA; (p.I2781Rfs X49) + c.11941C>T (p.H3981Y)+ c.10348-6C>G + c.14524G>A (p.V4842M)	Patient 5 (3). This boy is now 13 years of age. He had marked proximal weakness at birth with proximal joint contractures, myopathic faces and external ophthalmoplegia. His power appeared to improve with time and he acquired independent ambulation but not ambulation but can sit unaided.
Minicore SA 06 (South Africa)	Congenital myopathy with central nuclei	Compound Het RYR1 c.8342_8343delTA; (p.I2781Rfs X49) + c.11941C>T (p.H3981Y)+ c.10348-6C>G c.14524G>A; (p.V4842M)	Patient 6 (3). This boy was profoundly weak at birth with recurrent chest infections. He had myopathic facies and external ophthalmoplegia. He attained independent seating but not ambulation. His power has not deteriorated but appeared to plateau after some improvement up until 4 years of age.
Minicore SA 07 (South Africa)	Congenital myopathy with central nuclei	Compound Heterozygous c.3381+1 G>A + c.10348-6C>G+ c.14524G>A; (p.V4842M)	Patient 7 (3). This boy, now in his second decade, was weak from birth with external ophthalmoplegia, and myopathic facies. From infancy he did not have major feeding difficulties, but whilst his respiratory function appeared stable when well he decompensated rapidly with lower respiratory tract infections. He required several acute admissions with pneumonia in his first decade. He remains wheelchair bound but otherwise well with no new events in the last few years.
Minicore ISR 01 (Israel)	Recessive core myopathy	Compound HOM RYR1 Hom c.9047A>G (p.Y3016C) + Hom c.6178G>T (p.G2060C)	Myopathic face, waddling gait, slowly progressive weakness. No core like structures; patient V36 on the pedigree (8).
Minicore ISR 02 (Israel)	Recessive core myopathy	Compound HOM RYR1 Hom c.9047A>G (p.Y3016C) + Hom c.6178G>T (p.G2060C)	Myopathic face, waddling gait, difficulty climbing the stairs. Slowly progressive weakness. Early scoliosis. No core like structures; patient V31 on the pedigree (8).
NEM NL 01	Nemaline myopathy	Het mutation in KBTBD13 c.1222C>T (p.R408C), Daughter of NEM NL 04	Normal motor development. Gradual progressive muscle weakness from her teens, due to which sports in school became more difficult. No facial weakness. Mild proximal weakness in legs > arms (MRC 4). Biopsy (age 15): type I predominance, increase of internal nuclei, many nemaline rods.
NEM NL 04	Nemaline myopathy	Het mutation in KBTBD13 c.1222C>T (p.R408C)	Normal motor development. Mild muscle weakness and stiffness since her teens, non-progressive in adulthood, fast alternating movements are difficult. Biopsy (age 45): type I predominance, increase of internal nuclei, many nemaline rods, few cores on EM, much fatty infiltration. Cardiac evaluation normal.
NEM NL 03	Nemaline myopathy	Daughter of NEM NL_02; same phenotype as father, not genetically tested yet	Normal motor development. Remarkably strong compared to peers. Fast in running. Painful stiffness in lower arms, neck and back since her late twenties. Cramps in calves. Normal strength. Muscle biopsy (age 30): normal. EM: mild increase of fat vacuoles.
NEM NL 02	Nemaline myopathy	Het mutation in KBTBD13 Het mutation c.247G>C (p.E83Q)	Normal motor devolment. Myalgia since the age of 18, and diffuse muscle cramps. These occur frequently whenever he sits in the same position for a longer period. During endurance exercise at age 62, he cannot keep up with peers, whereas he was the fastest when he was younger. Muscle biopsy (age 60); cores, on EM Z-band streaming and cores.
NEM NL 05	Nemaline myopathy	Het mutation in KBTBD13 c.1222C>T (p.R408C)	Normal motor development. Difficulties in gymnastics (climbing ropes, high jumping). Difficulties climbing steep stairs (uses the railing). Falls several times a year since she cannot correct her balance fast enough. Mild proximal weakness (MRC 4) in arms, legs and axial muscles. Muscle biopsy (age 44): Type I predominance, increase of internal nuclei, cores, EM: abundance of rods.
NEM UK 01	Nemaline myopathy	Het de novo mutation in ACTA1 gene	Floppy at birth, swallowing difficulty, respiratory weakness and hypotonia. Muscle biopsy showed nemaline rods in Trichrome staining.

ID	Diagnosis	Mutation	Clinical features
NEM UK 02	Nemaline myopathy	Het mutation in *ACTA1* gene c.553C>G (p.R185G)	Difficulty in climbing, rising and walking fast, left facial weakness, hypotonia and joint laxity noted through infancy, feeding difficulties in first year, frequent respiratory infections in first 18 months, normal CK. Muscle biopsy showed nemaline rods.
NEM UK 03	Nemaline myopathy	Het mutation in *ACTA1* gene. C.16G>A (p.G6L)	Born prematurely at 33 weeks. Delayed motor milestones, recurrent chest infections, facial weakness, tires on exercise, abnormal gait, exaggerated lordosis, weak neck flexors, hyper extensible joints at elbows and knees, nasal tone of voice, mild spinal rigidity.
NEM UK 04 6105	Nemaline myopathy	Compound het mutations in *NEB* . C.21837dupC (p.D7280fs) + c.24209_24212dupTGTT (p.L8071fs)	Scoliosis, tight TA, muscle thin and hypotonic. The first biopsy at 3 years old showed fibre type disproportion, myofibrillar loss and disruption. The second muscle biopsy at 7 years old showed significant population of nemaline rods in Trichrome staining.
NEM UK 05	Nemaline myopathy	Het mutation in *ACTA1* gene. C.16G>A (p.G6L)	Born prematurely at 33 weeks. Delayed motor milestones, recurrent chest infections, facial weakness, tires on exercise, abnormal gait, exaggerated lordosis, weak neck flexors, hyper extensible joints at elbows and knees, nasal tone of voice, mild spinal rigidity.
NEM UK 06	Nemaline myopathy	Heterozygous for *RYR1* c.890C>A, p.G297D Compound heterozygous for *NEB* c.12736delA: p.I4246fs het and *NEB* c.24562C>T: p.Q8188T het	Early-onset with marked hypotonia and weakness and associated bulbar and respiratory involvement, requiring respiratory support and tube feeding. Muscle biopsy performed in infancy showing increased variability in fibre size, discrete nemaline rods and few cores.

Sato, I., Wu, S., Ibarra, M.C., Hayashi, Y.K., Fujita, H., Tojo, M., Oh, S.J., Nonaka, I., Noguchi, S. and Nishino, I. (2008) Congenital neuromuscular disease with uniform type 1 fiber and RYR1 mutation. *Neurology* **70**, 114-122.

Dowling, J.J., Lillis, S., Amburgey, K., Zhou, H., Al-Sarraj, S., Buk, S.J., Wraige, E., Chow, G., Abbs, S., Leber, S., Lachlan, K., Baralle, D., Taylor, A., Sewry, C., Muntoni, F. and Jungbluth, H. (2011) King-Denborough syndrome with and without mutations in the skeletal muscle ryanodine receptor (RYR1) gene. *Neuromuscl. Disord.* **21**, 420-427.

Supplementary Table 2

Expression levels (mean ± S.E.M. of n values) of mef2 and non –muscle miRs in
FDB fibers over-expressing HDAC-4 and HDAC-5

Transcript analysed	Control	HDAC-4/HDAC-5 over-expressing fibres	Statistical significance (Student's t test)
Mef2 C	1.0±0.10 n=6	1.39±0.16 n=6	P =0.072 N.S.
Mef2 D	1.0±0.14 n=6	1.56±0.22 n=6	P =0.505 N.S.
miR-486	1.0±0.17 n=6	0.73±0.34 n=6	P = 0.495 N.S.
miR-221	1.0±0.25 n=6	039±0.42 n=6	P = 0.826 N.S.
miR-126	1.0±0.19 n=6	0.81±0.21 n=6	P = 0.531 N.S.

Supplementary Table 3. Primers used for PCR:

Gene and species	Forward	Reverse
Human *RYR1*	5'-ATCTCCCGCCTTAGCCATTTT-3'	5'-GGACCTCTACGGCCCTGTATC- 3'
Human *HDAC4*	5'-GGCCCACCGGAATCTGAA - 3'	5'-GAACTCTGGTCAAGGGAAACTG- 3'
Human *DES*	5'-AACCAGGAGTTTCTGACCACG-3'	5'-TTGAGCCGGTTCACTTCGG- 3'
Human *MEF2A*	5'- GGTCRGCCACCTCAGAACTTT-3'	5'-CCCTGGGTTAGTGTGTAGGACAA- 3'
Human *MEF2C*	5'-CTGGTGTAACACATGGACCTC- 3'	5'-GATTGCCATACCCGTTCCCT- 3'
Human *MEF2D*	5'-GGTGCCGCCGTGTCCAATCAG - 3'	5'- GGTCCGTGAGGGATGATGTC- 3'
Human *DMNT1*	5'- AGAACGGTGCTCATGCTTACA- 3'	5'- CTCTACGGGCTTCACTTCTTG- 3'
Human *DMNT2*	5'- TGCCAAGACGGATTGAAGGCAT - 3'	5'- GCAGGGAGGGCTCATTAAAAT- 3'
Human *DMNT3*	5'- AGGGAAGACTCGATCCTCGTC - 3'	5'- GTGTGTTAGCTTAGCAGACTGG- 3'
Human *ACTN2*	5'- GACATCGTGAACACCCCTAAAC - 3'	5'- CCGCAAAAGCGTGGTAGAA - 3'
Mouse *RYR1*	5'- TCACTCACAATGGAAAGCAG-3'	5'-AGCAGAATGACGATAACGA - 3'
Mouse *DES*	5'- TGAGACCATCGCGGCTAAGA - 3'	5'- GTGTCGGTATTCCATCATCTCC - 3'
Mouse *HDAC4*	5'-CACTGCATTCCAGGGATCC - 3'	5'- AGGACGGGGGGTGGTTGTAGGA - 3'
Mouse *HDAC5*	5'- GACTTTCCCTCCGTAAAACG - 3'	5'- TGCCATCCTTTCGACGGCAG - 3'
Mouse *MYOM1*	5'- AACAGCAATGGTCCACTCTTCA - 3'	5'- TGAACATTGCAGGGCTGGGA - 3'
Mouse *MEF2C*	5'- ATCCCGGATGCAGAGACGATTCAG-3'	5'- AAGAGCACACAATCTTTGCCT-3'
Mouse *MEF2D*	5'- CGAGATCGGGGCTCATCATCTT - 3'	5'- AGGCGTTGAAACCCTTCTTCC - 3'

115

Human *RYR1* CG-rich	5'-TTGGGTGGGTTGATCTTGTC-3'	5'-CTCCTTTCAGACTCCCAGAAC-3'
Human *RYR1* Control	5'-CGAGACTCCATCTCAGAAACAAA-3'	5'-GCCTGTAATCCCAGCTACTC-3'

Additional Unpublished Data:

Histone methyltransferase; SMYD1 increases in patients with minicores:

SMYD family (SMYD1-SMYD4) plays a critical role in myofibril assembly during development. There are two highly conserved domains in SMYD family; SET domain and MYND domain. These domains are involved in lysine methylation and protein-protein interactions, respectively. SMYD1 is a histone methyltransferase that is highly expressed in striated muscle and is mainly located at the M Band of the sarcomere. SMYD1 is regulated by sumoylation, which regulates its nuclear export and its translocation to the M band during sarcomerogenesis. The translocation of SMYD1 to the M band has a potential to regulate the activity of myosin and muscle type Creatine kinase [149]. The levels of several muscle enriched histone methyl-transferases were quantified in patients with recessive RYR1 mutations, using qPCR and were not found different. However the transcript level of SMYD1 was higher in muscles of patients with recessive RYR1 mutations compared to muscles of healthy individuals. (Figure R3.1).
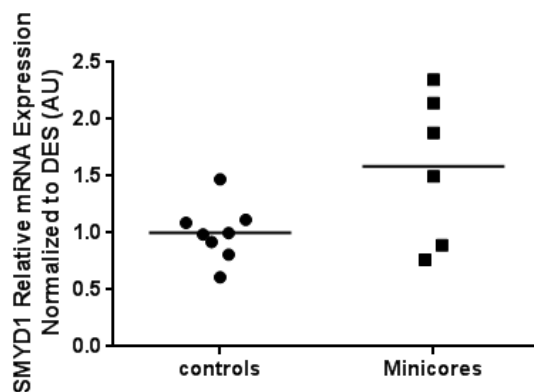
Figure R3.1: Expression levels of SMYD1 in muscles of patients with Recessive RYR1 mutations. Transcript levels were quantified and normalized to Desmin Expression levels (Controls: 1.00±0.08858 n=8, Minicores: 1.586±0.2674 n=6, student *t* test P=0.0374).

As mentioned previously, patients with minicores show a major disruption of the myofibrillar architecture and this may be related, at least in part to the up-regulation of SMYD1. SMYD1 is known to tri-methylate Histone 3 lysine 4 (H3K4me3), which has been associated with transcription activation although it was not ruled out that SMYD1 can also methylate other lysine residues [150].

MEF2 co-localization with HDAC4 in muscle biopsy:

In addition to the co-localization experiments that were performed in our 3rd manuscript, co-localization of HDAC4 and MEF2 (figure R3.2b) and the co-localization of MEF2 in the nucleus (figure R3.2a) were measured using confocal microscopy and analyzed with image J. The purpose of this experiment is to understand whether the increased nuclear localization of HDAC4 in muscles of patients with minicores, increases the nuclear co-localization of HDAC4 with MEF2.
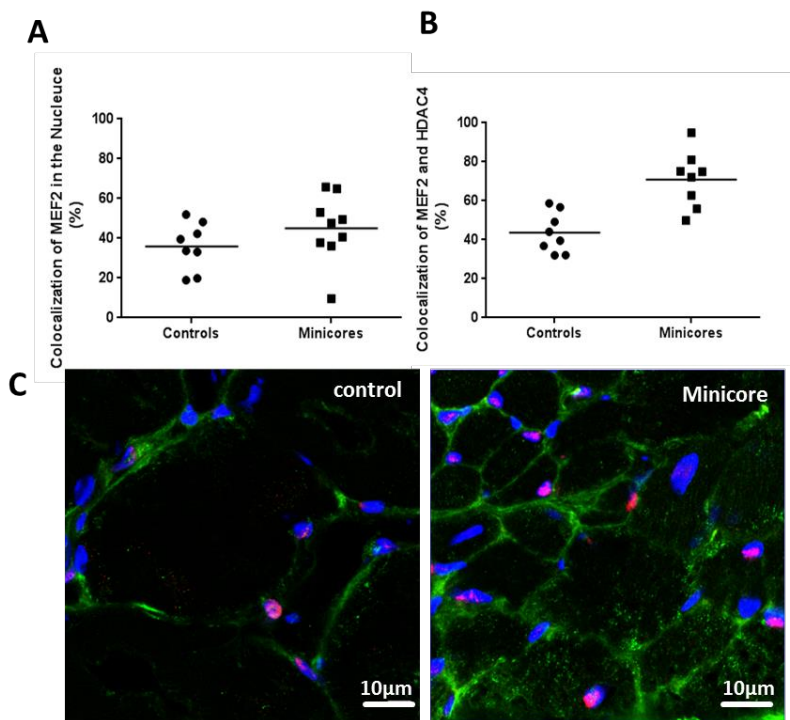
Figure R3.2: **Co-localization of MEF2 in the nucleus and with HDAC4.** A- Co localization of MEF2 in the nucleus (not significant). B- Co localization of HDAC4 with MEF2 (control 43.67%±3.679 minicore 70.85%±5.086, P<0.001). C- confocal images of Minicore and healthy individuals (**Blue – DAPI**, **Green- HDAC4** and **Red- MEF2**).

These results show that a higher degree of co-localization of HDAC4 and MEF2 in the nucleus is seen, indicating a potential shutting off of MEF2 dependent transcripts.

MicroRNA22 over expression in FDB fibers reduces the expression of RYR1 mRNA:
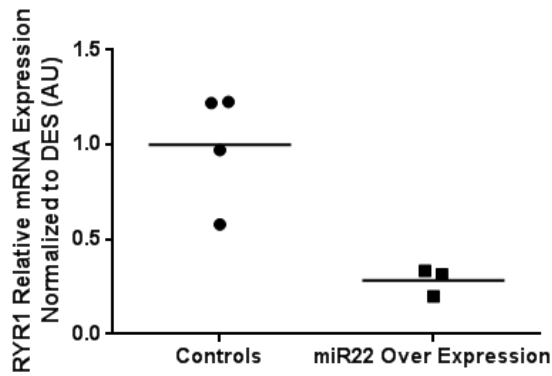
Figure R3.3: **Expression levels of RYR1 in FDB fibers transfected with miR22.** Transcript levels were quantified and normalized to Desmin Expression levels (Controls: 1.00±0.1521 n=4, Minicores: 0.2832±0.04214 n=3, student *t* test P=0.0113).

As described previously, miR22 and miR124 are predicted to bind the 3' UTR of the RYR1. Similar to the decrease of RYR1 transcript induced by over-expression of miR124 in FDB fibers, over-expression of miR22 reduced the levels of RYR1. This experiment was conducted in mouse FDB fibers as described in our 3rd publication.

Chapter 3 – Conclusions and future prospective:

Congenital myopathies are clinical conditions causing a number of symptoms including delayed motor development, muscle weakness, rigidity and hypotonia. Each year there are 6 newborns diagnosed with a congenital myopathy out of every 100,000 live births. The three main congenital myopathies are Nemaline myopathy, Core myopathies and Centronuclear myopathy. During this work we focused our studies on myopathies caused by mutations in RYR1, the gene encoding the skeletal muscle SR calcium release channel. Mutations in this gene have been associated with CCD, MmD, CNM and CFTD. In our laboratory Ca^{2+} release in myotubes isolated from biopsies were extensively investigated, these myotubes originate from patients with congenital myopathies and healthy control individuals. Live imaging in combination with the use of fluorescent Ca^{2+}-sensitive dyes such as Fura-2 (a ratiometric dye) and Fluo-4 were used to study Ca^{2+} release from the Sarcoplasmic reticulum. As mentioned in the results section of our 1st paper, working with primary cell cultures such as myotubes has several technical drawbacks, which could be potentially overcome by using immortalized human muscle cell lines. In our 1st publication the ECC properties of a human muscle cell line were characterized, both biochemically and physiologically. We describe that HMCL are suitable for experiments involving calcium homeostasis and in the future, immortalized cells from patients may also be used to characterize ECC, thus overcoming the problem of having a limited number of precious cells to study. As several different kinds of manipulations can be performed with immortalized muscle cells and as demonstrated on the HMCL, we think that such a model is amenable to investigate many aspects relevant to normal and diseased muscle, including myoblast differentiation, calcium homeostasis, cell fusion, intracellular trafficking, etc. In the last two decades the mouse muscle cell line C2C12 has been extensively used by laboratories throughout the world, for many research purposes in order to understand the physiology and plasticity of muscle differentiation. We think that HMCL in general or other similar immortalized cells offer a useful alternative for many experiments. In our 2nd publication, HMCL was used in

121

order to reproduce the conditions found in muscles of patients with congenital myopathies due to recessive RYR1 mutations, leading to reduced RyR1 content. Silencing of RyR1 expression in HMCL by siRNA was showed to cause reduction of RyR1, but also the up-regulation of InsP3R, similar to what we observed in patients. Clearly, up-regulation of InsP3R does not functionally compensate for the reduced RyR1 content. Intriguingly, the motive for the decreased RyR1 expression was still obscure and was addressed in our 3rd publication, where we found common epigenetic mechanisms leading to transcriptional repression that may be part of the underlying cause of muscle weakness seen in patients with congenital myopathies. The concluding figure represents our working hypothesis for the causes for RyR1 reduction, namely that over expression of HDAC4 and HDAC5 cause a decrease in the expression of MEF2 dependent genes and concomitantly cause hypermethylation of DNA. Sequestration of MEF2 also leads to a decrease of the expression of muscle-specific microRNAs. A pathological loop is then established whereby the decreased microRNAs expressions lead to further upregulation of class II HDACs. Interestingly, similar findings were made in muscle samples of patients with recessive RYR1 mutations as well as muscles of patients with Nemaline myopathy. Nevertheless, part of the pathological mechanism is still obscure as we cannot reveal exactly how recessive RYR1 mutations activate the above described epigenetic "loop".
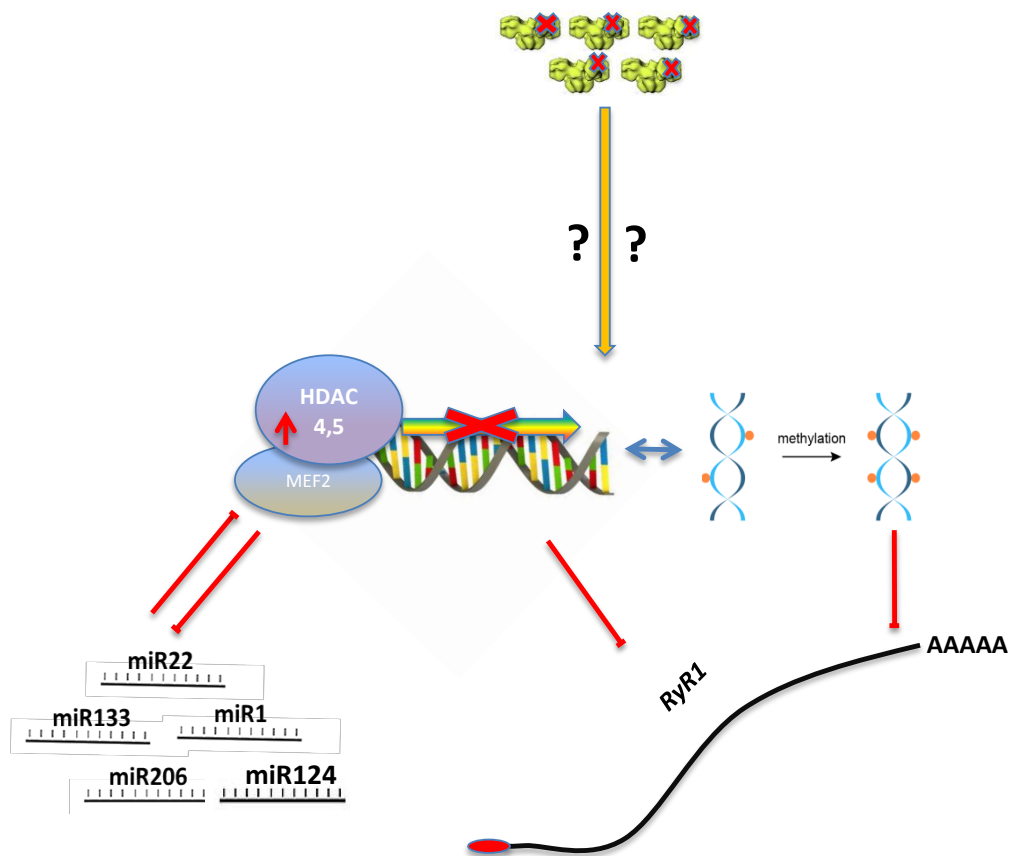
Concluding figure: Cartoon depicting how mutations in RYR1 lead to a decrease in RyR1 content thereby leading to weak muscles.

Our work describes the proposed mechanisms responsible for the down regulation of RyR1 expression in muscles of patients with congenital myopathies. Additionally, we have shown for the first time that when over-expressed in mouse FDB fibers, microRNAs that are predicted to bind to the 3`untranslated region of the RYR1 mRNA (namely, miR22 and miR124) downregulate RyR1 expression .Interestingly, the upregulation of HDAC4 in muscle biopsies from patients with mincores was remarkable (6-30 times higher) and such high levels of expression have not described so far in any other neuromuscular disorder. The treatment of patients with drugs that block the activity of class II HDACs or drugs that block the activity of DNA methyltransferases may significantly improve the symptoms of muscle weakness and

atrophy in patients with congenital muscle disorders. In order to verify and confirm the above pathological mechanisms the creation of a RYR1 mutant, compound heterozygous mouse will be necessary. Such a tool would also be useful in order to verify the impact of HDAC/DNMT inhibitors on muscle function. Amelioration of the phenotype needs to be assessed by physiological and biochemical characterization.

In brief, these results demonstrate that muscle weakness and atrophy in congenital myopathies can be initiated by a mutation in muscle specific gene, but the secondary effects of this mutation can be the major determinates of the phenotype. Thus targeting common downstream pathways activated in muscles of patients with congenital myopathies offers an interesting new approach for the amelioration of muscle function.

References:

1. McComas, B.R.M.P.F.G.A.J., *Skeletal Muscle : Form and Function 2nd*. 2nd 2e ed. 2006: Human Kinetics. 432.

2. Zalk, R., et al., *Structure of a mammalian ryanodine receptor.* Nature, 2015. **517**(7532): p. 44-9.

3. Schneider, M.F. and W.K. Chandler, *Voltage dependent charge movement of skeletal muscle: a possible step in excitation-contraction coupling.* Nature, 1973. **242**(5395): p. 244-6.

4. Rios, E. and G. Pizarro, *Voltage sensor of excitation-contraction coupling in skeletal muscle.* Physiol Rev, 1991. **71**(3): p. 849-908.

5. Franzini-Armstrong, C. and A.O. Jorgensen, *Structure and development of E-C coupling units in skeletal muscle.* Annu Rev Physiol, 1994. **56**: p. 509-34.

6. Franzini-Armstrong, C., *The sarcoplasmic reticulum and the control of muscle contraction.* FASEB J, 1999. **13 Suppl 2**: p. S266-70.

7. Endo, M., M. Tanaka, and Y. Ogawa, *Calcium induced release of calcium from the sarcoplasmic reticulum of skinned skeletal muscle fibres.* Nature, 1970. **228**(5266): p. 34-6.

8. Figueroa, L., et al., *Synthetic localized calcium transients directly probe signalling mechanisms in skeletal muscle.* J Physiol, 2012. **590**(Pt 6): p. 1389-411.

9. Sandow, A., *Excitation-contraction coupling in muscular response.* Yale J Biol Med, 1952. **25**(3): p. 176-201.

10. Fill, M. and J.A. Copello, *Ryanodine receptor calcium release channels.* Physiol Rev, 2002. **82**(4): p. 893-922.

11. gallery, B., Wikiversity Journal of Medicine, 2014.

12. Treves, S., et al., *Minor sarcoplasmic reticulum membrane components that modulate excitation-contraction coupling in striated muscles.* J Physiol, 2009. **587**(Pt 13): p. 3071-9.

13. Gehlert, S., W. Bloch, and F. Suhr, *Ca2+-dependent regulations and signaling in skeletal muscle: from electro-mechanical coupling to adaptation.* Int J Mol Sci, 2015. **16**(1): p. 1066-95.

14. Huxley, H.E., *The mechanism of muscular contraction.* Science, 1969. **164**(3886): p. 1356-65.

15. Milner, R.E., K.S. Famulski, and M. Michalak, *Calcium binding proteins in the sarcoplasmic/endoplasmic reticulum of muscle and nonmuscle cells.* Mol Cell Biochem, 1992. **112**(1): p. 1-13.

16. Fohr, U.G., et al., *Human alpha and beta parvalbumins. Structure and tissue-specific expression.* Eur J Biochem, 1993. **215**(3): p. 719-27.

17. Leberer, E., et al., *Molecular-Cloning and Expression of Cdna-Encoding a Lumenal Calcium-Binding Glycoprotein from Sarcoplasmic-Reticulum.* Proceedings of the National Academy of Sciences of the United States of America, 1989. **86**(16): p. 6047-6051.

18. Shoshan-Barmatz, V. and R.H. Ashley, *The structure, function, and cellular regulation of ryanodine-sensitive Ca2+ release channels.* Int Rev Cytol, 1998. **183**: p. 185-270.

19. Dowling, P., P. Doran, and K. Ohlendieck, *Drastic reduction of sarcalumenin in Dp427 (dystrophin of 427 kDa)-deficient fibres indicates that abnormal calcium handling plays a key role in muscular dystrophy.* Biochem J, 2004. **379**(Pt 2): p. 479-88.

20. Yoshida, M., et al., *Impaired Ca2+ store functions in skeletal and cardiac muscle cells from sarcalumenin-deficient mice.* J Biol Chem, 2005. **280**(5): p. 3500-6.

21. Ito, K., et al., *Deficiency of triad junction and contraction in mutant skeletal muscle lacking junctophilin type 1.* J Cell Biol, 2001. **154**(5): p. 1059-67.

22. Anderson, A.A., et al., *The junctional SR protein JP-45 affects the functional expression of the voltage-dependent Ca2+ channel Cav1.1.* J Cell Sci, 2006. **119**(Pt 10): p. 2145-55.

23. Anderson, A.A., et al., *The novel skeletal muscle sarcoplasmic reticulum JP-45 protein. Molecular cloning, tissue distribution, developmental expression, and interaction with alpha 1.1 subunit of the voltage-gated calcium channel.* J Biol Chem, 2003. **278**(41): p. 39987-92.

24. Delbono, O., et al., *Loss of skeletal muscle strength by ablation of the sarcoplasmic reticulum protein JP45.* Proc Natl Acad Sci U S A, 2007. **104**(50): p. 20108-13.

25. Nagaraj, R.Y., et al., *Increased susceptibility to fatigue of slow- and fast-twitch muscles from mice lacking the MG29 gene.* Physiol Genomics, 2000. **4**(1): p. 43-9.

26. Pan, Z., et al., *Co-expression of MG29 and ryanodine receptor leads to apoptotic cell death: effect mediated by intracellular Ca2+ release.* J Biol Chem, 2004. **279**(19): p. 19387-90.

27. Hong, C.S., S.J. Kwon, and H. Kim do, *Multiple functions of junctin and junctate, two distinct isoforms of aspartyl beta-hydroxylase.* Biochem Biophys Res Commun, 2007. **362**(1): p. 1-4.

28. Treves, S., et al., *Junctate is a key element in calcium entry induced by activation of InsP3 receptors and/or calcium store depletion.* J Cell Biol, 2004. **166**(4): p. 537-48.

29. Somlyo, A.V., et al., *Calcium release and ionic changes in the sarcoplasmic reticulum of tetanized muscle: an electron-probe study.* J Cell Biol, 1981. **90**(3): p. 577-94.

30.   Yazawa, M., et al., *TRIC channels are essential for Ca2+ handling in intracellular stores.* Nature, 2007. **448**(7149): p. 78-82.

31.   Chen, Y.F., et al., *Remodeling of calcium signaling in tumor progression.* J Biomed Sci, 2013. **20**: p. 23.

32.   Kurebayashi, N. and Y. Ogawa, *Depletion of Ca2+ in the sarcoplasmic reticulum stimulates Ca2+ entry into mouse skeletal muscle fibres.* J Physiol, 2001. **533**(Pt 1): p. 185-99.

33.   Stiber, J., et al., *STIM1 signalling controls store-operated calcium entry required for development and contractile function in skeletal muscle.* Nat Cell Biol, 2008. **10**(6): p. 688-97.

34.   Lee, E.H., et al., *Functional coupling between TRPC3 and RyR1 regulates the expressions of key triadic proteins.* J Biol Chem, 2006. **281**(15): p. 10042-8.

35.   Rosenberg, P.B., *Calcium entry in skeletal muscle.* J Physiol, 2009. **587**(Pt 13): p. 3149-51.

36.   Lyfenko, A.D. and R.T. Dirksen, *Differential dependence of store-operated and excitation-coupled Ca2+ entry in skeletal muscle on STIM1 and Orai1.* J Physiol, 2008. **586**(Pt 20): p. 4815-24.

37.   Soukup, T., G. Zacharova, and V. Smerdu, *Fibre type composition of soleus and extensor digitorum longus muscles in normal female inbred Lewis rats.* Acta Histochem, 2002. **104**(4): p. 399-405.

38.   Schiaffino, S. and C. Reggiani, *Fiber types in mammalian skeletal muscles.* Physiol Rev, 2011. **91**(4): p. 1447-531.

39.   Periasamy, M. and A. Kalyanasundaram, *SERCA pump isoforms: their role in calcium transport and disease.* Muscle Nerve, 2007. **35**(4): p. 430-42.

40.   Macdonald, W.A. and D.G. Stephenson, *Effects of ADP on sarcoplasmic reticulum function in mechanically skinned skeletal muscle fibres of the rat.* J Physiol, 2001. **532**(Pt 2): p. 499-508.

41.   Giannini, G., et al., *The ryanodine receptor/calcium channel genes are widely and differentially expressed in murine brain and peripheral tissues.* J Cell Biol, 1995. **128**(5): p. 893-904.

42.   Smith, J.S., et al., *Purified ryanodine receptor from rabbit skeletal muscle is the calcium-release channel of sarcoplasmic reticulum.* J Gen Physiol, 1988. **92**(1): p. 1-26.

43.   Takeshima, H., et al., *Primary structure and expression from complementary DNA of skeletal muscle ryanodine receptor.* Nature, 1989. **339**(6224): p. 439-45.

44.   Gillespie, D., et al., *(De)constructing the ryanodine receptor: modeling ion permeation and selectivity of the calcium release channel.* J Phys Chem B, 2005. **109**(32): p. 15598-610.

45.   Hwang, J.H., et al., *Mapping domains and mutations on the skeletal muscle ryanodine receptor channel.* Trends Mol Med, 2012. **18**(11): p. 644-57.

46.   Murayama, T., N. Kurebayashi, and Y. Ogawa, *Role of Mg(2+) in Ca(2+)-induced Ca(2+) release through ryanodine receptors of frog skeletal muscle: modulations by adenine nucleotides and caffeine.* Biophys J, 2000. **78**(4): p. 1810-24.

47.   Fruen, B.R., et al., *Differential Ca(2+) sensitivity of skeletal and cardiac muscle ryanodine receptors in the presence of calmodulin.* Am J Physiol Cell Physiol, 2000. **279**(3): p. C724-33.

48.   Moore, C.P., et al., *Apocalmodulin and Ca2+ calmodulin bind to the same region on the skeletal muscle Ca2+ release channel.* Biochemistry, 1999. **38**(26): p. 8532-7.

49.   Balshaw, D.M., et al., *Calmodulin binding and inhibition of cardiac muscle calcium release channel (ryanodine receptor).* J Biol Chem, 2001. **276**(23): p. 20144-53.

50.   Ikemoto, T., M. Iino, and M. Endo, *Enhancing effect of calmodulin on Ca(2+)-induced Ca2+ release in the sarcoplasmic reticulum of rabbit skeletal muscle fibres.* J Physiol, 1995. **487 (Pt 3)**: p. 573-82.

51.   Heiny, J.A., *S100A1: a physiological modulator of RYR1, Ca2+ release, and contractility in skeletal muscle. Focus on "S100A1 promotes action potential-initiated calcium release flux and force production in skeletal muscle".* Am J Physiol Cell Physiol, 2010. **299**(5): p. C882-4.

52.   Wright, N.T., et al., *S100A1 and calmodulin compete for the same binding site on ryanodine receptor.* J Biol Chem, 2008. **283**(39): p. 26676-83.

53.   Reiken, S., et al., *PKA phosphorylation activates the calcium release channel (ryanodine receptor) in skeletal muscle: defective regulation in heart failure.* J Cell Biol, 2003. **160**(6): p. 919-28.

54.   Marx, S.O., et al., *PKA phosphorylation dissociates FKBP12.6 from the calcium release channel (ryanodine receptor): defective regulation in failing hearts.* Cell, 2000. **101**(4): p. 365-76.

55.   Timerman, A.P., et al., *Selective binding of FKBP12.6 by the cardiac ryanodine receptor.* J Biol Chem, 1996. **271**(34): p. 20385-91.

56.   Barg, S., J.A. Copello, and S. Fleischer, *Different interactions of cardiac and skeletal muscle ryanodine receptors with FK-506 binding protein isoforms.* Am J Physiol, 1997. **272**(5 Pt 1): p. C1726-33.

57.   Xiao, R.P., et al., *The immunophilin FK506-binding protein modulates Ca2+ release channel closure in rat heart.* Journal of Physiology-London, 1997. **500**(2): p. 343-354.

58.   Kaftan, E., A.R. Marks, and B.E. Ehrlich, *Effects of rapamycin on ryanodine receptor/Ca(2+)-release channels from cardiac muscle.* Circ Res, 1996. **78**(6): p. 990-7.

59.   Wehrens, X.H., et al., *Ca2+/calmodulin-dependent protein kinase II phosphorylation regulates the cardiac ryanodine receptor.* Circ Res, 2004. **94**(6): p. e61-70.

60. Catterall, W.A., et al., *International Union of Pharmacology. XLVIII. Nomenclature and structure-function relationships of voltage-gated calcium channels.* Pharmacol Rev, 2005. **57**(4): p. 411-25.

61. Pietri-Rouxel, F., et al., *DHPR alpha1S subunit controls skeletal muscle mass and morphogenesis.* EMBO J, 2010. **29**(3): p. 643-54.

62. Bidaud, I., et al., *Voltage-gated calcium channels in genetic diseases.* Biochim Biophys Acta, 2006. **1763**(11): p. 1169-74.

63. Hu, H., et al., *The molecular architecture of dihydropyrindine receptor/L-type Ca2+ channel complex.* Sci Rep, 2015. **5**: p. 8370.

64. Rosenberg, H., et al., *Malignant hyperthermia: a review.* Orphanet J Rare Dis, 2015. **10**(1): p. 93.

65. Rosenberg, H., et al., *Malignant hyperthermia.* Orphanet J Rare Dis, 2007. **2**: p. 21.

66. Dirksen, R.T. and G. Avila, *Altered ryanodine receptor function in central core disease: leaky or uncoupled Ca(2+) release channels?* Trends Cardiovasc Med, 2002. **12**(5): p. 189-97.

67. Dietze, B., et al., *Malignant hyperthermia mutation Arg615Cys in the porcine ryanodine receptor alters voltage dependence of Ca2+ release.* J Physiol, 2000. **526 Pt 3**: p. 507-14.

68. Gallant, E.M. and R.C. Jordan, *Porcine malignant hyperthermia: genotype and contractile threshold of immature muscles.* Muscle Nerve, 1996. **19**(1): p. 68-73.

69. Jungbluth, H., *Central core disease.* Orphanet J Rare Dis, 2007. **2**: p. 25.

70. Jungbluth, H., *Multi-minicore Disease.* Orphanet J Rare Dis, 2007. **2**: p. 31.

71. Tong, J., T.V. McCarthy, and D.H. MacLennan, *Measurement of resting cytosolic Ca2+ concentrations and Ca2+ store size in HEK-293 cells transfected with malignant hyperthermia or central core disease mutant Ca2+ release channels.* J Biol Chem, 1999. **274**(2): p. 693-702.

72. Tilgen, N., et al., *Identification of four novel mutations in the C-terminal membrane spanning domain of the ryanodine receptor 1: association with central core disease and alteration of calcium homeostasis.* Hum Mol Genet, 2001. **10**(25): p. 2879-87.

73. Ghassemi, F., et al., *A recessive ryanodine receptor 1 mutation in a CCD patient increases channel activity.* Cell Calcium, 2009. **45**(2): p. 192-7.

74. Jungbluth, H., C. Wallgren-Pettersson, and J. Laporte, *Centronuclear (myotubular) myopathy.* Orphanet J Rare Dis, 2008. **3**: p. 26.

75. Begley, M.J. and J.E. Dixon, *The structure and regulation of myotubularin phosphatases.* Curr Opin Struct Biol, 2005. **15**(6): p. 614-20.

76. Laporte, J., et al., *Mutations in the MTM1 gene implicated in X-linked myotubular myopathy. ENMC International Consortium on Myotubular Myopathy. European Neuro-Muscular Center.* Hum Mol Genet, 1997. **6**(9): p. 1505-11.

77. Nicot, A.S., et al., *Mutations in amphiphysin 2 (BIN1) disrupt interaction with dynamin 2 and cause autosomal recessive centronuclear myopathy.* Nat Genet, 2007. **39**(9): p. 1134-9.

78. Wilmshurst, J.M., et al., *RYR1 Mutations Are a Common Cause of Congenital Myopathies with Central Nuclei.* Annals of Neurology, 2010. **68**(5): p. 717-726.

79. North, K.N. and M.M. Ryan, *Nemaline Myopathy*, in *GeneReviews(R)*, R.A. Pagon, et al., Editors. 1993: Seattle (WA).

80. Marttila, M., et al., *Nebulin interactions with actin and tropomyosin are altered by disease-causing mutations.* Skelet Muscle, 2014. **4**: p. 15.

81. Ha, M. and V.N. Kim, *Regulation of microRNA biogenesis.* Nat Rev Mol Cell Biol, 2014. **15**(8): p. 509-24.

82. Kim, V.N. and J.W. Nam, *Genomics of microRNA.* Trends Genet, 2006. **22**(3): p. 165-73.

83. Hirai, H., et al., *MyoD regulates apoptosis of myoblasts through microRNA-mediated down-regulation of Pax3.* J Cell Biol, 2010. **191**(2): p. 347-65.

84. Pratt, A.J. and I.J. MacRae, *The RNA-induced silencing complex: a versatile gene-silencing machine.* J Biol Chem, 2009. **284**(27): p. 17897-901.

85. Iwasaki, S., T. Kawamata, and Y. Tomari, *Drosophila argonaute1 and argonaute2 employ distinct mechanisms for translational repression.* Mol Cell, 2009. **34**(1): p. 58-67.

86. Behm-Ansmant, I., et al., *mRNA degradation by miRNAs and GW182 requires both CCR4:NOT deadenylase and DCP1:DCP2 decapping complexes.* Genes Dev, 2006. **20**(14): p. 1885-98.

87. McCarthy, J.J. and K.A. Esser, *MicroRNA-1 and microRNA-133a expression are decreased during skeletal muscle hypertrophy.* J Appl Physiol (1985), 2007. **102**(1): p. 306-13.

88. Liu, N., et al., *An intragenic MEF2-dependent enhancer directs muscle-specific expression of microRNAs 1 and 133.* Proc Natl Acad Sci U S A, 2007. **104**(52): p. 20844-9.

89. Goljanek-Whysall, K., D. Sweetman, and A.E. Munsterberg, *microRNAs in skeletal muscle differentiation and disease.* Clinical Science, 2012. **123**(11-12): p. 611-625.

90. Yu, H., et al., *microRNA-133: expression, function and therapeutic potential in muscle diseases and cancer.* Curr Drug Targets, 2014. **15**(9): p. 817-28.

91. Koutsoulidou, A., et al., *Expression of miR-1, miR-133a, miR-133b and miR-206 increases during development of human skeletal muscle.* BMC Dev Biol, 2011. **11**: p. 34.

92.   Liu, N., et al., *Mice lacking microRNA 133a develop dynamin 2-dependent centronuclear myopathy.* J Clin Invest, 2011. **121**(8): p. 3258-68.

93.   Guller, I. and A.P. Russell, *MicroRNAs in skeletal muscle: their role and regulation in development, disease and function.* J Physiol, 2010. **588**(Pt 21): p. 4075-87.

94.   Weng, L., J. Brown, and C. Eng, *PTEN induces apoptosis and cell cycle arrest through phosphoinositol-3-kinase/Akt-dependent and -independent pathways.* Hum Mol Genet, 2001. **10**(3): p. 237-42.

95.   Dey, B.K., J. Gagan, and A. Dutta, *miR-206 and -486 induce myoblast differentiation by downregulating Pax7.* Mol Cell Biol, 2011. **31**(1): p. 203-14.

96.   Wu, R., et al., *MicroRNA-431 accelerates muscle regeneration and ameliorates muscular dystrophy by targeting Pax7 in mice.* Nat Commun, 2015. **6**: p. 7713.

97.   McCarthy, J.J., *The MyomiR network in skeletal muscle plasticity.* Exerc Sport Sci Rev, 2011. **39**(3): p. 150-4.

98.   Williams, A.H., et al., *MicroRNA-206 delays ALS progression and promotes regeneration of neuromuscular synapses in mice.* Science, 2009. **326**(5959): p. 1549-54.

99.   Eisenberg, I., et al., *Distinctive patterns of microRNA expression in primary muscular disorders.* Proc Natl Acad Sci U S A, 2007. **104**(43): p. 17016-21.

100.   Alexander, M.S., et al., *Regulation of DMD pathology by an ankyrin-encoded miRNA.* Skelet Muscle, 2011. **1**: p. 27.

101.   Dmitriev, P., et al., *Defective regulation of microRNA target genes in myoblasts from facioscapulohumeral dystrophy patients.* J Biol Chem, 2013. **288**(49): p. 34989-5002.

102.   Portilho, D.M., et al., *miRNA expression in control and FSHD fetal human muscle biopsies.* PLoS One, 2015. **10**(2): p. e0116853.

103.   Falcone, G., et al., *Noncoding RNAs: emerging players in muscular dystrophies.* Biomed Res Int, 2014. **2014**: p. 503634.

104.   Trojer, P. and D. Reinberg, *Facultative heterochromatin: is there a distinctive molecular signature?* Mol Cell, 2007. **28**(1): p. 1-13.

105.   Armstrong, L., *Epigenetics*. 2014: Garland Science.

106.   Burgess, R.J. and Z. Zhang, *Histone chaperones in nucleosome assembly and human disease.* Nat Struct Mol Biol, 2013. **20**(1): p. 14-22.

107.   Krebs, J.E. and C.L. Peterson, *Understanding "active" chromatin: a historical perspective of chromatin remodeling.* Crit Rev Eukaryot Gene Expr, 2000. **10**(1): p. 1-12.

108.   Thomas, J.O., *Histone H1: location and role.* Curr Opin Cell Biol, 1999. **11**(3): p. 312-7.

109.   Filippakopoulos, P. and S. Knapp, *Targeting bromodomains: epigenetic readers of lysine acetylation.* Nat Rev Drug Discov, 2014. **13**(5): p. 337-56.

110.   Roth, S.Y., J.M. Denu, and C.D. Allis, *Histone acetyltransferases.* Annu Rev Biochem, 2001. **70**: p. 81-120.

111.   Legube, G. and D. Trouche, *Regulating histone acetyltransferases and deacetylases.* EMBO Rep, 2003. **4**(10): p. 944-7.

112.   de Ruijter, A.J., et al., *Histone deacetylases (HDACs): characterization of the classical HDAC family.* Biochem J, 2003. **370**(Pt 3): p. 737-49.

113.   Haberland, M., R.L. Montgomery, and E.N. Olson, *The many roles of histone deacetylases in development and physiology: implications for disease and therapy.* Nat Rev Genet, 2009. **10**(1): p. 32-42.

114.   Delcuve, G.P., D.H. Khan, and J.R. Davie, *Roles of histone deacetylases in epigenetic regulation: emerging paradigms from studies with inhibitors.* Clin Epigenetics, 2012. **4**(1): p. 5.

115.   Villagra, A., et al., *The histone deacetylase HDAC11 regulates the expression of interleukin 10 and immune tolerance.* Nat Immunol, 2009. **10**(1): p. 92-100.

116.   Oehme, I., et al., *Histone deacetylase 10 promotes autophagy-mediated cell survival.* Proc Natl Acad Sci U S A, 2013. **110**(28): p. E2592-601.

117.   Choi, M.C., et al., *HDAC4 promotes Pax7-dependent satellite cell activation and muscle regeneration.* EMBO Rep, 2014. **15**(11): p. 1175-83.

118.   Wang, A.H., et al., *Regulation of histone deacetylase 4 by binding of 14-3-3 proteins.* Mol Cell Biol, 2000. **20**(18): p. 6904-12.

119.   Backs, J., et al., *CaM kinase II selectively signals to histone deacetylase 4 during cardiomyocyte hypertrophy.* J Clin Invest, 2006. **116**(7): p. 1853-64.

120.   Yao, Y.L. and W.M. Yang, *Beyond histone and deacetylase: an overview of cytoplasmic histone deacetylases and their nonhistone substrates.* J Biomed Biotechnol, 2011. **2011**: p. 146493.

121.   Ago, T., et al., *A redox-dependent pathway for regulating class II HDACs and cardiac hypertrophy.* Cell, 2008. **133**(6): p. 978-93.

122.   Liu, F., et al., *Caspase-mediated specific cleavage of human histone deacetylase 4.* J Biol Chem, 2004. **279**(33): p. 34537-46.

123.   Kirsh, O., et al., *The SUMO E3 ligase RanBP2 promotes modification of the HDAC4 deacetylase.* EMBO J, 2002. **21**(11): p. 2682-91.

124. Gregoire, S. and X.J. Yang, *Association with class IIa histone deacetylases upregulates the sumoylation of MEF2 transcription factors.* Mol Cell Biol, 2005. **25**(6): p. 2273-87.

125. Basile, V., R. Mantovani, and C. Imbriano, *DNA damage promotes histone deacetylase 4 nuclear localization and repression of G2/M promoters, via p53 C-terminal lysines.* J Biol Chem, 2006. **281**(4): p. 2347-57.

126. Gupta, M.P., et al., *HDAC4 and PCAF bind to cardiac sarcomeres and play a role in regulating myofilament contractile activity.* J Biol Chem, 2008. **283**(15): p. 10135-46.

127. Wei, J.Y., et al., *Intracellular translocation of histone deacetylase 5 regulates neuronal cell apoptosis.* Brain Res, 2015. **1604**: p. 15-24.

128. Raichur, S., et al., *Histone deacetylase 5 regulates glucose uptake and insulin action in muscle cells.* J Mol Endocrinol, 2012. **49**(3): p. 203-11.

129. McGee, S.L. and M. Hargreaves, *Histone modifications and skeletal muscle metabolic gene expression.* Clin Exp Pharmacol Physiol, 2010. **37**(3): p. 392-6.

130. Greer, E.L. and Y. Shi, *Histone methylation: a dynamic mark in health, disease and inheritance.* Nat Rev Genet, 2012. **13**(5): p. 343-57.

131. Moresi, V., et al., *Regulation of skeletal muscle development and homeostasis by gene imprinting, histone acetylation and microRNA.* Biochim Biophys Acta, 2015. **1849**(3): p. 309-16.

132. Bonizec, M., et al., *The ubiquitin-selective chaperone Cdc48/p97 associates with Ubx3 to modulate monoubiquitylation of histone H2B.* Nucleic Acids Res, 2014. **42**(17): p. 10975-86.

133. Tang, H., et al., *A histone deacetylase 4/myogenin positive feedback loop coordinates denervation-dependent gene induction and suppression.* Mol Biol Cell, 2009. **20**(4): p. 1120-31.

134. Moresi, V., et al., *Myogenin and class II HDACs control neurogenic muscle atrophy by inducing E3 ubiquitin ligases.* Cell, 2010. **143**(1): p. 35-45.

135. Bruneteau, G., et al., *Muscle histone deacetylase 4 upregulation in amyotrophic lateral sclerosis: potential role in reinnervation ability and disease progression.* Brain, 2013. **136**(Pt 8): p. 2359-68.

136. Minetti, G.C., et al., *Functional and morphological recovery of dystrophic muscles in mice treated with deacetylase inhibitors.* Nat Med, 2006. **12**(10): p. 1147-50.

137. Deaton, A.M. and A. Bird, *CpG islands and the regulation of transcription.* Genes Dev, 2011. **25**(10): p. 1010-22.

138. Goll, M.G. and T.H. Bestor, *Eukaryotic cytosine methyltransferases.* Annu Rev Biochem, 2005. **74**: p. 481-514.

139. Denis, H., M.N. Ndlovu, and F. Fuks, *Regulation of mammalian DNA methyltransferases: a route to new mechanisms.* EMBO Rep, 2011. **12**(7): p. 647-56.

140. Bronner, C., et al., *UHRF1 Links the Histone code and DNA Methylation to ensure Faithful Epigenetic Memory Inheritance.* Genet Epigenet, 2010. **2009**(2): p. 29-36.

141. Schaefer, M., et al., *RNA methylation by Dnmt2 protects transfer RNAs against stress-induced cleavage.* Genes Dev, 2010. **24**(15): p. 1590-5.

142. Yasin, R., et al., *A quantitative technique for growing human adult skeletal muscle in culture starting from mononucleated cells.* J Neurol Sci, 1977. **32**(3): p. 347-60.

143. Blau, H.M. and C. Webster, *Isolation and characterization of human muscle cells.* Proc Natl Acad Sci U S A, 1981. **78**(9): p. 5623-7.

144. Zhu, C.H., et al., *Cellular senescence in human myoblasts is overcome by human telomerase reverse transcriptase and cyclin-dependent kinase 4: consequences in aging muscle and therapeutic strategies for muscular dystrophies.* Aging Cell, 2007. **6**(4): p. 515-23.

145. Mamchaoui, K., et al., *Immortalized pathological human myoblasts: towards a universal tool for the study of neuromuscular disorders.* Skelet Muscle, 2011. **1**: p. 34.

146. Zhang, J., et al., *microRNA-22, downregulated in hepatocellular carcinoma and correlated with prognosis, suppresses cell proliferation and tumourigenicity.* Br J Cancer, 2010. **103**(8): p. 1215-20.

147. Sarkar, S., et al., *Histone deacetylase inhibitors reverse CpG methylation by regulating DNMT1 through ERK signaling.* Anticancer Res, 2011. **31**(9): p. 2723-32.

148. Espada, J., et al., *Human DNA methyltransferase 1 is required for maintenance of the histone H3 modification pattern.* J Biol Chem, 2004. **279**(35): p. 37175-84.

149. Du, S.J., X. Tan, and J. Zhang, *SMYD proteins: key regulators in skeletal and cardiac muscle development and function.* Anat Rec (Hoboken), 2014. **297**(9): p. 1650-62.

150. Tan, X., et al., *SmyD1, a histone methyltransferase, is required for myofibril organization and muscle contraction in zebrafish embryos.* Proc Natl Acad Sci U S A, 2006. **103**(8): p. 2713-8.

Curriculum vitae

Education:

2012 – Present **Doctor of Philosophy in Cell Biology**, Faculty of Science, Basel University.

Thesis: "The Molecular Dysregulation of Excitation Contraction Coupling in Patients with Congenital Muscle Disorders". Departments of Anesthesia and Biomedicine, Basel University Hospital, Switzerland.

Advisor: Prof Susan Treves

2009 - 2011 **Master of Science in Biotechnology,** Faculty of life science, Bar-Ilan university.

Thesis: "Characterization of Nek1 kinase Involvement in spermatogenesis", Ramat Gan Israel.

Advisor: Dr Benny Motro

2006 - 2009 **Bachelor of Science in Molecular, Cellular and Medical Biology,** Faculty of life science, Bar-Ilan university, Ramat Gan Israel .

2003 - 2005 **High School final certificate** - Majoring; Mathematics, English, Biology and Biotechnology, Yehud, Israel.

Additional Education:

LTK Module 1: Introductory Course in Laboratory Animal Science - FELASA Category B course (10/2012) Zurich University, Switzerland.

Writing to Be Published - Academic Writing Conventions and Style (02/2014), Basel University, Switzerland.

Teaching experience:

2009 – 2011 Teaching Assistant - Microbiology lab, Bar-Ilan University.

Fellowships and Prizes:

1. Scholarship for Academic merit - Banin Foundation/ UJA Federation of New York (5/2010).

2. Scholarship for Excellence - Salti Foundation (9/2010).

3. PhD support - Botnar stiftung (2012-2016).

Conferences and Communications:

11/2012 **9th Swiss Meeting on Muscle Research** Macolin / Magglingen, Switzerland. Pathophysiology of recessive RYR1 mutations in congenital myopathies: is there more than meets the eye? (Poster presentation) Ori Rokach, Marijana Sekulic, Mirko Vukcevic, Francesco Zorzato and Susan Treves.

2/2014 **Biophisical society annual meeting**, San Francisco, USA: BIOCHEMICAL, CELLULAR AND ELECTROPHYSIOLOGICAL CHARACTERIZATION OF HMCL-7304 A HUMAN SKELETAL MUSCLE-DERIVED CELL LINE. Ori Rokach, Nina D. Ullrich, Martin Rausch, Haiyan Zhou, Francesco Muntoni, Francesco Zorzato and Susan Treves.

11/2014 **10th Swiss Meeting on Muscle Research** Macolin / Magglingen, Switzerland. Mechanism of action of recessive RYR1 mutations. (Poster presentation) Ori Rokach, Heinz Jungbluth, Francesco Muntoni, Nicol Voermans, Baziel Van Engelen, Luc Heytens, Francesco Zorzato and Susan Treves.

5/2015 **EMBO conference; Chromatin and Epigenetics**, Heidelberg, Germany. Epigenetic changes as a common trigger of muscle weakness in congenital myopathies. (Poster presentation) Ori Rokach, Marijana Sekulic, Francesco Zorzato and Susan Treves.

6/2015 **34th meeting of the European Malignant Hyperthermia Group** (Oral presentation), Lille, France.

Languages:

1. Hebrew as mother tongue
2. Fluent English

List of Publications

Rokach, O., N. D. Ullrich, M. Rausch, V. Mouly, H. Zhou, F. Muntoni, F. Zorzato and S. Treves (2013). "Establishment of a human skeletal muscle-derived cell line: biochemical, cellular and electrophysiological characterization." Biochem J 455(2): 169-177.

Zhou, H., **O. Rokach**, L. Feng, I. Munteanu, K. Mamchaoui, J. M. Wilmshurst, C. Sewry, A. Y. Manzur, K. Pillay, V. Mouly, M. Duchen, H. Jungbluth, S. Treves and F. Muntoni (2013). "RyR1 deficiency in congenital myopathies disrupts excitation-contraction coupling." Hum Mutat 34(7): 986-996.

Attali, R., S. Aharoni, S. Treves, **O. Rokach**, M. Becker Cohen, Y. Fellig, R. Straussberg, T. Dor, M. Daana, S. Mitrani-Rosenbaum and Y. Nevo (2013). "Variable myopathic presentation in a single family with novel skeletal RYR1 mutation." PLoS One 8(7): e69296.

Rokach, O., M. Sekulic-Jablanovic, N. Voermans, J. Wilmshurst, K. Pillay, L. Heytens, H. Zhou, F. Muntoni, M. Gautel, Y. Nevo, S. Mitrani-Rosenbaum, R. Attali, A. Finotti, R. Gambari, B. Mosca, H. Jungbluth, F. Zorzato and S. Treves (2015). "Epigenetic changes as a common trigger of muscle weakness in congenital myopathies." Hum Mol Genet 24(16): 4636-4647.